

Accepted Manuscript

Design, synthesis and biological evaluation of 1,3-diphenyl-1H-pyrazole derivatives containing benzimidazole skeleton as potential anticancer and apoptosis inducing agents

T.Srinivasa Reddy, Hitesh Kulhari, V.Ganga Reddy, Vipul Bansal, Dr. Ahmed Kamal, Outstanding Scientist, Dr. Ravi Shukla

PII: S0223-5234(15)30163-X

DOI: [10.1016/j.ejmech.2015.07.031](https://doi.org/10.1016/j.ejmech.2015.07.031)

Reference: EJMECH 8015

To appear in: *European Journal of Medicinal Chemistry*

Received Date: 23 April 2015

Revised Date: 13 July 2015

Accepted Date: 16 July 2015

Please cite this article as: T.S. Reddy, H. Kulhari, V.G. Reddy, V. Bansal, A. Kamal, R. Shukla, Design, synthesis and biological evaluation of 1,3-diphenyl-1H-pyrazole derivatives containing benzimidazole skeleton as potential anticancer and apoptosis inducing agents, *European Journal of Medicinal Chemistry* (2015), doi: 10.1016/j.ejmech.2015.07.031.

This is a PDF file of an unedited manuscript that has been accepted for publication. As a service to our customers we are providing this early version of the manuscript. The manuscript will undergo copyediting, typesetting, and review of the resulting proof before it is published in its final form. Please note that during the production process errors may be discovered which could affect the content, and all legal disclaimers that apply to the journal pertain.



Graphical Abstract

Design, synthesis and biological evaluation of 1,3-diphenyl-1H-pyrazole derivatives containing benzimidazole skeleton as potential anticancer and apoptosis inducing agents

T. Srinivasa Reddy,^{a,b,c,d} Hitesh Kulhari,^{a,b,c,d} V. Ganga Reddy,^a Vipul Bansal,^{c,d} Ahmed Kamal,^{a,b,*} Ravi Shukla,^{c,d,e,*}

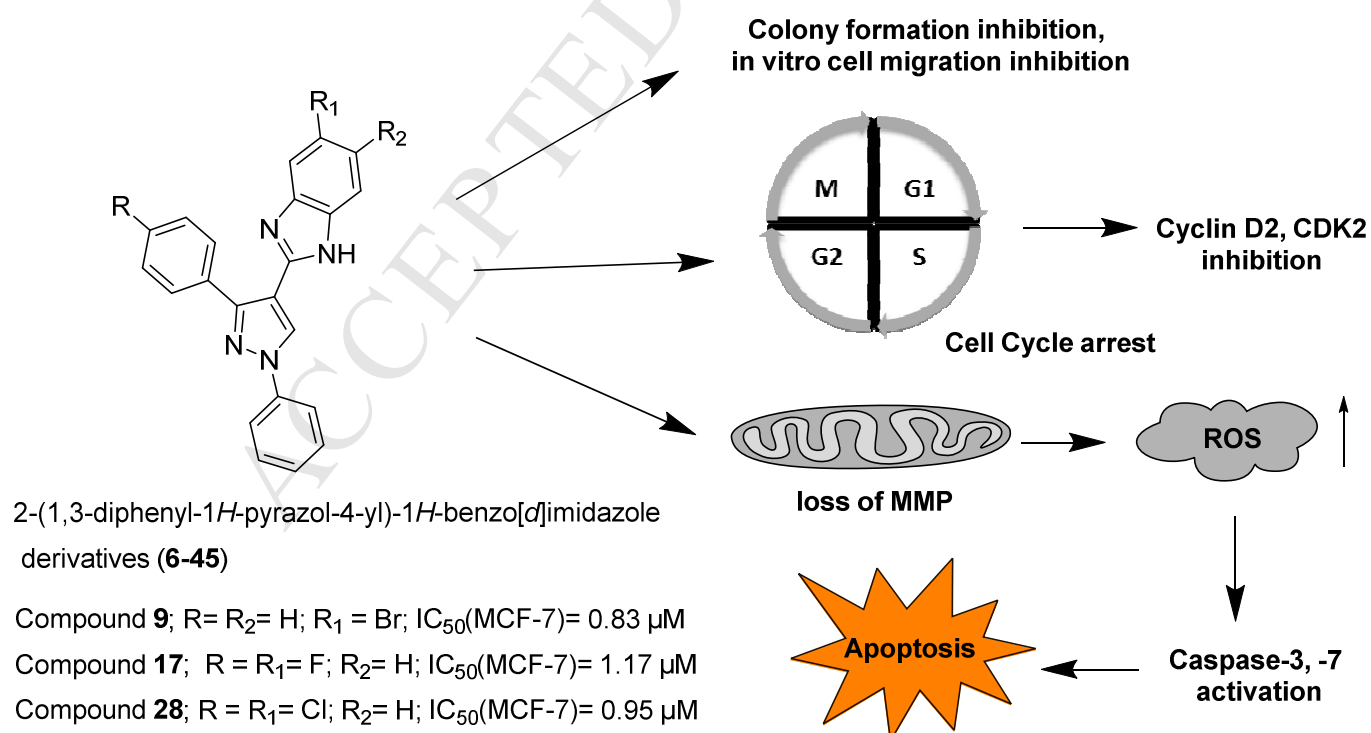
^a Medicinal Chemistry and Pharmacology, CSIR-Indian Institute of Chemical Technology, Hyderabad 500 007, India

^b IICT - RMIT Research Centre, CSIR-Indian Institute of Chemical Technology, Hyderabad 500 007, India

^c Ian Potter NanoBioSensing Facility, NanoBiotechnology Research Laboratory, School of Applied Sciences, RMIT University, Melbourne 3000, Australia

^d Health Innovations Research Institute, RMIT University, Melbourne 3083, Australia

^e Centre for Advanced Materials and Industrial Chemistry, RMIT University, Melbourne 3000, Australia



Design, synthesis and biological evaluation of 1,3-diphenyl-1H-pyrazole derivatives containing benzimidazole skeleton as potential anticancer and apoptosis inducing agents

T. Srinivasa Reddy,^{a,b,c,d} Hitesh Kulhari,^{a,b,c,d} V. Ganga Reddy,^a Vipul Bansal,^{c,d} Ahmed Kamal,^{a,b*} Ravi Shukla,^{c,d,e*}

^a *Medicinal Chemistry and Pharmacology, CSIR-Indian Institute of Chemical Technology, Hyderabad 500 007, India*

^b *IICT - RMIT Research Centre, CSIR-Indian Institute of Chemical Technology, Hyderabad 500 007, India*

^c *Ian Potter NanoBioSensing Facility, NanoBiotechnology Research Laboratory, School of Applied Sciences, RMIT University, Melbourne 3000, Australia*

^d *Health Innovations Research Institute, RMIT University, Melbourne 3083, Australia*

^e *Centre for Advanced Materials and Industrial Chemistry, RMIT University, Melbourne 3000, Australia*

*Corresponding authors:

Dr. Ravi Shukla

School of Applied Sciences, RMIT University
GPO Box 2476, Melbourne 3001 VIC Australia
E-mail: ravi.shukla@rmit.edu.au
Tel: 0061 3 9925 2970
Fax: 0061 3 9925 2882

Dr. Ahmed Kamal

Outstanding Scientist,
CSIR-Indian Institute of Chemical Technology,
Hyderabad, India-500 007.
E-mail: ahmedkamal@iict.res.in
Tel: +91-040-27193157;
Fax: +91-40-27193189

Abstract

A series of forty different pyrazole containing benzimidazole hybrids (**6-45**) have been designed, synthesized and evaluated for their potential anti-proliferative activity against three human tumor cell lines - lung (A549), breast (MCF-7), and cervical (HeLa). Some of the compounds, specifically **9**, **17**, and **28**, showed potent growth inhibition against all the cell lines tested, with IC₅₀ values in the range of 0.83-1.81 μM. Breast cancer cells were used for further detailed studies to understand the mechanism of cell growth inhibition and apoptosis inducing effect of compounds. The morphology, cell migration and long term clonogenic survival of MCF-7 breast cancer cells were severely affected by treatment with these compounds. Flow-cytometry revealed the compounds arrested MCF-7 cells in the G1 phase of the cell cycle via down regulation of cyclin D2 and CDK2. Fluorescent staining and DNA fragmentation studies showed that cell proliferation was inhibited by induction of apoptosis. Moreover, the compounds led to collapse of mitochondrial membrane potential (DΨm) and increased levels of reactive oxygen species (ROS) were noted. The ease of synthesis and the remarkable biological activities make these compounds promising new frameworks for the development of cancer therapeutics.

Key words

Pyrazole; benzimidazole; anti-proliferative activity; apoptosis; RT-PCR.

1.0 Introduction

Cancer is a major cause of death worldwide. Thus, the incidence of and mortality rate from cancer has become globally important [1]. Chemotherapy using drugs that target cell division, angiogenesis or that induce cancer cell death by various signaling pathways is one strategy to treat cancer. However, due to side effects and the development of drug resistance in cancer cells, there is need to design, synthesize and develop more potent and safer chemotherapeutic agents [2].

Apoptosis is a programmed cell death that plays an important role in the maintenance of tissue homeostasis. Generally, it is considered that apoptosis is regulated by pro and anti-apoptotic proteins, such as the Bcl-2 and inhibitor of apoptosis protein (IAP) family members, and executed through caspases; mainly via two major and inter-related pathways, the mitochondrial-dependent 'intrinsic' pathway and the death receptor-mediated 'extrinsic' caspase-8 pathway [3]. Disruption or inappropriate regulation of these processes results in several diseases including cancer [4]. Thus, targeting critical regulators of apoptosis with the goal of inducing apoptosis in cancer cells has emerged as an attractive strategy in cancer therapy [5].

Pyrazoles are an important class of heterocyclic compounds and are promising scaffolds in medicinal chemistry. Much attention has been paid to pyrazole based compounds because of their broad range of biological effects, including anti-inflammatory, anti-microbial, anti-oxidant, anti-depressant, anti-influenza and anti-cancer activities [6-10]. Several recent reports suggest pyrazole derivatives as promising anticancer agents, indicating their use in the development of new anticancer agents [11-14]. Among the anticancer pyrazoles, 1,3-diphenyl pyrazoles have been reported to be highly potent and efficient cytotoxic agents [15-17].

On the other hand, benzimidazole ring system has also emerged as an important heterocyclic system due to its wide range of biological activities, as well as synthetic applications in medicinal chemistry [18-19]. Recently, various benzimidazole derivatives have been reported to have potential anti-tumor/anti-proliferative activity against different cancers [20-22]. Due to the structural similarity of the benzimidazole nuclei with some of the naturally occurring moieties such as purines, they easily interact with biomolecules of living systems. Moreover, benzimidazoles attached to other heterocyclic moieties have resulted in compounds (hybrid molecules) with improved anti-cancer activities [23-24].

A pharmacophore hybridization approach for the synthesis of new bioactive compounds is an effective strategy and is being used in modern medicinal chemistry. Hybridization of two different bioactive molecules with complementary pharmacophoric functions or with different mechanisms of action often show enhanced effects [25-26]. Prompted by these observations, and continuing our work on benzimidazole and pyrazole derivatives with significant anti-cancer activities [27-28], we synthesized pyrazole containing benzimidazole derivatives (**6-45**) with a view to producing promising anti-cancer agents.

2.0 Results and Discussion

2.1 Chemistry

The synthetic route for 2-(1,3-diphenyl-1*H*-pyrazol-4-yl)-1*H*-benzo[*d*]imidazoles (**6-45**) is outlined in Scheme 1. These analogs were synthesized by adapting a reported procedure [13,16]. The key aldehyde intermediates (**4a-d**) were prepared in two steps. Condensation of the acetophenones (**1a-d**) with phenyl hydrazine (**2**) in ethanol produced the corresponding acetophenone phenyl hydrazones (**3a-d**). This was followed by cyclization of the acetophenone phenyl hydrazones via the Vilsmeier–Haack reaction. The desired target

compounds (**6-45**) were obtained in good yields by refluxing aldehyde intermediates (**4a-d**) with different substituted *O*-phenylenediamines (**5a-d**) in ethanol and sodium metabisulphate.

<Scheme 1>

2.2 *In vitro* anticancer activity

All the newly synthesized 2-(1,3-diphenyl-1*H*-pyrazol-4-yl)-1*H*-benzo[*d*]imidazoles (**6-45**) were evaluated for their cytotoxicity against three human tumor cell lines: lung (A549), breast (MCF-7), cervical (HeLa) and against normal keratinocyte (HaCaT) cells using the 3-(4,5-dimethylthiazol-2-yl)-2,5-diphenyltetrazolium bromide (MTT) growth inhibition assay. 5-Fluorouracil was used as a positive control and the results are summarized in Table.1. As shown in Table 1, compounds **9**, **17** and **28** exhibited potent broad spectrum anti-proliferative activity against the three cancer cell lines, with IC₅₀ values of 0.83-1.81 μM. These were superior to 5-fluorouracil which showed IC₅₀ values of 2.13-4.16 μM. The highest growth inhibitory activity observed in the series was against the MCF-7 cancer cell line, with compound **9** being most potent (IC₅₀-0.83 μM), followed by the compounds **17** (IC₅₀-0.93 μM) and **28** (IC₅₀-1.17 μM). The other two cancer cell lines, A549 and HeLa, also showed sensitivity towards these three compounds with not more than 1.81 μM concentration. All compounds, with the exception of **13-15**, **23-25**, **33-35** and **43-45**, exhibited higher or comparable cytotoxic activity against certain cell lines with respect to the standard, 5-Fluorouracil. The intermediates 1,3- diphenyl pyrazole carboxaldehyde (**4 a-d**) displayed moderate growth inhibition on the tested cancer cells with IC₅₀ values of 8.66-29.5 μM. We also investigated the effect of these compounds on normal human keratinocytes (HaCaT) proliferation. Interestingly, most of the synthesized compounds had no effect on keratinocyte cell growth (IC₅₀ >50 μM). The exceptions were compounds **12**, **14**, **19**, **24**, **31** and **43**, that exhibited IC₅₀ values in the range of 21.35-44.67 μM (Table. 1). These results indicate

selectivity of 1,3-diphenyl-1*H*-pyrazole derivatives towards tumor cells compared to the normal HaCaT cells.

By investigating the variation in selectivity of the three cell lines to the compounds, it was revealed that structural variations and modification on the B ring of pyrazolo-benzimidazole derivatives led to different cytotoxic activities. Structure–activity relationships in these hybrids demonstrated that compounds **7-9**, **17-19**, **27-29** and **37-39**, with mono-substituted halogens (fluorine, chlorine, and bromine) on the benzimidazole B ring, exhibited more potent activities than compounds **11**, **20**, **30** and **40** or **10**, **21**, **31** and **42** with methoxy and methyl substitutions, respectively. An electron withdrawing trifluoromethyl (CF₃) substitution on the B-ring of compounds **12**, **22**, **31** and **41** resulted in moderate to lower cytotoxic activity. In addition, the presence of dichloro groups (**14**, **24**, **34** and **44**) on the phenyl ring and dimethyl groups (**13**, **23**, **33** and **43**) on the benzimidazole B ring also caused lower inhibitory activities. In contrast, varying the substitution groups on the A-ring did not impact anti-proliferative activity of these hybrids.

<Table.1>

An *in silico* study of compounds **6-45** was performed in QikProp 3.7 (Schrödinger, 2013) [29] to determine the Lipinski's parameters and the predicted human oral absorption (% ABS) (Table. S1 Supplementary information). According to the 'Lipinski's rule of five', compounds that violate more than one of these rules (no. of violations), may face bioavailability issues. It was observed that all the compounds followed the rule, indicative of their 'drug-like' nature. The predicted percent human oral absorption (% ABS) was 100% indicating complete absorption via the oral route. Moreover, the number of likely metabolic reactions (#metab) was between 0-3, indicating lower propensity for metabolic degradation.

2.3 Morphological analysis

Based on promising cytotoxic activity, the three most potent compounds from this series, compounds **9**, **17** and **28** were used for further mechanistic studies. To determine whether these compounds could cause loss of cell viability, MCF-7 cells were treated with the IC₅₀ concentrations for 48 h and cells were observed under a phase contrast microscope. As shown in Figure 1, as determined by the distinctive morphological features of cells including detachment and cell shrinkage, numbers of viable MCF-7 cells were significantly reduced after treatment with the compounds compared to control, untreated cells.

<Figure 1>

2.4 Colony formation inhibition assay

In order to investigate the long term cytotoxic potential of compounds **9**, **17** and **28**, clonogenic cell survival assay was performed. This assay measures the ability of a single cell to grow into a colony. Because it reflects all modes of cell death or arrest, it is considered a standard for measuring long term cell viability [30]. As shown in Figure 2, exposure of MCF-7 cells to the compounds inhibited the colony formation of MCF-7 cells, with all reducing clonogenic survival by approximately 50%. These results are in agreement with GI₅₀ values, indicating the compounds can effectively suppress growth and proliferation of MCF-7 cells.

<Figure 2>

2.5 *In vitro* cell migration assay

In vitro cell migration assay/wound healing assay was then performed. Migration of cancer cells is a key step in tumor metastasis, and as such, measures of migration capacity correlate with the metastatic potential of cancer cells [31]. Migration was assessed by comparing the number of cells moving into the induced wound area in control and treatment wells. Photographs, taken at different time intervals during the assay (0, 24, 48 and 72 h),

showed the number of invasive breast cancer cells penetrating into the respective wound areas were inhibited after treatment with these compounds (**9**, **17** and **28**) when compared to the control group (Figure 3). These results indicate that the compounds can suppress the migration of MCF-7 cells.

<Figure 3>

2.6 Effect on mRNA expression levels of markers of cell adhesion

Cellular migration and invasiveness are considered to be associated with decrease in the expression of cell adhesion markers, such as E-cadherin and β -catenin [32]. E-cadherin is a trans-membrane protein acting at cell-to-cell junctions where it influences epithelial-mesenchymal transition. Studies have shown down-regulation of the E-cadherin expression in tumors of many organs, including human breast [33]. β -catenin plays an important role in the regulation of the Wnt signaling pathway that is crucial for cell-to-cell interactions in organ development [34]. To evaluate the effect of these compounds (**9**, **17** and **28**) on E-cadherin and β -catenin levels, total RNA was extracted from compound treated MCF-7 cells and relative E-cadherin, β -catenin expression levels were determined by RT-PCR. Results shown in Figure 4 indicate the pyrazolo-benzimidazole hybrids enhanced the expression of E-cadherin (1.6-2.2 times) and β -catenin (1.4-1.6 times) in MCF-7 cancer cells. Compound **9**, which more potently inhibits cell migration, increased expression of E-cadherin 2.2 times. These results suggest the hybrids, at least in part, may inhibit cell migration via up-regulation of cell adhesion markers in MCF-7 cells.

<Figure 4>

2.7 Cell cycle analysis

We then used flow cytometry to explore the effects of the compounds **9**, **17** and **28** on cell cycle. MCF-7 cells were treated with the IC_{50} concentrations of the compounds for 24 h,

fixed with ethanol and stained with propidium iodide. As shown in Figure 5, treatment of MCF-7 cells with compounds **9**, **17** and **28** increased cell cycle arrest at the G1 phase, resulting in cell population increase in the G1 phase (85.2%, 84.7% and 81.3%, respectively) compared to the control cells (72.3%). In line with this finding, the cell populations in S and G2/M phases decreased significantly after treatments. These results demonstrate that, in MCF-7 cells, cell cycle arrest in the G0/G1 phase contributes to the cytotoxicity of the compounds.

<Figure 5>

2.8 Effect of compounds on expression levels of cell cycle check point markers

To study possible mechanisms responsible for arrest at G1 phase, we examined effects on expression levels of some cell cycle specific genes such as cyclins and cyclin dependent kinases (CDKs) by RT-PCR. As shown in Figure 6, treatment with hybrids **9**, **17** and **28** resulted in significantly decreased levels of cyclin D1; a known regulator of G1/S phase transition. There was a small increase of 1.1 to 1.3 times in levels of cyclin B1, whereas the mRNA levels of CDK1 were not significantly changed. Thus, pyrazole-benzimidazole hybrids may decrease levels of cell cycle regulators such as cyclin D1 and CDK2 in MCF-7 cells, leading to the cell cycle arrest and inhibition of cell growth.

<Figure 6>

2.9 Studies of apoptosis

Apoptosis is one of the major pathways that leads to the process of cell death and is associated with chromatin condensation, nuclear shrinking and fragmented nuclei. Tumor cells often have irregular apoptotic pathways and induction of tumor cell apoptosis by natural or synthetic compounds is considered an effective therapy for cancer [35-36]. Moreover,

many pyrazole and benzimidazole derivatives induce apoptosis in different cancer cell lines [37-40]. Hence it was of interest to investigate the effects of the hybrid compounds on apoptosis inducing effect of these hybrids in MCF-7 breast cancer cells.

2.9.1 Hoechst staining

To examine apoptosis inducing effect, MCF-7 cells were treated with the IC_{50} concentration of compounds **9**, **17** and **28** for 24 h and morphological changes studied following Hoechst 33242 staining. As shown in Figure 7, control cells treated with DMSO exhibited uniformly dispersed chromatin, whereas 25-34% of compound treated cells showed typical apoptotic characteristics; including condensation of chromatin (brightly stained cells) and appearance of nuclear fragmentation (arrowheads indicate an apoptotic nucleus). Among them, compound **9** was the most potent in inducing apoptosis (42% apoptotic cells) compared to the other two compounds; that is **17** (26% apoptotic cells) and **28** (32% apoptotic cells). These results demonstrate the hybrids have the potential to induce cellular apoptosis in MCF-7 cells.

<Figure 7>

2.9.2 DNA fragmentation assay

During the apoptotic process, activated nucleases degrade the higher order chromatin structure of DNA into mono and oligo nucleosomal DNA-fragments. Thus, fragmentation of DNA leads to loss of DNA content which results in a characteristic DNA ladder on agarose gel electrophoresis [41]. Thus, DNA fragmentation assay was carried out to further confirm the apoptosis inducing effect of these hybrids. MCF-7 cells were treated with the IC_{50} concentration of compounds **9**, **17** and **28** for 24 h and chromosomal DNA was extracted. Apoptotic degradation of DNA was analyzed by agarose gel electrophoresis. A typical DNA smeared ladder pattern, indicative of fragmentation, was observed in DNA from the pyrazole-

benzimidazole compound treated cells (Figure 8). The observed smear is the result of DNA breaks at multiple positions across the chromosomal DNA. The smear intensity was most obvious in DNA from compound **9** and **28** treated cells, whereas compound **17** resulted in moderate smear formation. In contrast, there was little or no degradation of DNA from control cells. The findings support the concept that compounds **9**, **17** and **28** induce apoptosis in MCF-7 cells.

<Figure 8>

2.9.3 Effect of compounds on mitochondrial membrane potential

The maintenance of mitochondrial membrane potential ($\Delta\Psi_m$) is important for mitochondrial integrity and bioenergetic function. Previous reports suggest loss of mitochondrial membrane potential leads to apoptosis [42]. To examine this possibility, MCF-7 cells were treated with hybrid compounds **9**, **17** and **28** for 24 h and incubated with rhodamine 123. Mitochondria that maintain normal $\Delta\Psi_m$ retain the dye, which gives strong green fluorescence. However, loss of mitochondrial membrane potential leads to depolarization which results in less uptake of rhodamine 123 [43]. As shown in Figure 9a, compared with the untreated control, compounds **9**, **17** and **28** treated cells exhibit a marked reduction in green fluorescence. Quantitation of fluorescence intensity demonstrated the compound treated cells exhibit 44-62% loss of mitochondrial membrane potential compared to the control cells (Figure 9b). Among the hybrids, compound **9** is more potent in inducing mitochondrial depolarization (62%). The results suggest that, in MCF-7 cells, collapse of mitochondrial membrane potential also contributes to the apoptotic effects of the compounds.

<Figure 9>

2.9.4 Effect of compounds on reactive oxygen species (ROS) levels

The increase in levels of the ROS in the mitochondrion may result in oxidative damage to the mitochondrial membrane which leads to apoptosis [44]. Thus, we next examined the effects of these hybrids **9**, **17** and **28** on ROS generation using carboxy-2',7'-dichlorofluorescein diacetate (Carboxy-DCFDA) dye which upon cleavage by intracellular esterases oxidizes to highly fluorescent carboxy-2',7'-dichlorofluorescein (Carboxy-DCF). As shown in Figure 10a, increased ROS production was observed in compound treated cells that showed strong green fluorescence in comparison to the control cells. Quantitative analysis by spectrofluorometry revealed that the ROS levels increased 2-4 times higher when compared to control cells (Figure 10b). This data suggests cytotoxicity of the hybrids is also dependent on ROS production.

<Figure 10>

2.9.5 Effect on the mitochondrial mediated apoptotic pathway

Mitochondria play an important role in cell death signaling pathways such as apoptosis [45]. Mitochondrial dependent apoptotic pathway is regulated by proteins of the Bcl-2 family which are associated with both pro and anti-apoptotic effects in cancer cells. The relative equilibrium of proapoptotic (Bax) and anti-apoptotic (Bcl-2) proteins is critical for maintaining cellular homeostasis. A change in the Bax/Bcl-2 ratio induces the release of cytochrome C from mitochondria into the cytosol leading to activation of caspases and induction of apoptosis [46]. To examine the possible role of mitochondrial mediated apoptotic pathway, the effect of these hybrids (**9**, **17** and **28**) on the expression of levels of Bcl-2, Bax and caspases-3 and 7 was analysed by RT-PCR. As shown in Figure 11, treatment of MCF-7 cells with IC₅₀ concentrations of **9**, **17** and **28** resulted in significantly increased levels of bax (proapoptotic) and reduced levels of Bcl-2 (anti-apoptotic) mRNAs. In addition, as shown in Figure 11, the compounds upregulated expression of the proapoptotic, caspase-3

and 7. Thus, these mitochondrial mediated pathways may also play a role in induction of apoptosis by pyrazole-benzimidazole hybrids.

<Figure 11>

3.0 Conclusion

In summary, we synthesized a series of pyrazole-benzimidazole hybrids (**6-45**) and investigated their antiproliferative activities on four different human tumor cell lines. The results reveal most of the synthesized compounds significantly inhibit cancer cell proliferation; some with superior antiproliferative activity than 5-fluorouracil. Compounds **9**, **17** and **28** showed potent broad spectrum cytotoxic activity against all tested cancer cell lines. Preliminary structure-activity relationships among the series are discussed. The compounds inhibit *in vitro* cell migration, possibly through restoration of E-cadherin, β -catenin expression and also inhibit the long term colonogenic survival of MCF-7 cells. Moreover, the compounds induces G1 phase cell cycle arrest in MCF-7 cells through down regulation of cyclin D1 as well as CDK2. The apoptotic effects of these compounds on MCF-7 cells was studied by Hoechst staining and the DNA ladder assay. Results suggest the compounds induce apoptosis via increased production of ROS, elevation of Bax/Bcl-2 ratio, and activation of caspase-3 and 7. Therefore, these results imply that the pyrazolyl-benzimidazole hybrids represent targets for further optimization and development of anticancer agents to treat breast cancer.

4.0 Experimental Section

4.1 Chemistry

All reagents and solvents used were of commercial grade and were used without any further purification. Progress of reactions was monitored by thin layer chromatography (TLC) performed on silica gel glass plates containing 60 F-254 and visualized on TLC was achieved under UV light or with iodine indicator. Melting points were measured with an Electro-

thermal melting point apparatus, and are uncorrected. ^1H and ^{13}C NMR spectra were recorded on INOVA (400 MHz) or Gemini Varian-VXR-unity (200 MHz) or Bruker UXNMR/XWIN-NMR (300 MHz) instruments. Chemical shifts (δ) are reported in ppm downfield from internal TMS standards. Signal multiplicities are represented by s (singlet), d (doublet), t (triplet), ds (double singlet), dd (double doublet), m (multiplet) and br s (broad singlet). ESI spectra were recorded on Micro mass, Quattro LC using ESI+ software with capillary voltage 3.98 kV and ESI mode positive ion trap detector. IR spectra were recorded on KBr disc using a FTIR Bruker Vector 22 Spectrophotometer.

4.1.1 General procedure for the synthesis of 1, 3 diphenyl pyrazole carboxaldehydes (**4a-d**)

The 1,3-diphenyl-1*H*-pyrazole-4-carboxaldehydes intermediates (**4a-d**) were synthesized based on a literature method as follows: *para*-substituted acetophenones (**1a-d**, 20 mmol) interact with phenylhydrazine (**2**, 25 mmol) in anhydrous ethanol to form acetophenonephenylhydrazones (**3a-d**), which were added to a cold solution of DMF (25 mL) and POCl_3 (5 mL) and stirred at 50–60 °C for 6 h. The resulting mixture was poured into ice-cold water, a saturated solution of sodium bicarbonate was added to neutralize the mixture, extracted with ethyl acetate and then concentrated *in vacuo*. The resulting residue was purified by column chromatography to afford pure 1,3-diphenyl-1*H*-pyrazole-4-carbaldehydes (**4a-d**) in good yields. The spectroscopic data of the obtained aldehyde compounds was in agreement with the reported data [16,47].

4.1.2 General procedure for the synthesis of 2-(1,3-diphenyl-1*H*-pyrazol-4-yl)-1*H*-benzo[*d*]imidazole derivatives (**6-45**)

A solution of $\text{Na}_2\text{S}_2\text{O}_5$ (40 mmol) in H_2O (1.6 mL) was added to a mixture of appropriate 1,3-diphenyl carboxaldehydes (10 mmol) and different substituted *o*-phenylenediamines (10

mmol) in ethanol. After completion of the reaction, the resulting mixture was stirred at reflux for 4 h, the mixture diluted with 50 mL of H₂O and then extracted with ethyl acetate (2X40 mL). The combined extracts were washed with brine, dried over Na₂SO₄, and evaporated *in vacuo*. The crude product was purified by column chromatography using EtOAc/hexane as the eluent to produce pure 2-(1,3-diphenyl-1*H*-pyrazol-4-yl)-1*H*-benzo[*d*]imidazole derivatives in good yields.

4.1.2.1 2-(1,3-diphenyl-1*H*-pyrazol-4-yl)-1*H*-benzo[*d*]imidazole (6)

White solid, yield 77%, Mp: 178-182 °C.; ¹H NMR (300 MHz, CDCl₃+DMSO-*d*6) δ 8.60 (s, 1H), 7.82 – 7.73 (m, 4H), 7.55 (dd, *J* = 6.0, 3.1 Hz, 2H), 7.45 (t, *J* = 7.8 Hz, 2H), 7.39 – 7.27 (m, 4H), 7.20 (dd, *J* = 6.0, 3.2 Hz, 2H). ¹³C NMR (75 MHz, CDCl₃+DMSO-*d*6) δ 150.2, 145.2, 138.7, 138.3, 131.8, 128.8, 128.7, 127.8, 127.7, 126.3, 121.5, 118.2, 114.3, 112.3. MS (ESI): *m/z* 337 [M+H]⁺. HRMS (ESI) calcd for C₂₂H₁₆N₄ [M+H]⁺ 337.14477; found: 337.14257.

4.1.2.2 2-(1,3-diphenyl-1*H*-pyrazol-4-yl)-6-fluoro-1*H*-benzo[*d*]imidazole (7)

Light brown solid, yield 71%, Mp: 189-192 °C.; ¹H NMR (300 MHz, CDCl₃) δ 8.63 (s, 1H), 7.74 (d, *J* = 7.8 Hz, 2H), 7.71-7.62 (m, 2H), 7.59-7.46 (m, 6H), 7.37 (t, *J* = 7.36 Hz, 2H), 7.03 – 6.93 (m, 1H). ¹³C NMR (75 MHz, CDCl₃) δ 161.1, 157.9, 150.7, 146.9, 139.2, 132.3, 129.5, 129.2, 129.1, 128.8, 128.6, 127.4, 119.1, 112.5, 111.0, 110.7.; MS (ESI): *m/z* 355 [M+H]⁺. HRMS (ESI) calcd for C₂₂H₁₆N₄F [M+H]⁺ 355.13535; found: 355.13342.

4.1.2.3 6-chloro-2-(1,3-diphenyl-1*H*-pyrazol-4-yl)-1*H*-benzo[*d*]imidazole (8)

White solid, yield 69%, Mp: 196-198 °C.; ¹H NMR (300 MHz, CDCl₃) δ 8.67 (s, 1H), 7.77 (d, *J* = 7.8 Hz, 2H), 7.68 (dd, *J* = 6.4, 3.0 Hz, 2H), 7.55 – 7.42 (m, 6H), 7.35 (t, *J* = 7.4 Hz, 2H), 7.20 (d, *J* = 7.4 Hz, 1H). ¹³C NMR (75 MHz, DMSO-*d*6) δ 150.1, 147.4, 138.4, 131.4,

128.8, 128.7, 127.7, 127.6, 126.31, 124.6, 118.1, 117.8, 111.5.; MS (ESI): m/z 371 $[M+H]^+$. HRMS (ESI) calcd for $C_{22}H_{16}N_4Cl$ $[M+H]^+$ 371.10580; found: 371.10401.

4.1.2.4 6-bromo-2-(1,3-diphenyl-1H-pyrazol-4-yl)-1H-benzo[d]imidazole (9)

Light brown solid, yield 75%, Mp: 184-187 °C.; 1H NMR (500 MHz, $CDCl_3$) δ 8.67 (s, 1H), 7.78 (d, $J = 7.62$ Hz, 2H), 7.74-7.67 (m, 2H), 7.53 – 7.45 (m, 6H), 7.34 (t, $J = 7.32$ Hz, 2H), 6.87 (dd, $J = 8.69, 2.28$ Hz, 1H). ^{13}C NMR (75 MHz, $CDCl_3$) δ 150.8, 146.6, 139.1, 132.2, 129.5, 129.2, 129.1, 128.9, 128.6, 127.3, 125.8, 119.1, 115.6, 112.3.; MS (ESI): m/z 415 $[M+H]^+$. HRMS (ESI) calcd for $C_{22}H_{16}N_4Br$ $[M+H]^+$ 415.05529; found: 415.05284.

4.1.2.5 2-(1,3-diphenyl-1H-pyrazol-4-yl)-6-methyl-1H-benzo[d]imidazole (10)

Light brown solid, yield 67%, Mp: 175-177 °C.; 1H NMR (300 MHz, $CDCl_3$) δ 8.64 (s, 1H), 7.77 (d, $J = 7.6$ Hz, 2H), 7.69 (d, $J = 3.2$ Hz, 2H), 7.55 – 7.39 (m, 6H), 7.34 (d, $J = 7.4$ Hz, 2H), 7.06 (d, $J = 7.5$ Hz, 1H), 2.45 (s, 3H). ^{13}C NMR (126 MHz, $CDCl_3$) δ 150.7, 145.8, 139.3, 132.2, 129.5, 129.2, 129.0, 128.8, 128.7, 127.4, 127.1, 126.5, 124.1, 119.3, 119.1, 118.8, 113.0, 21.6.; MS (ESI): m/z 351 $[M+H]^+$. HRMS (ESI) calcd for $C_{23}H_{19}N_4$ $[M+H]^+$ 351.16042; found: 351.15831.

4.1.2.6 2-(1,3-diphenyl-1H-pyrazol-4-yl)-6-methoxy-1H-benzo[d]imidazole (11)

Light yellow solid, yield 73%, Mp: 191-193 °C.; 1H NMR (500 MHz, $CDCl_3$) δ 8.67 (s, 1H), 7.80 – 7.75 (m, 2H), 7.70 (ddd, $J = 10.8, 5.8, 3.4$ Hz, 2H), 7.53 – 7.44 (m, 6H), 7.34 (t, $J = 7.4$ Hz, 2H), 6.88 (dd, $J = 8.8, 2.4$ Hz, 1H), 3.83 (s, 3H). ^{13}C NMR (126 MHz, $CDCl_3$) δ 156.5, 150.7, 145.3, 139.3, 132.6, 129.5, 129.3, 129.0, 128.7, 127.9, 127.4, 127.1, 119.3, 119.1, 118.8, 112.9, 112.2, 55.8.; MS (ESI): m/z 367 $[M+H]^+$. HRMS (ESI) calcd for $C_{23}H_{19}ON_4$ $[M+H]^+$ 367.15534; found: 367.15330.

4.1.2.7 2-(1,3-diphenyl-1H-pyrazol-4-yl)-6-(trifluoromethyl)-1H-benzo[d]imidazole (12)

Brown solid, yield 73%, Mp: 201-203 °C.; ¹H NMR (500 MHz, CDCl₃) δ 8.71 (s, 1H), 7.77 (d, *J* = 7.3 Hz, 2H), 7.70-7.64 (m, 2H), 7.55 – 7.43 (m, 7H), 7.35 (t, *J* = 6.9 Hz, 1H), 7.21 (s, 1H). ¹³C NMR (75 MHz, CDCl₃) δ 150.9, 148.0, 139.1, 132.1, 129.6, 129.3, 129.1, 128.6, 127.4, 126.5, 125.2, 124.8, 119.7, 119.2, 112.1.; MS (ESI): *m/z* 405 [M+H]⁺. HRMS (ESI) calcd for C₂₃H₁₆N₄F₃ [M+H]⁺ 405.13216; found: 405.12978.

4.1.2.8 2-(1,3-diphenyl-1H-pyrazol-4-yl)-5,6-dimethyl-1H-benzo[d]imidazole (13)

Light brown solid, yield 73%, Mp: 184-186 °C.; ¹H NMR (300 MHz, CDCl₃) δ 8.55 (s, 1H), 7.78 – 7.59 (m, 5H), 7.46-7.35 (m, 3H), 7.34 (s, 2H), 7.17 (t, *J* = 8.6 Hz, 2H), 2.35 (s, 6H). MS (ESI): *m/z* 365 [M+H]⁺, HRMS (ESI) calcd for C₂₄H₂₁N₄ [M+H]⁺ 365.17612; found: 365.17662.

4.1.2.9 5,6-dichloro-2-(1,3-diphenyl-1H-pyrazol-4-yl)-1H-benzo[d]imidazole (14)

Light brown solid, yield 66%, Mp: 213-215 °C.; ¹H NMR (300 MHz, DMSO-*d*₆) δ 8.90 (s, 1H), 7.85 – 7.72 (m, 5H), 7.68 (s, 2H), 7.46 (t, *J* = 7.8 Hz, 2H), 7.31-7.38 (m, 3H); ¹³C NMR (75 MHz, DMSO) δ 150.1, 147.4, 138.4, 131.4, 128.8, 128.7, 127.7, 127.6, 126.3, 124.6, 118.1, 111.5.; MS (ESI): *m/z* 405 [M+H]⁺. HRMS (ESI) calcd for C₂₂H₁₅N₄Cl₂ [M+H]⁺ 405.06683; found: 405.06473.

4.1.2.10 2-(1,3-diphenyl-1H-pyrazol-4-yl)-1H-naphtho[2,3-*d*]imidazole (15)

Light brown solid, yield 76%, Mp: 197-199 °C.; ¹H NMR (300 MHz, CDCl₃) δ 8.61 (s, 1H), 7.92-7.83 (m, 4H), 7.81 – 7.70 (m, 4H), 7.48 (d, *J* = 7.7 Hz, 2H), 7.39 (d, *J* = 7.1 Hz, 2H), 7.34 (s, 2H), 7.20 (t, *J* = 8.5 Hz, 2H). ¹³C NMR (75 MHz, CDCl₃) δ 151.2, 149.7, 139.2,

132.3, 130.6, 129.6, 129.4, 129.3, 129.1, 128.9, 127.8, 127.3, 123.9, 119.2, 112.7.; MS (ESI): m/z 387 $[M+H]^+$. HRMS (ESI) calcd for $C_{26}H_{19}N_4$ $[M+H]^+$ 387.16081; found: 387.16105.

4.1.2.11 2-(3-(4-fluorophenyl)-1-phenyl-1*H*-pyrazol-4-yl)-1*H*-benzo[*d*]imidazole (16)

White solid, yield 73%, Mp: 179-182 °C.; 1H NMR (300 MHz, $CDCl_3$) δ 8.71 (s, 1H), 7.89-7.79 (m, 3H), 7.68-7.44 (m, 5H), 7.36 (s, 2H), 7.22-7.13 (m, 3H). ^{13}C NMR (75 MHz, $CDCl_3$ +DMSO-*d*6) δ 163.7, 160.4, 149.2, 145.1, 138.6, 129.6, 129.5, 128.8, 128.7, 127.9, 127.9, 126.2, 121.3, 118.1, 114.5, 114.2, 112.2.; MS (ESI): m/z 355 $[M+H]^+$. HRMS (ESI) calcd for $C_{22}H_{16}FN_4$ $[M+H]^+$ 355.13496; found: 355.13483.

4.1.2.12 5-fluoro-2-(3-(4-fluorophenyl)-1-phenyl-1*H*-pyrazol-4-yl)-1*H*-benzo[*d*]imidazole (17)

Light brown solid, yield 79%, Mp: 189-192 °C.; 1H NMR (500 MHz, $CDCl_3$) δ 8.54 (s, 1H), 7.69 (d, $J = 7.4$ Hz, 2H), 7.66 – 7.60 (m, 2H), 7.52-7.41 (m, 4H), 7.33 (t, $J = 7.4$ Hz, 1H), 7.12 (t, $J = 8.6$ Hz, 2H), 7.00 (td, $J = 9.2, 2.4$ Hz, 1H). ^{13}C NMR (126 MHz, $CDCl_3$) δ 164.4, 162.3, 160.6, 158.7, 149.7, 139.2, 130.5, 129.6, 128.9, 128.4, 127.4, 119.2, 116.3, 116.1, 112.5, 111.2, 111.0.; MS (ESI): m/z 373 $[M+H]^+$. HRMS (ESI) calcd for $C_{22}H_{15}F_2N_4$ $[M+H]^+$ 373.12647; found: 373.12513.

4.1.2.13 5-chloro-2-(3-(4-fluorophenyl)-1-phenyl-1*H*-pyrazol-4-yl)-1*H*-benzo[*d*]imidazole (18)

White solid, yield 77%, Mp: 198-200 °C.; 1H NMR (300 MHz, $CDCl_3$) δ 8.62 (s, 1H), 7.75 (d, $J = 7.7$ Hz, 2H), 7.70 – 7.62 (m, 2H), 7.54 – 7.45 (m, 3H), 7.38 -7.31 (m, 2H), 7.23-7.19 (m, 2H), 6.90 (dt, $J = 16.4, 8.5$ Hz, 1H); ^{13}C NMR (75 MHz, $CDCl_3$) δ 163.5, 160.2, 149.1, 145.4, 138.0, 137.2, 135.0, 129.4, 128.6, 127.1, 126.3, 122.3, 118.0, 114.5, 113.6, 109.7; MS

(ESI): m/z 389 $[M+H]^+$. HRMS (ESI) calcd for $C_{22}H_{15}ClFN_4$ $[M+H]^+$ 389.09655; found: 389.09677.

4.1.2.14 5-bromo-2-(3-(4-fluorophenyl)-1-phenyl-1*H*-pyrazol-4-yl)-1*H*-benzo[*d*]imidazole (19)

Light brown solid, yield 71%, Mp: 207-209 °C.; 1H NMR (500 MHz, $CDCl_3$) δ 8.67 (s, 1H), 7.96 – 7.86 (m, 2H), 7.82 (d, $J = 7.4$ Hz, 2H), 7.75 – 7.61 (m, 1H), 7.54-7.46 (m, 3H), 7.35 (t, $J = 6.5$ Hz, 1H), 7.28 (dd, $J = 8.3, 1.4$ Hz, 1H), 7.13 – 7.00 (m, 2H). ^{13}C NMR (75 MHz, $CDCl_3$) δ 163.5, 160.3, 149.1, 146.1, 138.4, 129.6, 129.5, 128.7, 127.7, 126.1, 124.1, 117.9, 114.3, 114.1, 113.9, 111.6.; MS (ESI): m/z 433 $[M+H]^+$. HRMS (ESI) calcd for $C_{22}H_{25}BrFN_4$ $[M+H]^+$ 433.04641; found: 433.04597.

4.1.2.15 2-(3-(4-fluorophenyl)-1-phenyl-1*H*-pyrazol-4-yl)-5-methoxy-1*H*-benzo[*d*]imidazole (20)

Light yellow solid, yield 77%, Mp: 213-215 °C.; 1H NMR (300 MHz, $CDCl_3$) δ 8.58 (s, 1H), 7.78 – 7.62 (m, 4H), 7.47 (t, $J = 7.8$ Hz, 2H), 7.34 (t, $J = 7.4$ Hz, 1H), 7.28 (s, 1H), 7.16 (t, $J = 8.6$ Hz, 2H), 7.01 (s, 1H), 6.91 (dd, $J = 8.8, 2.4$ Hz, 1H), 3.85 (s, 3H). ^{13}C NMR (75 MHz, $CDCl_3$) δ 164.8, 161.4, 156.6, 149.6, 139.1, 130.5, 130.4, 129.5, 128.71, 128.5, 127.1, 119.0, 116.1, 115.8, 112.8, 112.3, 55.7.; MS (ESI): m/z 385 $[M+H]^+$. HRMS (ESI) calcd for $C_{23}H_{18}FN_4O$ $[M+H]^+$ 385.14507; found: 385.14507.

4.1.2.16 2-(3-(4-fluorophenyl)-1-phenyl-1*H*-pyrazol-4-yl)-5-methyl-1*H*-benzo[*d*]imidazole (21)

Light brown solid, yield 65%, Mp: 185-187 °C.; 1H NMR (500 MHz, $CDCl_3$) δ 8.35 (s, 1H), 7.58 – 7.49 (m, 4H), 7.40 (d, $J = 7.3$ Hz, 1H), 7.34 (t, $J = 7.4$ Hz, 2H), 7.28 – 7.22 (m, 2H), 7.06 (dd, $J = 8.2, 1.0$ Hz, 1H), 6.98 (t, $J = 8.69$ Hz, 2H), 2.44 (s, 3H). ^{13}C NMR (126 MHz,

CDCl₃) δ 164.1, 162.1, 149.8, 145.23, 139.2, 132.7, 130.4, 130.3, 129.5, 128.8, 128.4, 127.1, 124.2, 119.0, 115.9, 115.8, 112.7, 21.6.; MS (ESI): m/z 369 [M+H]⁺. HRMS (ESI) calcd for C₂₃H₁₈FN₄ [M+H]⁺ 369.15027; found: 369.15027.

4.1.2.17 2-(3-(4-fluorophenyl)-1-phenyl-1*H*-pyrazol-4-yl)-5-(trifluoromethyl)-1*H*-benzo[*d*]imidazole (22)

Light brown solid, yield 70%, Mp: 217-219 °C.; ¹H NMR (500 MHz, CDCl₃) δ 8.78 (s, 1H), 7.98 – 7.91 (m, 2H), 7.88-7.82 (m, 3H), 7.72-7.67 (m, 1H), 7.49 (t, J = 7.47 Hz, 2H), 7.46 (dd, J = 8.4, 1.2 Hz, 1H), 7.35 (t, J = 7.47 Hz, 1H), 7.10 (t, J = 8.71 Hz, 2H). ¹³C NMR (75 MHz, CDCl₃) δ 163.6, 160.3, 149.3, 147.0, 138.8, 138.2, 137.1, 129.49, 128.7, 127.3, 126.3, 125.7, 123.6, 123.2, 122.1, 118.5, 114.2, 111.9, 110.3.; MS (ESI): m/z 423 [M+H]⁺. HRMS (ESI) calcd for C₂₃H₁₅F₄N₄ [M+H]⁺ 423.12182; found: 423.12187.

4.1.2.18 2-(3-(4-fluorophenyl)-1-phenyl-1*H*-pyrazol-4-yl)-5,6-dimethyl-1*H*-benzo[*d*]imidazole (23)

Light brown solid, yield 73%, Mp: 187-189 °C.; ¹H NMR (300 MHz, CDCl₃) δ 8.56 (s, 1H), 7.78 – 7.59 (m, 4H), 7.46 (t, J = 7.8 Hz, 2H), 7.34 (t, J = 7.4 Hz, 2H), 7.25 (s, 1H), 7.14 (t, J = 8.6 Hz, 2H), 2.38 (s, 6H). ¹³C NMR (75 MHz, CDCl₃) δ 164.7, 161.4, 149.8, 144.7, 139.1, 131.7, 130.3, 130.2, 129.4, 128.6, 128.4, 127.0, 118.9, 115.8, 115.5, 112.7, 20.3.; MS (ESI): m/z 383 [M+H]⁺. HRMS (ESI) calcd for C₂₄H₂₀FN₄ [M+H]⁺ 383.16617; found: 383.16614.

4.1.2.19 5,6-dichloro-2-(3-(4-fluorophenyl)-1-phenyl-1*H*-pyrazol-4-yl)-1*H*-benzo[*d*]imidazole (24)

Light brown solid, yield 79%, Mp: 203-205 °C.; ¹H NMR (300 MHz, CDCl₃) δ 8.74 – 8.60 (m, 1H), 7.93-7.82 (m, 4H), 7.62 (s, 2H), 7.47 (t, J = 7.0 Hz, 2H), 7.39 – 7.27 (m, 1H), 7.06 (t, J = 7.6 Hz, 2H). ¹³C NMR (126 MHz, CDCl₃) δ 163.9, 161.9, 150.0, 148.0, 139.1, 130.3,

130.2, 129.5, 129.3, 128.2, 127.1, 125.9, 118.8, 115.3, 112.0, 30.8, 29.5.; MS (ESI): m/z 423 [M+H]⁺. HRMS (ESI) calcd for C₂₂H₁₄ClFN₄ [M+H]⁺ 423.05680; found: 423.05699.

4.1.2.20 2-(3-(4-fluorophenyl)-1-phenyl-1H-pyrazol-4-yl)-1H-naphtho[2,3-d]imidazole (25)

Brown solid, yield 70%, Mp: 193-195 °C.; ¹H NMR (500 MHz, CDCl₃) δ 8.74 (s, 1H), 7.89-7.84 (m, 3H), 7.78 – 7.69 (m, 4H), 7.47 (t, J = 7.8 Hz, 2H), 7.40 (dq, J = 6.2, 3.1 Hz, 2H), 7.35 (t, J = 7.1 Hz, 1H), 7.25 (s, 1H), 7.20 (t, J = 8.5 Hz, 2H). ¹³C NMR (126 MHz, CDCl₃) δ 163.7, 161.8, 150.2, 150.0, 139.1, 130.5, 130.4, 130.1, 129.7, 129.4, 128.4, 127.6, 127.0, 123.4, 118.7, 115.1, 114.9, 112.6.; MS (ESI): m/z 405 [M+H]⁺. HRMS (ESI) calcd for C₂₆H₁₈FN₄ [M+H]⁺ 405.15063; found: 405.15071.

4.1.2.21 2-(3-(4-chlorophenyl)-1-phenyl-1H-pyrazol-4-yl)-1H-benzo[d]imidazole (26)

Light brown solid, yield 73%, Mp: 177-179 °C.; ¹H NMR (500 MHz, CDCl₃) δ 8.55 (s, 1H), 7.66 (d, J = 7.7 Hz, 2H), 7.59 (d, J = 8.54 Hz, 2H), 7.56-7.52 (m, 2H), 7.42 (t, J = 7.9 Hz, 2H), 7.36 (d, J = 8.4 Hz, 2H), 7.31 (t, J = 7.47 Hz, 1H), 7.28 – 7.23 (m, 2H). ¹³C NMR (126 MHz, CDCl₃) δ 149.6, 145.3, 139.1, 135.1, 130.7, 129.8, 129.5, 129.1, 127.3, 123.0, 119.1, 112.3.; MS (ESI): m/z 371 [M+H]⁺; HRMS (ESI) calcd for C₂₂H₁₆ClN₄ [M+H]⁺ 371.10567; found: 371.10580.

4.1.2.22 2-(3-(4-chlorophenyl)-1-phenyl-1H-pyrazol-4-yl)-5-fluoro-1H-benzo[d]imidazole (27)

Light brown solid, yield 69%, Mp: 188-191 °C.; ¹H NMR (300 MHz, CDCl₃) δ 8.69 (s, 1H), 7.91-7.80 (m, 4H), 7.60 (s, 1H), 7.52-7.46 (m, 3H), 7.36 (d, J = 7.55 Hz, 2H), 7.25 (d, J = 9.1 Hz, 1H), 6.97 (t, J = 9.2 Hz, 1H). ¹³C NMR (75 MHz, CDCl₃) δ 149.7, 147.8, 139.08, 134.2,

130.7, 129.7, 129.5, 129.4, 128.3, 127.1, 125.4, 118.8, 112.2. MS (ESI): m/z 389 $[M+H]^+$; HRMS (ESI) calcd for $C_{22}H_{15}ClFN_4$ $[M+H]^+$ 389.09671; found: 389.09636.

4.1.2.23 5-chloro-2-(3-(4-chlorophenyl)-1-phenyl-1*H*-pyrazol-4-yl)-1*H*-benzo[*d*]imidazole (28)

Light brown solid, yield 71%, Mp: 208-210 °C.; 1H NMR (300 MHz, $CDCl_3$) δ 8.78 (d, $J = 8.7$ Hz, 1H), 7.90 (dd, $J = 16.6, 8.0$ Hz, 4H), 7.72 (d, $J = 11.1$ Hz, 1H), 7.65 – 7.48 (m, 4H), 7.41 (d, $J = 7.9$ Hz, 2H), 7.21 (d, $J = 8.3$ Hz, 1H). MS (ESI): m/z 405 $[M+H]^+$; HRMS (ESI) calcd for $C_{22}H_{15}Cl_2N_4$ $[M+H]^+$ 405.06729; found: 405.06685.

4.1.2.24 5-bromo-2-(3-(4-chlorophenyl)-1-phenyl-1*H*-pyrazol-4-yl)-1*H*-benzo[*d*]imidazole (29)

Light brown solid, yield 76%, Mp: 202-204 °C.; 1H NMR (300 MHz, $CDCl_3$) δ 8.87 (s, 1H), 7.96 (d, $J = 8.5$ Hz, 2H), 7.93 – 7.83 (m, 3H), 7.54 (t, $J = 7.8$ Hz, 2H), 7.44-7.34 (m, 4H), 7.29 (d, $J = 8.4$ Hz, 1H). ^{13}C NMR (75 MHz, $CDCl_3$) δ 147.9, 145.2, 137.5, 132.1, 129.5, 128.5, 128.0, 126.5, 125.4, 123.2, 117.1, 111.0.; MS (ESI): m/z 449 $[M+H]^+$. HRMS (ESI) calcd for $C_{22}H_{15}BrClN_4$ $[M+H]^+$ 449.01686; found: 449.01589.

4.1.2.25 2-(3-(4-chlorophenyl)-1-phenyl-1*H*-pyrazol-4-yl)-5-methoxy-1*H*-benzo[*d*]imidazole (30)

Light brown solid, yield 75%, Mp: 191-193 °C.; 1H NMR (500 MHz, $CDCl_3$) δ 8.55 (s, 1H), 7.70 (d, $J = 7.7$ Hz, 2H), 7.61 (d, $J = 8.54$ Hz, 2H), 7.48-7.43 (m, 3H), 7.41 (d, $J = 8.39$ Hz, 2H), 7.38-7.29 (m, 2H), 6.90 (dd, $J = 8.8, 2.4$ Hz, 1H), 3.84 (s, 3H). ^{13}C NMR (75 MHz, $CDCl_3$) δ 155.3, 148.7, 144.4, 138.5, 133.2, 130.3, 128.9, 128.4, 127.5, 126.2, 118.0, 112.3, 110.8, 96.5, 54.9.; MS (ESI): m/z 401 $[M+H]^+$. HRMS (ESI) calcd for $C_{23}H_{18}ClN_4O$ $[M+H]^+$ 401.11680; found: 401.11694.

4.1.2.26 2-(3-(4-chlorophenyl)-1-phenyl-1H-pyrazol-4-yl)-5-(trifluoromethyl)-1H-benzo[d]imidazole (31)

Light brown solid, yield 71%, Mp: 216-218 °C.; ¹H NMR (500 MHz, CDCl₃) δ 8.55 (s, 1H), 7.71 (d, *J* = 8.39 Hz, 2H), 7.60 – 7.55 (m, 3H), 7.51 (d, *J* = 7.78 Hz, 2H), 7.45 (t, *J* = 8.39 Hz, 2H), 7.42 – 7.37 (m, 2H), 7.34 (dt, *J* = 7.47, 1.52 Hz, 1H). ¹³C NMR (75 MHz, CDCl₃) δ 149.8, 148.0, 139.0, 134.1, 130.7, 129.7, 129.6, 129.4, 128.3, 127.1, 118.8, 112.3.; MS (ESI): *m/z* 439 [M+H]⁺. HRMS (ESI) calcd for C₂₃H₁₅ClF₃N₄ [M+H]⁺ 439.09211; found: 439.09206.

4.1.2.27 2-(3-(4-chlorophenyl)-1-phenyl-1H-pyrazol-4-yl)-5-methyl-1H-benzo[d]imidazole (32)

Light brown solid, yield 67%, Mp: 176-178 °C.; ¹H NMR (300 MHz, CDCl₃) δ 8.48 (s, 1H), 7.63 (d, *J* = 7.8 Hz, 2H), 7.56 (d, *J* = 8.4 Hz, 2H), 7.45-7.28 (m, 7H), 7.08 (d, *J* = 8.12 Hz, 1H), 2.46 (s, 3H). ¹³C NMR (75 MHz, CDCl₃) δ 148.3, 144.1, 138.0, 132.6, 130.4, 130.0, 128.6, 128.3, 127.0, 125.7, 122.3, 117.5, 111.9, 20.4.; MS (ESI): *m/z* 385 [M+H]⁺. HRMS (ESI) calcd for C₂₃H₁₇ClN₄ [M+H]⁺ 385.12185; found: 385.12093.

4.1.2.28 2-(3-(4-chlorophenyl)-1-phenyl-1H-pyrazol-4-yl)-5,6-dimethyl-1H-benzo[d]imidazole (33)

Light brown solid, yield 71%, Mp: 182-184 °C.; ¹H NMR (500 MHz, CDCl₃) δ 8.41 (s, 1H), 7.56 (d, *J* = 8.08 Hz, 2H), 7.48 (t, *J* = 8.39 Hz, 2H), 7.36-7.30 (m, 3H), 7.26-7.21 (m, 4H), 2.34 (s, 6H). ¹³C NMR (75 MHz, CDCl₃) δ 149.7, 143.3, 134.4, 133.1, 130.0, 129.5, 129.2, 128.7, 128.4, 127.9, 127.3, 126.9, 126.5, 119.2, 118.8, 114.3, 110.7, 109.3, 20.3.; MS (ESI): *m/z* 399 [M+H]⁺.; HRMS (ESI) calcd for C₂₄H₂₀ClN₄ [M+H]⁺ 399.13745; found: 399.13714.

4.1.2.29 5,6-dichloro-2-(3-(4-chlorophenyl)-1-phenyl-1H-pyrazol-4-yl)-1H-benzo[d]imidazole (34)

Brown solid, yield 72%, mp: 195-197 °C; ¹H NMR (300 MHz, CDCl₃) δ 8.39 (s, 1H), 7.92-7.80 (m, 4H), 7.65 (s, 1H), 7.52 (t, *J* = 7.74 Hz, 2H) 7.4 – 7.32 (m, 4H). MS (ESI): *m/z* 439 [M+H]⁺; HRMS (ESI) calcd for C₂₂H₁₄Cl₃N₄ [M+H]⁺ 439.0284; found: 439.0282.

4.1.2.30 2-(3-(4-chlorophenyl)-1-phenyl-1H-pyrazol-4-yl)-1H-naphtho [2,3-d]imidazole (35)

Light brown solid, yield 75%, Mp: 184-186 °C.; ¹H NMR (500 MHz, CDCl₃) δ 8.65 (s, 1H), 7.92-7.84 (m, 3H), 7.70 – 7.59 (m, 4H), 7.45 – 7.37 (m, 6H), 7.32 (t, *J* = 7.4 Hz, 1H), 7.25 (s, 1H). ¹³C NMR (75 MHz, CDCl₃) δ 150.0, 149.8, 139.1, 134.3, 130.8, 130.3, 129.9, 129.4, 128.4, 127.7, 127.1, 123.5, 118.8, 112.7.; MS (ESI): *m/z* 421 [M+H]⁺; HRMS (ESI) calcd for C₂₆H₁₈ClN₄ [M+H]⁺ 421.12184; found: 421.12176.

4.1.2.31 2-(3-(4-methoxyphenyl)-1-phenyl-1H-pyrazol-4-yl)-1H-benzo[d]imidazole (36)

Light yellow solid, yield 78%, Mp: 179-182 °C.; ¹H NMR (300 MHz, CDCl₃+DMSO-*d*6) δ 8.69 (s, 1H), 7.81 (dd, *J* = 8.2, 3.4 Hz, 4H), 7.56 (dd, *J* = 5.9, 3.1 Hz, 2H), 7.48 (t, *J* = 7.9 Hz, 2H), 7.32 (t, *J* = 7.4 Hz, 1H), 7.23 – 7.14 (m, 2H), 6.89 (d, *J* = 8.8 Hz, 2H), 3.77 (s, 3H). ¹³C NMR (75 MHz, CDCl₃+DMSO-*d*6) δ 158.6, 149.5, 145.0, 138.2, 128.5, 128.3, 128.2, 125.6, 123.8, 120.8, 117.5, 112.5, 111.5, 54.0.; MS (ESI): *m/z* 367 [M+H]⁺. HRMS (ESI) calcd for C₂₃H₁₉ON₄ [M+H]⁺ 367.15534; found: 367.15330.

4.1.2.32 6-fluoro-2-(3-(4-methoxyphenyl)-1-phenyl-1H-pyrazol-4-yl)-1H-benzo[d]imidazole (37)

Light brown solid, yield 71%, Mp: 176-179 °C.; ¹H NMR (500 MHz, CDCl₃) δ 8.64 (s, 1H), 7.73 (d, *J* = 7.9 Hz, 2H), 7.63 (d, *J* = 8.54 Hz, 2H), 7.47-7.43 (m, 4H), 7.32 (t, *J* = 7.4 Hz, 1H), 7.02-6.95 (m, 3H), 3.85 (s, 3H); ¹³C NMR (126 MHz, CDCl₃) δ 160.2, 159.9, 158.3, 150.7, 147.2, 139.3, 129.6, 129.4, 128.9, 126.8, 124.6, 118.8, 113.9, 112.3, 110.4, 110.2, 55.1.; MS (ESI): *m/z* 385 [M+H]⁺; HRMS (ESI) calcd for C₂₃H₁₈ON₄F [M+H]⁺ 385.1464; found: 385.1506.

4.1.2.33 6-chloro-2-(3-(4-methoxyphenyl)-1-phenyl-1*H*-pyrazol-4-yl)-1*H*-benzo[*d*]imidazole (38)

Light brown solid, yield 75%, Mp: 188-190 °C; ¹H NMR (300 MHz, CDCl₃) δ 8.47 (s, 1H), 7.62 (d, *J* = 7.74 Hz, 2H), 7.50-7.39 (m, 4H), 7.36-7.24 (m, 3H), 7.18 (d, *J* = 7.6 Hz, 1H), 6.89 (d, *J* = 8.5 Hz, 2H), 3.78 (s, 3H). ¹³C NMR (75 MHz, CDCl₃) δ 160.1, 150.7, 147.0, 139.0, 129.7, 129.4, 128.7, 128.1, 127.1, 124.2, 123.1, 118.9, 114.2, 112.0, 55.2.; MS (ESI): *m/z* 401 [M+H]⁺. HRMS (ESI) calcd for C₂₃H₁₈ON₄Cl [M+H]⁺ 401.11637; found: 401.11412.

4.1.2.34 6-bromo-2-(3-(4-methoxyphenyl)-1-phenyl-1*H*-pyrazol-4-yl)-1*H*-benzo[*d*]imidazole (39)

Light brown solid, yield 78%, Mp: 194-196 °C.; ¹H NMR (300 MHz, CDCl₃) δ 8.67 (s, 1H), 7.81 (d, *J* = 8.1 Hz, 2H), 7.68 (d, *J* = 8.3 Hz, 2H), 7.57-7.42 (m, 4H), 7.36 (t, *J* = 7.2 Hz, 1H), 7.11-7.02 (m, 3H), 3.87 (s, 3H); ¹³C NMR (75 MHz, CDCl₃) δ 160.2, 151.1, 146.8, 139.5, 129.8, 129.5, 128.8, 127.1, 125.6, 124.3, 119.0, 115.5, 114.3, 112.0, 55.2.; MS (ESI): *m/z* 445 [M+H]⁺; HRMS (ESI) calcd for C₂₃H₁₈BrN₄O [M+H]⁺ 445.06593; found: 445.06581.

4.1.2.35 6-methoxy-2-(3-(4-methoxyphenyl)-1-phenyl-1*H*-pyrazol-4-yl)-1*H*-benzo[*d*]imidazole (40)

Light yellow solid, yield 74%, Mp: 177-179 °C.; ¹H NMR (300 MHz, CDCl₃) δ 8.69 (s, 1H), 7.90 – 7.66 (m, 4H), 7.59-7.48 (m, 3H), 7.45 (t, *J* = 7.6 Hz, 2H), 7.33 (d, *J* = 7.2 Hz, 1H), 6.89 (d, *J* = 8.5 Hz, 2H), 3.82 (s, 3H), 3.78 (s, 3H). ¹³C NMR (75 MHz, CDCl₃) δ 162.0, 160.0, 158.7, 138.3, 136.1, 130.3, 129.1, 128.6, 125.7, 123.8, 118.1, 115.9, 112.5, 105.8, 101.6, 55.4, 55.3.; MS (ESI): *m/z* 397 [M+H]⁺. HRMS (ESI) calcd for C₂₄H₂₁O₂N₄ [M+H]⁺ 397.16590; found: 397.16368.

4.1.2.36 2-(3-(4-methoxyphenyl)-1-phenyl-1*H*-pyrazol-4-yl)-5-(trifluoromethyl)-1*H*-benzo[*d*]imidazole (41)

Brown solid, yield 71%, Mp: 190-192 °C.; ¹H NMR (300 MHz, CDCl₃) δ 8.63 (s, 1H), 7.72 (d, *J* = 7.7 Hz, 2H), 7.57 (d, *J* = 8.6 Hz, 2H), 7.55-7.46 (m, 4H), 7.33 (t, *J* = 7.3 Hz, 1H), 7.11 (d, *J* = 7.2 Hz, 1H), 6.98 (d, *J* = 8.6 Hz, 2H), 3.84 (s, 3H). ¹³C NMR (75 MHz, CDCl₃) δ 160.0, 150.8, 147.9, 138.8, 129.4, 127.2, 123.8, 119.9, 118.9, 114.1, 110.6, 54.9. MS (ESI): *m/z* 435 [M+H]⁺. HRMS (ESI) calcd for C₂₄H₁₈ON₄F₃ [M+H]⁺ 435.14272; found: 435.13945.

4.1.2.37 2-(3-(4-methoxyphenyl)-1-phenyl-1*H*-pyrazol-4-yl)-6-methyl-1*H*-benzo[*d*]imidazole (42)

Light brown solid, yield 68%, Mp: 175-177 °C.; ¹H NMR (500 MHz, CDCl₃) δ 8.53 (s, 1H), 7.66 (d, *J* = 7.8 Hz, 2H), 7.55 (d, *J* = 8.7 Hz, 2H), 7.40 (t, *J* = 7.9 Hz, 2H), 7.30 (dd, *J* = 12.4, 5.0 Hz, 4H), 6.94 – 6.90 (m, 2H), 3.80 (s, 3H), 2.33 (s, 3H). ¹³C NMR (75 MHz, CDCl₃) δ 160.2, 150.6, 145.5, 139.3, 132.5, 130.0, 129.5, 129.2, 128.8, 128.6, 127.0, 126.4, 124.7, 124.1, 119.0, 118.7, 114.4, 114.0, 112.8, 110.1, 55.3, 21.6.; MS (ESI): *m/z* 381 [M+H]⁺. HRMS (ESI) calcd for C₂₄H₂₁ON₄ [M+H]⁺ 381.17099; found: 381.16916.

4.1.2.38 2-(3-(4-methoxyphenyl)-1-phenyl-1*H*-pyrazol-4-yl)-5,6-dimethyl-1*H*-benzo[*d*]imidazole (43)

Light brown solid, yield 67%, Mp: 187-189 °C.; ¹H NMR (300 MHz, CDCl₃) δ 8.93 (s, 1H), 7.65 (d, *J* = 7.5 Hz, 2H), 7.45 – 7.30 (m, 4H), 7.26 – 7.11 (m, 2H), 6.78 (d, *J* = 8.6 Hz, 2H), 6.68-6.73 (m, 1H), 3.71 (s, 3H), 2.33 (s, 6H); ¹³C NMR (75 MHz, CDCl₃) δ 160.2, 150.5, 145.0, 139.4, 131.5, 130.0, 129.5, 129.2, 128.7, 128.5, 126.9, 126.4, 124.7, 119.8, 119.1, 118.7, 114.3, 112.9, 110.8, 55.3, 20.3.; MS (ESI): *m/z* 395 [M+H]⁺. HRMS (ESI) calcd for C₂₅H₂₃ON₄ [M+H]⁺ 395.18664; found: 395.18477.

4.1.2.39 5,6-dichloro-2-(3-(4-methoxyphenyl)-1-phenyl-1*H*-pyrazol-4-yl)-1*H*-benzo[*d*]imidazole (44)

Light brown solid, yield 79%, Mp: 208-210 °C.; ¹H NMR (500 MHz, CDCl₃) δ 8.73 (s, 1H), 7.82 (d, *J* = 7.7 Hz, 2H), 7.78 (d, *J* = 8.6 Hz, 2H), 7.66 (s, 2H), 7.49 (dd, *J* = 10.7, 5.1 Hz, 2H), 7.33 (t, *J* = 7.4 Hz, 1H), 6.95 – 6.86 (m, 2H), 3.81 (s, 3H). ¹³C NMR (75 MHz, CDCl₃) δ 159.3, 150.3, 148.0, 138.8, 129.2, 129.1, 126.5, 124.7, 124.2, 118.2, 113.2, 111.5, 54.7.; MS (ESI): *m/z* 435 [M+H]⁺. HRMS (ESI) calcd for C₂₃H₁₇ON₄Cl₂ [M+H]⁺ 435.07739; found: 435.07502.

4.1.2.40 2-(3-(4-methoxyphenyl)-1-phenyl-1*H*-pyrazol-4-yl)-1*H*-naphtho[2,3-*d*]imidazole (45)

Light brown solid, yield 76%, Mp: 211-213 °C.; ¹H NMR (500 MHz, CDCl₃) δ 8.75 (s, 1H), 7.89-7.81 (s, 4H), 7.74 (d, *J* = 7.8 Hz, 2H), 7.64 (d, *J* = 8.6 Hz, 2H), 7.45 (t, *J* = 7.9 Hz, 2H), 7.39 (dq, *J* = 6.5, 3.3 Hz, 2H), 7.32 (t, *J* = 7.4 Hz, 1H), 7.01 (d, *J* = 8.6 Hz, 2H), 3.83 (s, 3H). ¹³C NMR (75 MHz, CDCl₃) δ 149.2, 147.2, 142.9, 139.0, 138.4, 130.9, 127.2, 123.5, 121.2,

114.1, 110.3, 108.5, 105.7, 101.8, 101.6, 55.4.; MS (ESI): m/z 417 $[M+H]^+$; HRMS (ESI) calcd for $C_{27}H_{21}N_4O$ $[M+H]^+$ 417.17142; found: 417.17126.

4.2 Cell Culture

MCF-7 (breast), HeLa (cervical) and A549 (lung) cancer cells were purchased from ATCC (Manassas, VA). The A549 cells were grown in RPMI 1640 medium (GIBCO-Invitrogen, NY) with 10% fetal bovine serum (FBS) and supplemented with glutamine (2 mmol/L), penicillin G (100 μ g/mL), and streptomycin (100 μ g/mL) at 37 °C under 5% CO_2 . MCF-7 and HeLa cells were maintained in Dulbecco's modified Eagle's medium (DMEM) containing 10% fetal bovine serum (FBS), 1% penicillin/streptomycin at 37 °C under 5% CO_2 . The culture medium was replaced with fresh medium every two days. After reaching 80-90% confluence, cells were treated with 0.25% trypsin-EDTA for further passages. Cells were used at passages 4-8 for all the experiments.

4.2.1 MTT assay

The *in vitro* cytotoxicity of test compounds on MCF-7, HeLa and A549 cells was performed using the MTT assay. Cells under study were seeded into 96 well plates at a density of 3000-5000 cells per well depending on their doubling times and allowed to adhere for 24 h at 37 °C and 5% CO_2 . After 24 h incubation, the medium was replaced with culture medium containing test compounds dissolved in dimethyl sulphoxide (DMSO) and culture medium (DMSO) only was included as a control. After 48 h incubation, the medium containing test compounds was aspirated and 100 μ L of culture media containing 5 mg/mL MTT (Thiazoyl blue tetrazolium bromide) was added to each well and cells were further incubated for 4 hours in dark at 37 °C. After 4 hours incubation, the media containing MTT was removed and 100 μ L DMSO was added to each well to solubilize the crystallized formazan product. The plates were read on a micro-plate reader at 570 nm and a reference

wavelength of 630 nm. The percent growth inhibition was calculated as $100 - [(Mean\ OD\ of\ treated\ cell \times 100) / Mean\ OD\ of\ vehicle\ treated\ cells\ (DMSO)]$. The IC_{50} values were calculated using Probit Software. All tests were repeated in at least three independent experiments.

4.2.2 *In vitro* cell migration assay

MCF-7 cells (5×10^5 cells/well) were cultured in a 6 well plate as confluent monolayer for 24 h. The monolayers were then scratched with 200 μ L pipette tip. The wounded monolayers were washed twice with 150 mM PBS (pH 7.4) to remove non-adherent cells. Media containing IC_{50} concentrations of the compounds **9**, **17** and **28** was then added to each well. Cells which migrated across the inflicted wound were photographed under the phase contrast microscope microscopy at 0, 24 , 48 and 72 h time intervals after treatment in three or more randomly selected fields.

4.2.3 Colony formation inhibition assay

MCF-7 cells at the exponential phase were plated into 6-well culture plates at a single cell density (500 cells/well) and allowed to adhere for 24 h before treatment. Cells were incubated with culture medium containing IC_{50} concentrations of the compounds **9**, **17** and **28**. After 24 h the medium was replaced with fresh medium and cells were incubated for 14 days. Cells were then washed with 150 mM PBS (pH 7.4), fixed with 4 % paraformaldehyde and stained with 0.5% methylene blue in 10% ethanol for 30 min and rinsed with distilled water to remove excess dye. Plates were photographed with a digital camera.

4.2.4 Cell cycle analysis

MCF-7 Cells (1×10^6 cells/well) were seeded in 6 well plates and incubated overnight. Cells were treated with IC_{50} concentrations of compounds **9**, **17** and **28** for 24 h. Vehicle (DMSO) treated cells were used as controls. After 24 h treatment, both floating and adherent, trypsinized cells were collected and washed with 150 mM PBS (pH 7.4). The pellet was resuspended in 1 mL of PBS at room temperature and all suspended cells added to 9 ml of 70% ethanol by pipetting the cell suspension slowly in to ethanol, while and then vortexing at high speed. Cells were kept at 4 °C. After 30 min, ethanol was removed by centrifuging the cells. After tapping the tube to loosen the pellet, 5 mL PBS was added at room temp. Cells were allowed to rehydrate for 15 min and then centrifuged. The cell pellet was resuspended in propidium iodide staining buffer (PI (200 µg), 0.1% (v/v) Triton X-100, 2 mg DNase-free RNase A (Sigma) in 10 mL PBS), and incubated for 15 min at room temp in dark. The samples were analysed for PI fluorescence from 10000 events in a FACScanto -II flow cytometer (BD), using a linear scale for the cell cycle and a logarithmic scale to determine the sub- G1 fraction. Results were analyzed with FlowJo software (v 7.6.5, Tree Star, Inc.).

4.2.5 Hoechst staining

MCF-7 cells were seeded at a density of 5×10^4 cells/well in 12 well tissue culture plates and incubated for 24 h. The culture medium was then replaced with media containing IC_{50} concentrations of the compounds **9**, **17** and **28** and incubated for 24 h. After 24 h treatment, cells were fixed with 4% para formaldehyde and stained with Hoechst 33242 (5 µg/mL) for 30 min at room temp. Excess dye was removed by washing the cells twice with 150 mM PBS (pH 7.4). Images of stained nuclei from each well were captured from randomly selected fields under fluorescence microscopy (filters, excitation 350 nm and emissions 460 nm) to detect apoptotic cells.

4.2.6 DNA fragmentation assay

MCF-7 Cells were seeded (1×10^6 cells/well) in six-well plates. After incubation for 24 h, cells were treated with IC_{50} concentrations of compounds **9**, **17** and **28** for 24 h. Cells were harvested by trypsinisation and centrifuged at 2500 rpm for 5 min at 4 °C. The pellet was collected and washed with phosphate buffered saline (150 mM PBS; pH 7.4). 250 μ L of lysis buffer (100 mM NaCl, 5 mM EDTA, 10 mM Tris HCl pH 8.0, 0.25% SDS) containing 400 μ g/mL DNase free RNase A was added and incubated at 37 °C for 90 min, followed by incubation with proteinase K (200 μ g/mL) at 50 °C for 1 h. Samples were centrifuged at 3000 rpm for 5 min at 4 °C and supernatant collected. 65 μ L of 10 M ammonium acetate and 500 μ L of ice cold ethanol was added and mixed well. These samples were incubated at -80 °C for 1 h. After incubation, samples were centrifuged at 12000 rpm for 20 min at 4 °C and the pellet washed with 80% ethanol and air-dried for 10 min at room temperature. The pellet was dissolved in 50 μ L of TBE buffer and DNA laddering was visualised by using 1.5% agarose gel electrophoresis in TBE Buffer followed by ethidium bromide staining and photography.

4.2.7 Measurement of mitochondrial membrane potential

MCF-7 cells (5×10^5 cells/mL) were seeded in 6 well plates and allowed to adhere overnight. Cells were treated with IC_{50} concentrations of compounds **9**, **17** and **28**. After 24 h treatment, cells were harvested by trypsinisation, washed with 150 mM PBS (pH 7.4) and resuspended in a solution of rhodamine 123 (5 μ g/mL). The cells were washed twice with PBS followed by 30 min incubation at room temperature then resuspended in PBS. Samples were then subjected to flow cytometric analysis on a FACScan (Becton Dickinson) to detect loss of mitochondrial membrane potential. For qualitative analysis, cells were observed under a fluorescence microscope (Nikon, 10X Magnification).

4.2.8 Measurement of reactive oxygen species (ROS) levels

MCF-7 cells were plated in 6 well plates at a density of 1×10^5 cells/mL and allowed to adhere overnight. Cells were then treated with IC_{50} concentrations of compounds **9**, **17** and **28**

for 24 h. After 24 h treatment, the medium was replaced with culture medium containing carboxy-DCFDA (10 μ M) and further incubated for 30 min at room temperature in dark. Cells were collected, washed twice with 150 mM PBS (pH 7.4) and resuspended at a density of 5×10^4 cells/mL. The fluorescence intensity from each sample was analysed by spectrofluorometry at excitation and emission wavelengths of 488 and 525 nm, respectively. Qualitative cellular fluorescence images were captured by using a Nikon ECLIPSETE2000-S fluorescence microscope.

4.2.9 RNA extraction

MCF-7 cells (1×10^6 cells/ well) were plated in 6-well plates and allowed to adhere for 24h. After 24 h, cells were treated with IC_{50} concentrations of compounds **9**, **17** and **28**. After 24h incubation time, total RNA was extracted using TRIZOL reagent (Life Technologies, Carlsbad, CA, 12183-555) according to the manufacturer's instructions. Briefly, cells were washed twice with 2 mL cold 1 x PBS followed by addition of 1 mL of Trizol. Cell lysis was performed by incubating the cells with Trizol for 5 min at room temperature, samples transferred to 1.5 mL eppendorf centrifuge tubes and 0.12 mL of chloroform added. Tubes were then inverted vigorously for 15 seconds and incubated on ice for 10 min followed by centrifugation at 12000 rpm for 15 min at 4 °C. The aqueous phase was withdrawn and transferred to new 1.5 mL eppendorf tubes. 0.3 mL of isopropanol was added to the aqueous phase and RNA precipitated. Samples were centrifuged at 8000 rpm for 30 min at 4 °C. The supernatant was removed and the resulting pellet washed with 0.6 mL of 75% ethanol. Samples were then centrifuged at 8000 rpm for 20 min at 4 °C, the supernatant was discarded and the pellet was air-dried then resuspended in 20 μ L of DEPC water. RNA was stored at -80 °C. RNA concentration was determined with a Nano drop (Thermo Scientific, USA). This method yielded an average of 40 μ g total RNA from 10^6 cells.

4.2.10 cDNA Synthesis

cDNA synthesis from RNA was carried out in a volume of 20 μ L reaction mixture containing 1 μ g of RNA in 10 μ L nuclease free water, 2 μ L of 10X RT buffer, 0.8 μ L of 25X dNTP mix (100 mM), 2 μ L of 10X random primers and 3.2 μ L of nuclease free water. The thermal PCR cycles used in thermal cycler for reverse transcription were: 25 °C for 10 min followed by 37 °C for 2 h, 85 °C for 5 min and finally hold at 4 °C. The resulting cDNA was stored at -20 °C until use.

4.2.11 Real Time PCR

Fold change in mRNA expression levels were determined by the comparative CT method. Each 10 μ L PCR reaction in PCR fast reaction tubes (Applied Biosystems) contained 2.5 μ L of De Ionised water, 5 μ L of TaqMan Universal Master Mix (Applied Biosystems), 0.5 μ L (300 nM) of assay primers (Eurofins, Germany) and 2 μ L of cDNA. Samples were subjected to real-time quantitative PCR (Applied Biosystems-7500 Fast, USA). Specific gene primers (Bax, Bcl-2, CASP-3, CASP-7, E-cadherin and the internal control gene β -actin) were used to amplify the target genes. The sequences of the human genome based primers used for RT-PCR were

E-cadherin (CGCGTCCTGGGCAGAGTGAATTTTG)

β -catenin (CGCCAGGATGATCCTAGCTATCGTT),

cyclin-D1 (CTCTGTGCCACAGATGTGAAGTTCA),

Bax (CTGGTGCTCAAGGCCCTGTGCACCA),

Bcl-2 (CGGAGGCTGGGATGCCTTTGTGGAA),

caspase-3 (CATAAAAGCACTGGAATGACATCTC),

caspase-7 (TATTCCACGGTTCCAGGCTATTACT),

β -actin (CCTTTGCCGATCCGCCGCCCGTCCA),

Each reaction was performed in triplicate and threshold cycle numbers (CT) determined using the Applied Biosystems-7500 Fast software and the mean CT of triplicate reactions determined. Expression levels of specific genes were normalized to β -actin levels. The levels of the target gene expression can be expressed as $2^{\Delta\Delta CT}$ fold, where $\Delta\Delta CT = (C_{T,target} - C_{T,actin})_{Time\ 24\ h} - (C_{T,target} - C_{T,actin})_{Time\ 0\ h}$. The ΔCT value is inversely proportional to the levels of mRNA expression of the samples in this formula. The PCR cycles used were: 1 cycle of 95 °C for 3 min, followed by 40 cycles of 95 °C for 1 second (denaturation) and 60 °C for 20 seconds (annealing and extension). The PCR products were separated on a 1.5 % agarose gel containing ethidium bromide and viewed under UV light. Signal intensities for the PCR products were analysed using Quantiscan software (Biosoft, Cambridge, MA, USA).

Acknowledgements

T.S.R. and H.K. are thankful to IICT-RMIT research centre for the award of research fellowships. A.K. also acknowledges CSIR for financial support under the 12th Five Year plan project 'Affordable Cancer Therapeutics (ACT)' (CSC0301). V.B. acknowledges the Australian Research Council (ARC) for a Future Fellowship (FT140101285). V.B. and R.S. acknowledge the ARC for research support through the ARC-Linkage (LP130100437) scheme and Ian Potter Foundation for establishing the Ian Potter NanoBioSensing Facility and equipment support at RMIT University. We thank Dr. Suzane Rogers for proof reading of manuscript.

5.0 References

- [1] M. Gallorini, A. Cataldi, V. di Giacomo, Cyclin-dependent kinase modulators and cancer therapy, *Biodrugs* 26 (2012) 377–391.
- [2] G. Kibria, H. Hatakeyama, H. Harashima, Cancer multidrug resistance: mechanisms involved and strategies for circumvention using a drug delivery system, *Arch. Pharm. Res.* 37 (2014) 4-15.
- [3] S. Fulda, Tumor resistance to apoptosis, *Int. J. Cancer* 124 (2009) 511-515.
- [4] J.C. Reed, Apoptosis-based therapies, *Nat. Rev. Drug Disc.* 1 (2002) 111-121.
- [5] W. Hu, J.J. Kavanagh, Anticancer therapy targeting the apoptotic pathway, *Lancet Oncol.* 4 (2003) 721-729.
- [6] F.K. Keter, J. Darkwa, Perspective: the potential of pyrazole-based compounds in medicine, *Biometals* 25 (2012) 9–21.
- [7] V. Kumar, K. Kaur, G.K. Gupta, A.K. Sharma, Pyrazole containing natural products: synthetic preview and biological significance, *Eur. J. Med. Chem.* 69 (2013) 735-753.
- [8] B. Caliskan, A. Yilmaz, I. Evren, S. Menevse, O. Uludag, E. Banoglu, Synthesis and evaluation of analgesic, anti-inflammatory, and anticancer activities of new pyrazole-3(5)-carboxylic acid derivatives, *Med. Chem. Res.* 22 (2013) 782–793.
- [9] N. Gokhan-Kelekci, S. Koyunoglu, S. Yabanoglu, K. Yelekci, O. Ozgen, G. Ucar, K. Erol, E. Kendi, A. Yesilada, New pyrazoline bearing 4(3H)-quinazolinone inhibitors of monoamine oxidase: synthesis, biological evaluation, and structural determinants of MAO-A and MAO-B selectivity, *Bioorg. Med. Chem.* 17 (2009) 675–689.
- [10] S.R. Shih, T.Y. Chu, G. Reddy, S.N. Tseng, H.L. Chen, W.F. Tang, M.S. Wu, J.Y. Yeh, Y.S. Chao, J. Hsu, H.P. Hsieh, J.T. Horng, Pyrazole compound BPR1P0034 with potent and selective anti-influenza virus activity, *J. Biomed. Sci.* 17 (2010) 13.

- [11] H. Kumar, D. Saini, S. Jain, N. Jain, Pyrazole scaffold: A remarkable tool in the development of anticancer agents, *Eur. J. Med. Chem.* 70 (2013) 248-258.
- [12] I. Koca, A. Ozgur, K.A. Coskun, Y. Tutar, Synthesis and anticancer activity of acyl thioureas bearing pyrazole moiety, *Bioorg. Med. Chem.* 21 (2013) 3859-3865.
- [13] A.M. Farag, K.A.K. Ali, T.M.A. El-Debss, A.S. Mayhoub, A.E. Amr, N.A. Abdel-Hafez, M.M. Abdulla, Design, synthesis and structure-activity relationship study of novel pyrazole-based heterocycles as potential antitumor agents, *Eur. J. Med. Chem.* 45 (2010) 5887–5898.
- [14] Y.R. Liu, J.Z. Luo, P.P. Duan, J. Shao, B.X. Zhao, J.Y. Miao, Synthesis of pyrazole peptidomimetics and their inhibition against A549 lung cancer cells, *Bioorg. Med. Chem. Lett.* 22 (2012) 6882–6887.
- [15] Y. Yao, C. Liao, Z. Li, Z. Wang, Q. Sun, C. Liu, Y. Yang, Z. Tu, S. Jiang, Design, synthesis, and biological evaluation of 1, 3-disubstituted-pyrazole derivatives as new class I and IIb histone deacetylase inhibitors, *Eur. J. Med. Chem.* 86 (2014) 639-652.
- [16] H. Xian-Feng Huang, L. Xiang, Z. Yong, S. Guo-Qiang, H. Qi-Long, L. Qing-Shan, Y. Xian-Hui, W. Yao, Z. Hai-Liang, Synthesis, biological evaluation, and molecular docking studies of *N*-((1,3-diphenyl-1*H*-pyrazol-4-yl)methyl) aniline derivatives as novel anticancer agents, *Bioorg. Med. Chem.* 20 (2012) 4895-4900.
- [17] Y. Xia, C.D. Fan, B.X. Zhao, J. Zhao, D.S. Shin, J.Y. Miao, Synthesis and structure–activity relationships of novel 1-arylmethyl-3-aryl-1*H*-pyrazole-5-carbohydrazide hydrazone derivatives as potential agents against A549 lung cancer cells, *Eur. J. Med. Chem.* 43 (2008) 2347–2353.
- [18] K. Shah, S. Chhabra, S.K. Shrivastava, P. Mishra, Benzimidazole, a promising pharmacophore, *Med. Chem. Res.* 22 (2013) 5077-5104.

- [19] B. Narasimhan, D. Sharma, P. Kumar, Benzimidazole: a medicinally important heterocyclic moiety, *Med. Chem. Res.* 21 (2012) 269-283.
- [20] A.A.O. Sarhan, A. Al-Dhfyhan, M.A. Al-Mozaini, C.N. Adra, T.A. Fadl, Cell cycle disruption and apoptotic activity of 3-aminothiazolo[3,2-*a*]benzimidazole-2-carbonitrile and its homologues, *Eur. J. Med. Chem.* 45 (2010) 2689-2694.
- [21] A.A. El Rashedy, H.Y. Aboul-Enein, Benzimidazole derivatives as potential anticancer agents, *Mini Rev. Med. Chem.* 13 (2013) 399-407.
- [22] Q. Guan, C. Han, D. Zuo, M. Zhai, Z. Li, Q. Zhang, Y. Zhai, X. Jiang, K. Bao, Y. Wu, W. Zhang, Synthesis and evaluation of benzimidazole carbamates bearing indole moieties for antiproliferative and antitubulin activities, *Eur. J. Med. Chem.* 87 (2014) 306-315.
- [23] A. Husain, M. Rashid, M. Shaharyar, A.A. Siddiqui, R. Mishra, Benzimidazole clubbed with triazolo-thiadiazoles and triazolo-thiadiazines: New anticancer agents, *Eur. J. Med. Chem.* 62 (2013) 785-798.
- [24] K. Paul, S. Bindal, V. Luxami, Synthesis of new conjugated coumarinbenzimidazole hybrids and their anticancer activity, *Bioorg. Med. Chem.* 15 (2013) 3667-3672.
- [25] C.V. Junior, A. Danuello, V.d.S. Bolzani, E.J. Barreiro, C.A.M. Fraga, Molecular hybridization: a useful tool in the design of new drug prototypes, *Curr. Med. Chem.* 14 (2007) 1829-1852.
- [26] L.K. Gediya, V.C. Njar, Promise and challenges in drug discovery and development of hybrid anticancer drugs, *Expert Opin. Drug Discov.* 4 (2009) 1099-1111.
- [27] A. Kamal, T.S. Reddy, S. Polepalli, N. Shalini, V.G. Reddy, A.S. Rao, N. Jain, N. Shankaraiah, Synthesis and biological evaluation of podophyllotoxin congeners as tubulin polymerization inhibitors, *Bioorg. Med. Chem.* 22 (2014) 5466-5475.
- [28] A. Kamal, V. Srinivasulu, V.L. Nayak, M. Sathish, N. Shankaraiah, C. Bagul, N.V.S. Reddy, N. Rangaraj, N. Nagesh, Design and Synthesis of C3-Pyrazole/Chalcone-Linked

Beta-Carboline Hybrids: Antitopoisomerase I, DNA-Interactive, and Apoptosis-Inducing Anticancer Agents, *ChemMedChem* 9 (2014) 2084-2098.

[29] QikProp, version 3.8, Schrödinger, LLC, New York, NY, 2013.

[30] N.A Franken, H.M. Rodermond, J. Stap, J. Haveman, C. van Bree, Colonogenic assay of cells *in vitro*, *Nat. Protoc.* 1 (2006) 2315-2319.

[31] L.G. Rodriguez, X. Wu, J. L. Guan, Wound healing assay, *Methods Mol. Biol.* 294 (2005) 23–29.

[32] U.H Frixen, J. Behrens, M. Sachs, G. Eberle, B. Voss, A. Warda, D. Lochner, W. Birchmeier, E-cadherin-mediated cell-cell adhesion prevents invasiveness of human carcinoma cells, *J. Cell Biol.* 113 (1991) 173-185.

[33] H. Oka, H. Shiozaki, K. Kobayashi, M. Inoue, H. Tahara, T. Kobayashi, Y. Takatsuka, N. Matsuyoshi, S. Hirano, M. Takeichi, T. Mori, Expression of E-cadherin cell adhesion molecules in human breast cancer tissues and its relationship to metastasis, *Cancer Res.* 53 (1993) 1696-1701.

[34] M.E. Menezes, A. Mitra, L.A. Shevde, R.S. Samant, DNAJB6 governs a novel regulatory loop determining Wnt/ β -catenin signalling activity, *Biochem. J.* 444 (2012) 573-580.

[35] S. Fulda, K.M. Debatin, Extrinsic versus intrinsic apoptosis pathways in anticancer chemotherapy, *Oncogene* 25 (2006) 4798–4811.

[36] T.T. Tan, E. White, Therapeutic targeting of death pathways in cancer: mechanisms for activating cell death in cancer cells, *Adv. Exp. Med. Biol.* 615 (2008) 81–104.

[37] F.M. Mohamed, M.S. Mohamed, M.M. Fathi, S.A. Shouman, I.A. Abdelhamid, Chalcones Incorporated Pyrazole Ring Inhibit Proliferation, Cell Cycle Progression, Angiogenesis and Induce Apoptosis of MCF-7 Cell Line, *Anti-Cancer Agents Med. Chem.* 14 (2014) 1282-1292.

- [38] L.W. Zheng, Y. Li, D. Ge, B.X. Zhao, Y.R. Liu, H.S. Lv, J. Ding, J.Y. Miao, Synthesis of novel oxime-containing pyrazole derivatives and discovery of regulators for apoptosis and autophagy in A549 lung cancer cells, *Bioorg. Med. Chem. Lett.* 20 (2010) 4766–4770.
- [39] L.W. Zheng, L.L. Wu, B.X. Zhao, W.L. Dong, J.Y. Miao, Synthesis of novel substituted pyrazole-5-carbohydrazide hydrazone derivatives and discovery of a potent apoptosis inducer in A549 lung cancer cells, *Bioorg. Med. Chem.* 17 (2009) 1957–1962.
- [40] E. Toton, E. Ignatowicz, M.K. Bernard, J. Kujawski, M. Rybczynska, Evaluation of apoptotic activity of new condensed pyrazole derivatives, *J. Physiol. Pharmacol.* 64 (2013) 115-123.
- [41] Q. Hou, T.B. Zhao, H.L. Zhang, H.X. Lu, Q.X. Zhang, L. Sun, Z. Fan, Granzyme H induces apoptosis of target tumor cells characterized by DNA fragmentation and BID - dependent mitochondrial damage, *Mol. Immunol.* 45 (2008) 1044-1055.
- [42] X.D. Wang, The expanding role of mitochondria in apoptosis, *Genes Dev* 15 (2001) 2922–2933.
- [43] R.D. Miao, Y. Han, L.Z. An, J.B. Yang, Q. Wang, Seleno-podophyllotoxin derivatives induce hepatoma SMMC-7721 cell apoptosis through Bax pathway, *Cell Biol. Int.* 32 (2008) 217-223.
- [44] H.U. Simon, A.H. Yehia, F.L. Schaffer, Role of reactive oxygen species (ROS) in apoptosis induction, *Apoptosis* 5 (2000) 415–418.
- [45] G. Kroemer, J.C. Reed, Mitochondrial control of cell death, *Nature Med.* 6 (2000) 513–519.
- [46] D.G. Breckenridge, D. Xue, Regulation of mitochondrial membrane permeabilisation by Bcl-2 family proteins and caspases, *Curr. Opin. Cell Biol.* 16 (2004) 647–652.
- [47] X. Li, X. Lu, M. Xing, X.H. Yang, T.T. Zhao, H.B. Gong, H.L. Zhu, Synthesis, biological evaluation, and molecular docking studies of *N*,1,3-triphenyl-1*H*-pyrazole-4-

carboxamide derivatives as anticancer agents, *Bioorg. Med. Chem. Lett.* 22 (2012) 3589-3593.

Figure/Scheme Captions

Table. 1 *in vitro* anticancer activity (IC_{50}) of the pyrazolo-benzimidazole derivatives (**6-45**)

Figure. 1 Morphology of MCF-7 cells treated with IC_{50} concentrations of compounds **9**, **17** and **28** for 48 h.

Figure. 2 Colony formation inhibition assay: MCF-7 cells were exposed to DMSO (control)/compounds **9**, **17** and **28** for 24 h. Medium was removed, and cells then incubated in fresh medium for 14 days. The viable cells formed colonies that were stained with crystal violet.

Figure. 3 Effect of compounds **9**, **17** and **28** on migration of MCF-7 cells. The images were captured using phase contrast microscopy immediately (0 h), 24, 48 and 72 h after treatment.

Figure. 4 Effect of compounds on E-cadherin and β -catenin mRNA expression levels. MCF-7 cells were treated with IC_{50} concentrations of compounds **9**, **17** and **28** for 24 h and total RNA was extracted. mRNA levels were measured by RT-PCR. Target gene expression is normalized to β -actin. Each histogram represents the mean \pm standard deviation of three independent experiments.

Figure. 5 **a)** Cell cycle analysis of MCF-7 cells treated with compounds **9**, **17** and **28** for 24 h. Cells were fixed with ethanol, stained with propidium iodide, and then cell cycle distribution was analyzed by flow-cytometry (BD FACS-Canto-II). Data from 10,000 cells were collected for each data file. **b)** The percentage of cells in G0/G1, S and G2/M phases were quantified using Flowjo software.

Figure. 6 Effect of compounds on mRNA expression levels of cell cycle regulatory molecules. MCF-7 cells were treated with IC₅₀ concentrations of compounds **9**, **17** and **28** for 24 h and total RNA was extracted. mRNA levels of cyclin B1, cyclin D1, CDK1 and CDK2 were measured by RT-PCR. Target gene expression is normalized to β -actin. Each histogram represents the mean \pm standard deviation of three independent experiments.

Figure. 7 a) Compounds **9**, **17** and **28** induced nuclear morphological changes of MCF-7 cells after treatment for 24 h. **b)** Quantitative analysis of apoptosis induced by the compounds **9**, **17** and **28**. Data are mean \pm Standard deviation from three independent experiments.

Figure. 8 DNA ladder assay. MCF-7 cells were treated with IC₅₀ concentrations of compounds **9**, **17** and **28** for 24 h. Genomic DNA was extracted, and resolved on 1.5 % agarose gels. Lanes 1-3 are DNA from compound treated cells, lane 4 from control cells and M the molecular weight marker.

Figure. 9 a) Compounds **9**, **17** and **28** induced loss of mitochondrial membrane potential in MCF-7 cells as demonstrated with rhodamine 123 staining. **b)** The quantitative determination of loss in fluorescence intensity was measured by spectrofluorometry.

Figure. 10 Effect of compounds on reactive oxygen species levels. **a)** MCF-7 cells were treated with compounds **9**, **17**, and **28**, incubated with carboxy-DCFH-DA. The cells were observed for DCF-DA fluorescence in the cells observed under fluorescence microscope. **b)** Quantitative estimation of ROS was done fluorimetrically with DCF-DA, using an excitation wavelength of 485 nm and an emission wavelength of 535 nm.

Figure. 11 Effect of compounds **9**, **17** and **28** on the mRNA expression levels of apoptotic signaling molecules in MCF-7 cells. Agarose gel show bax, bcl-2, caspase-3 and caspase-7 amplification with respect to β -actin (house keeping gene). The relative mRNA expression levels were analyzed by real-time PCR. Each histogram represents the mean values \pm standard deviation of three dependent experiments.

Table. 1 *in vitro* anticancer activity (^aIC₅₀) of the pyrazolo-benzimidazole derivatives (**6-45**)

Compound	R	R ₁	R ₂	A549 ^b	MCF-7 ^c	HeLa ^d	HaCaT ^e
4a	H	-	-	13.71±1.3	18.24±2.1	21.32±1.6	>50
4b	F	-	-	8.66±0.9	24.76±1.7	16.64±3.1	>50
4c	Cl	-	-	29.5±2.5	9.65±0.7	15.53±1.2	>50
4d	OMe	-	-	2.71±0.6	3.19±0.9	1.55±0.4	>50
6	H	H	H	2.71±0.6	3.19±0.9	1.55±0.4	>50
7	H	F	H	1.72±0.5	2.43±1.1	3.61±1.3	>50
8	H	Cl	H	2.37±0.2	1.96±0.6	3.48±0.3	>50
9	H	Br	H	1.81±0.4	0.83±0.3	1.76±0.7	>50
10	H	Me	H	3.61±0.1	5.94±1.3	6.56±1.6	>50
11	H	OMe	H	1.23±0.3	1.59±0.4	2.87±0.2	>50
12	H	CF ₃	H	5.93±0.7	2.66±0.9	1.92±0.3	37.23±2.1
13	H	Me	Me	14.5±3.3	>50	41.5±6.9	>50
14	H	Cl	Cl	11.1±1.9	7.56±1.0	13.4±1.5	29.65±3.7
15	H	cbz ^f		19.3±2.7	12.6±1.4	21.3±3.2	>50
16	F	H	H	1.51±0.3	3.20±0.6	2.33±0.8	>50
17	F	F	H	1.13±0.2	0.95±0.3	1.57±0.3	>50
18	F	Cl	H	1.32±0.5	2.23±0.7	2.77±0.3	>50
19	F	Br	H	5.83±0.8	3.21±0.3	4.94±0.9	21.79±1.8
20	F	OMe	H	1.96±0.3	0.97±0.2	7.51±1.9	>50
21	F	Me	H	1.44±0.4	1.12±0.3	3.63±0.6	>50
22	F	CF ₃	H	2.34±1.4	2.13±0.6	3.52±0.7	>50
23	F	Me	Me	>50	27.2±4.2	10.2±2.6	>50

24	F	Cl	Cl	15.7±3.1	6.93±1.0	11.6±2.7	44.62±2.3
25	F	cbz		21.5±2.9	9.24±1.4	23.6±4.1	>50
26	Cl	H	H	5.96±1.8	3.03±1.1	1.65±0.7	>50
27	Cl	F	H	4.61±0.9	2.83±1.2	2.77±1.2	>50
28	Cl	Cl	H	1.34±0.2	1.17±0.2	1.63±0.3	>50
29	Cl	Br	H	2.17±0.3	1.92±0.2	2.16±0.5	>50
30	Cl	OMe	H	2.42±0.4	1.76±0.6	3.63±0.8	>50
31	Cl	CF ₃	H	3.36±0.3	4.21±1.1	4.42±0.9	41.77±2.8
32	Cl	Me	H	4.64±1.5	8.23±1.0	5.36±1.7	>50
33	Cl	Me	Me	17.7±2.3	13.0±1.6	21.8±2.5	>50
34	Cl	Cl	Cl	19.1±3.1	48.3±5.7	12.1±1.9	>50
35	Cl	cbz		7.73±1.8	13.9±2.5	8.13±1.7	>50
36	OMe	H	H	2.36±0.6	2.54±0.3	3.67±0.5	>50
37	OMe	F	H	1.98±0.7	1.51±0.4	1.74±0.6	>50
38	OMe	Cl	H	3.13±1.1	1.76±0.3	1.29±0.2	>50
39	OMe	Br	H	6.37±0.8	1.83±0.7	1.06±0.4	>50
40	OMe	OMe	H	22.7±2.9	3.13±1.1	1.14±0.2	>50
41	OMe	CF ₃	H	4.82±1.2	5.73±1.7	2.76±0.7	>50
42	OMe	Me	H	5.07±1.3	6.61±2.0	3.29±0.4	>50
43	OMe	Me	Me	5.85±0.43	12.8±2.7	8.93±2.5	21.35±3.8
44	OMe	Cl	Cl	7.33±1.2	13.2±1.1	6.6±1.2	>50
45	OMe	cbz		11.9±2.3	7.46±1.3	12.4±2.7	>50
	Nocodazole			1.87±0.5	1.6±0.2	2.83±0.3	8.9±2.6
	5-Fluorouracil			2.13±0.3	2.36±0.2	4.6±0.9	15.26±1.7

^a IC₅₀ values are the concentrations that cause 50 % inhibition of cancer cell growth (μM). Data represent the mean values \pm standard deviation of three independent experiments performed in triplicate; ^b lung cancer cell line; ^c breast cancer cell line; ^d cervical cancer cell line; ^e human keratinocyte cells, ^f condensed benzene ring.

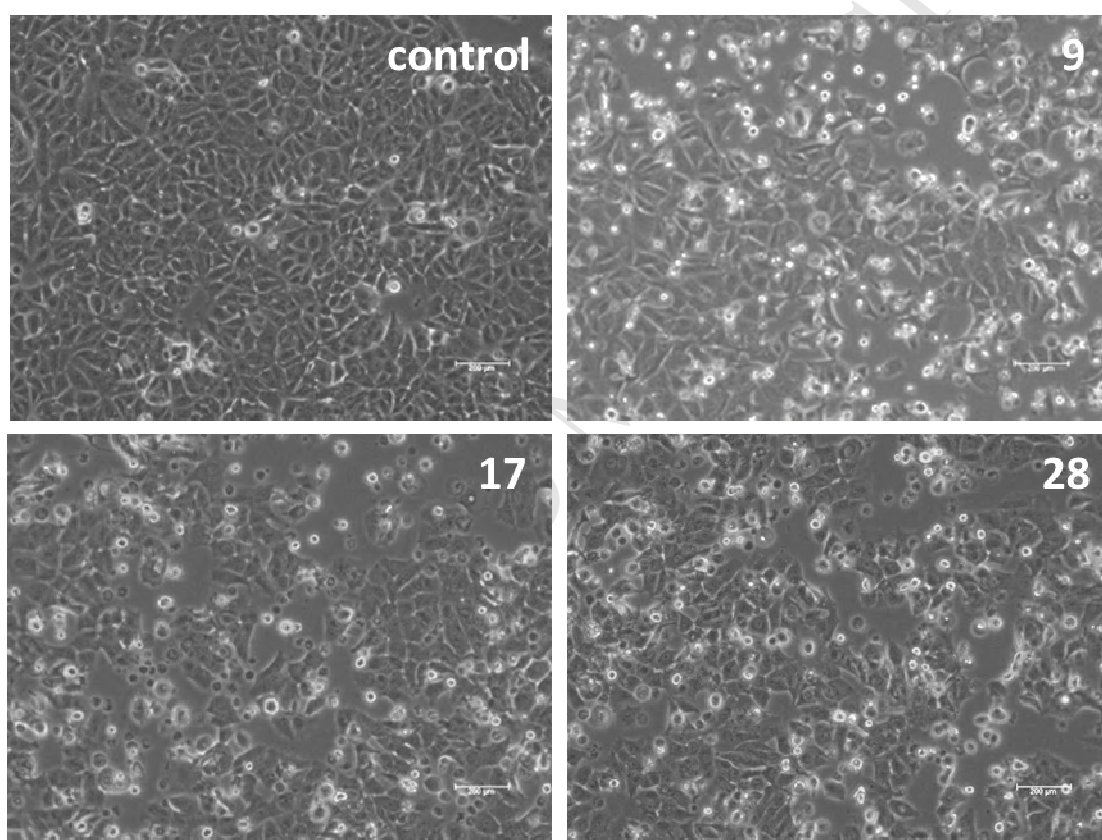


Figure. 1 Morphology of MCF-7 cells treated with IC₅₀ concentrations of the compounds **9**, **17** and **28** for 48 h.

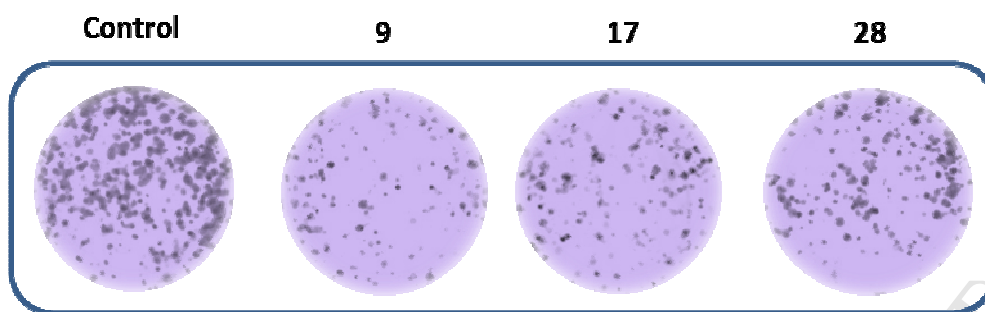


Figure. 2 Colony formation inhibition assay: MCF-7 cells were exposed to DMSO (control)/compounds **9**, **17** and **28** for 24 h. Medium was removed, and cells then incubated in fresh medium for 14 days. The viable cells formed colonies that were stained with crystal violet.

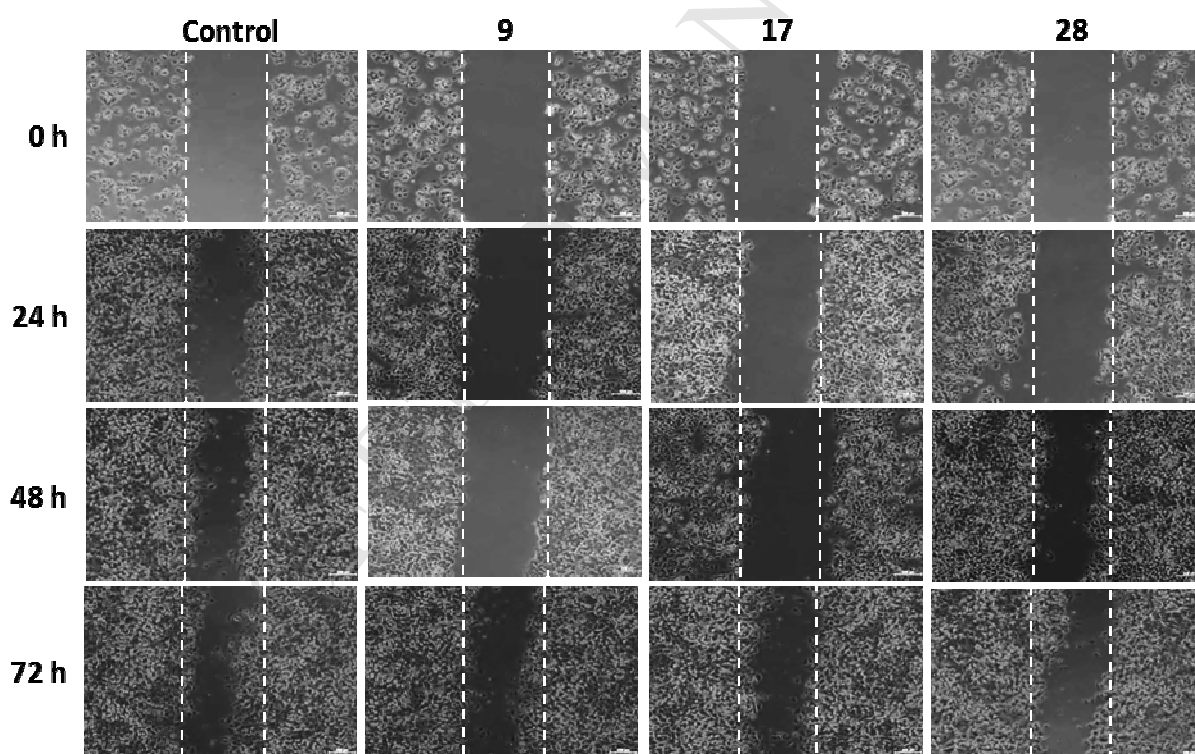


Figure. 3 Effect of compounds **9**, **17** and **28** on migration of MCF-7 cells. The images were captured using phase contrast microscopy immediately (0 h), 24, 48 and 72 h after treatment.

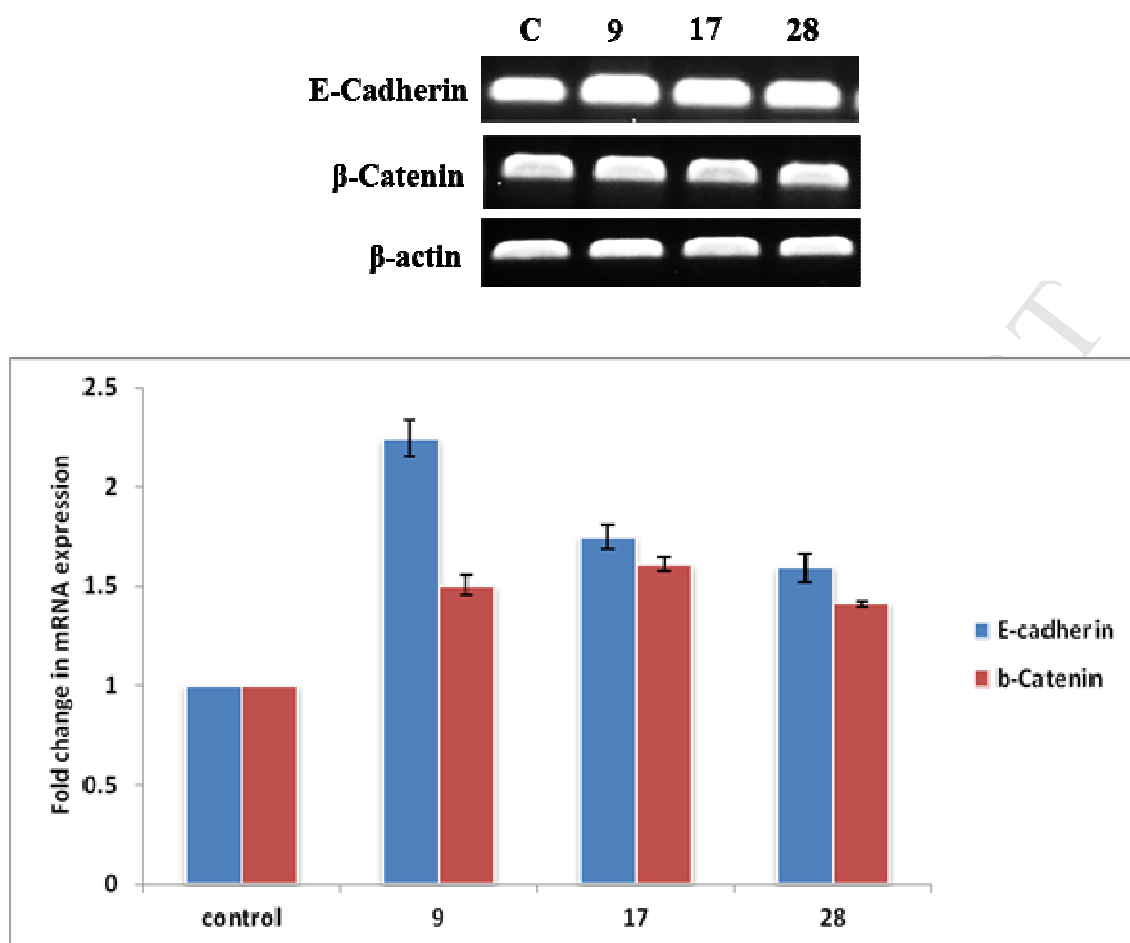
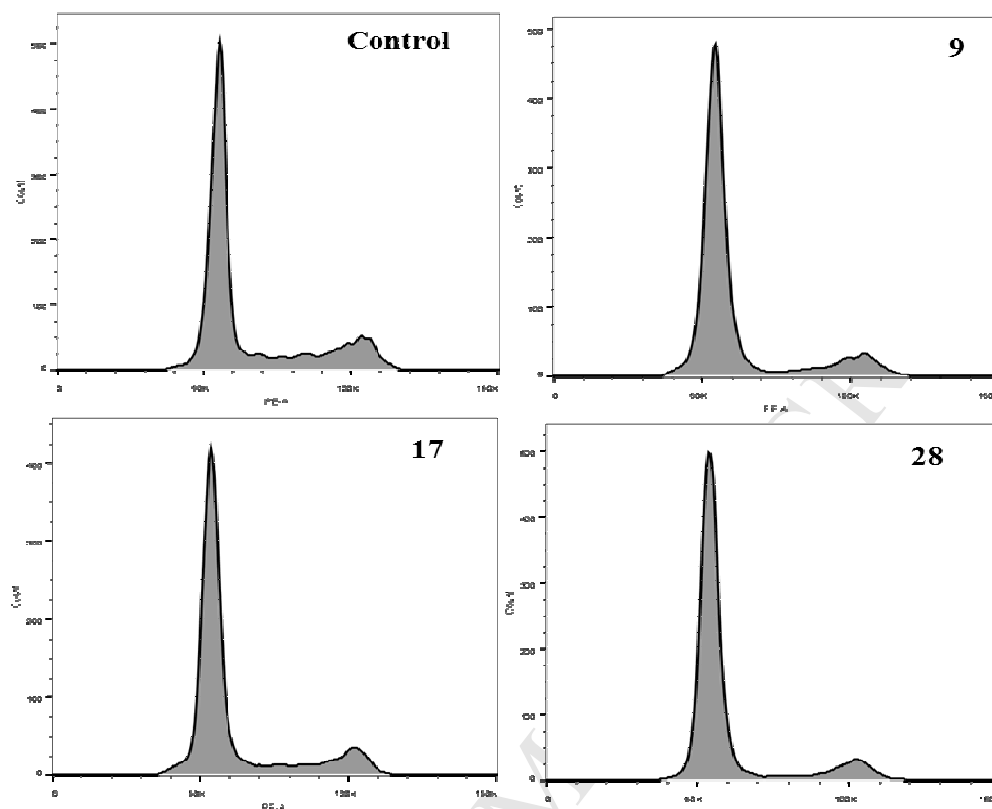


Figure. 4 Effect of compounds on E-cadherin and β -catenin mRNA expression levels. MCF-7 cells were treated with IC_{50} concentrations of compounds **9**, **17** and **28** for 24 h and total RNA was extracted. mRNA levels were measured by RT-PCR. Target gene expression is normalized to β -actin. Each histogram represents the mean \pm standard deviation of three independent experiments.

a)



b)

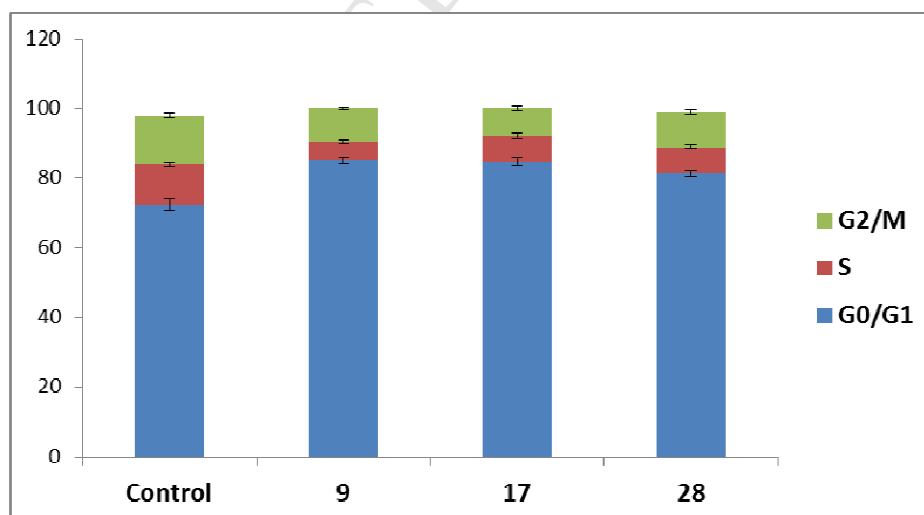


Figure. 5 a) Cell cycle analysis of MCF-7 cells treated with compounds **9**, **17** and **28** for 24 h. Cells were fixed with ethanol, stained with propidium iodide, and then cell cycle distribution was analyzed by flow-cytometry (BD FACS-Canto-II). Data from 10,000 cells

were collected for each data file. **b)** The percentage of cells in G0/G1, S and G2/M phases were quantified using Flowjo software.

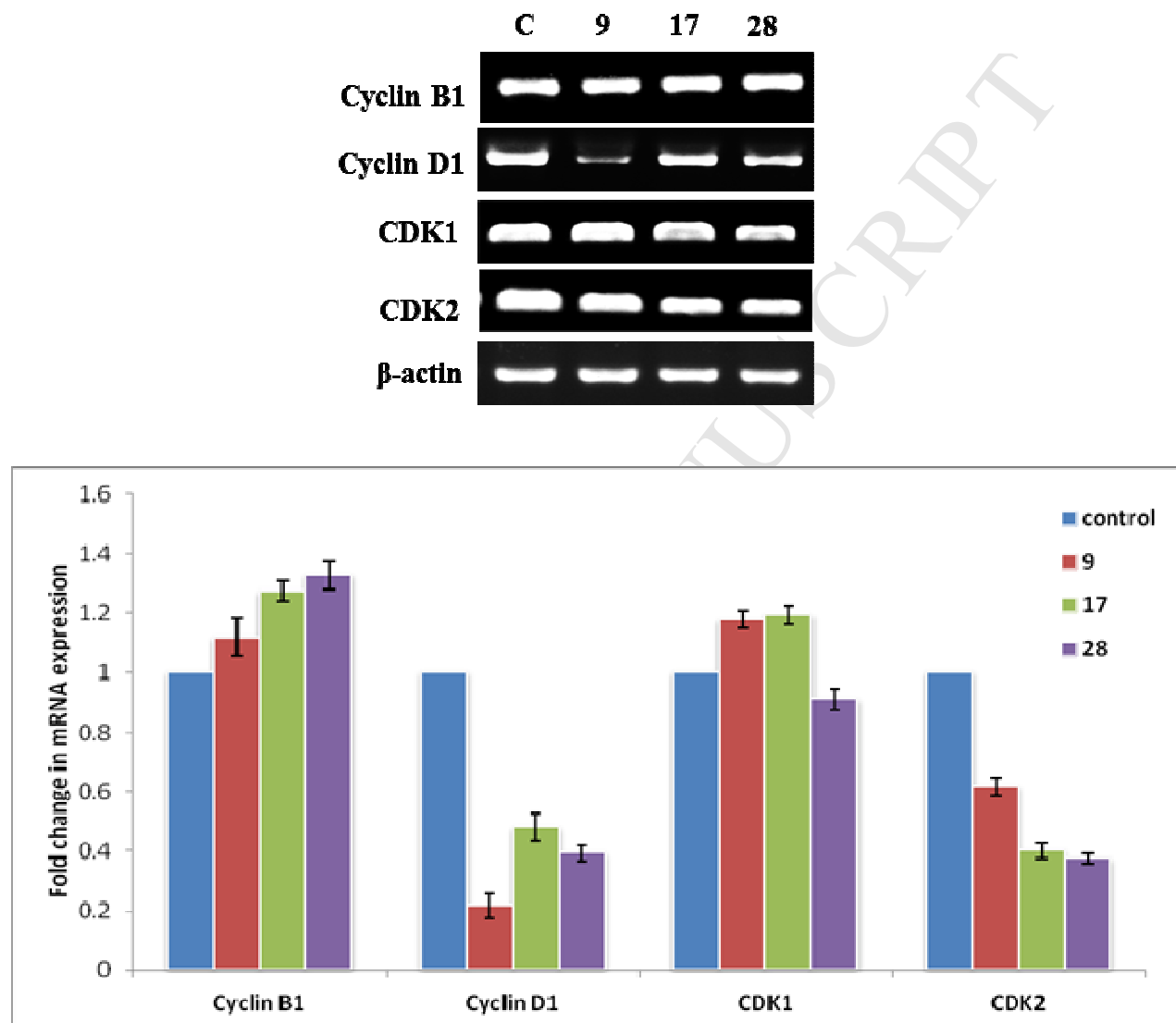
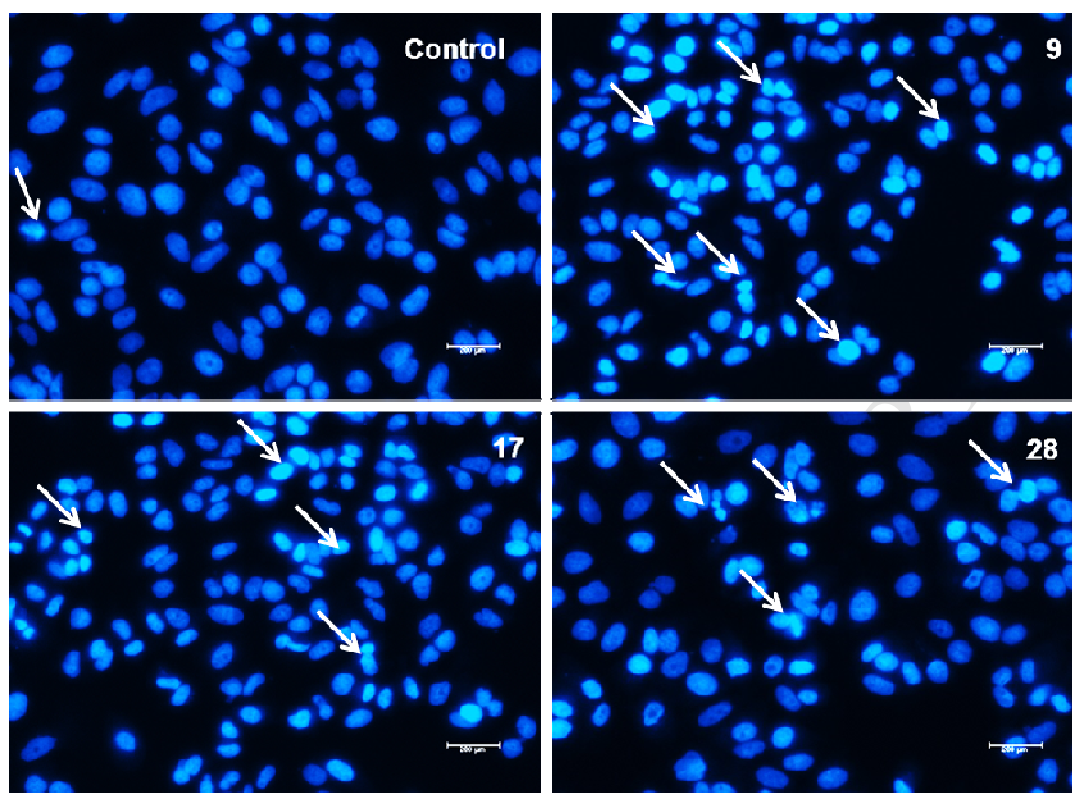


Figure. 6 Effect of compounds on mRNA expression levels of cell cycle regulatory molecules. MCF-7 cells were treated with IC_{50} concentrations of compounds **9**, **17** and **28** for 24 h and total RNA was extracted. mRNA levels of cyclin B1, cyclin D1, CDK1 and CDK2 were measured by RT-PCR. Target gene expression is normalized to β -actin. Each histogram represents the mean \pm standard deviation of three independent experiments.

a)



b)

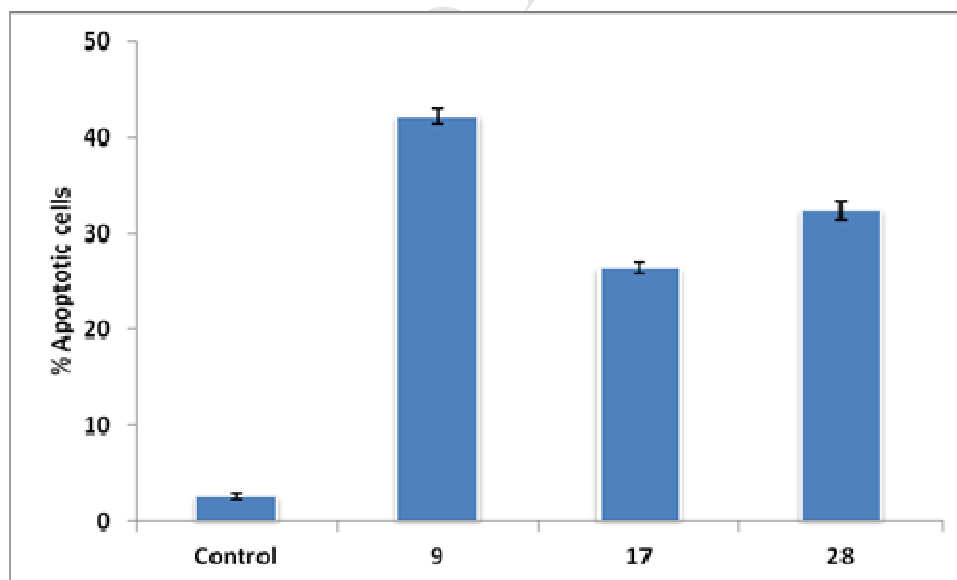


Figure. 7 a) Compounds **9**, **17** and **28** induced nuclear morphological changes of MCF-7 cells after treatment for 24 h. b) Quantitative analysis of apoptosis induced by the compounds **9**, **17** and **28**. Data are mean \pm Standard deviation from three independent experiments.

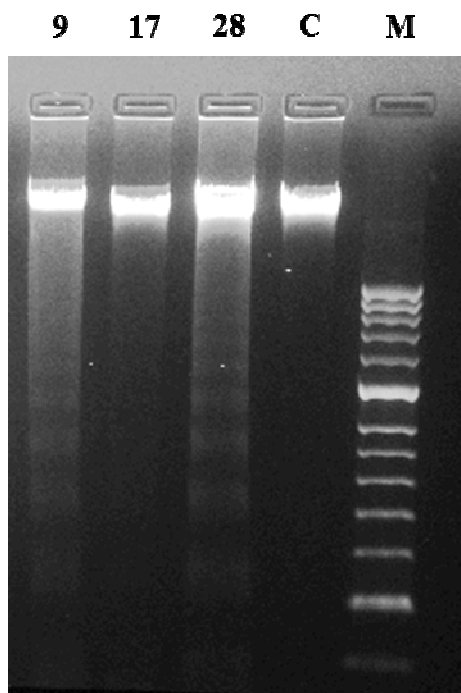
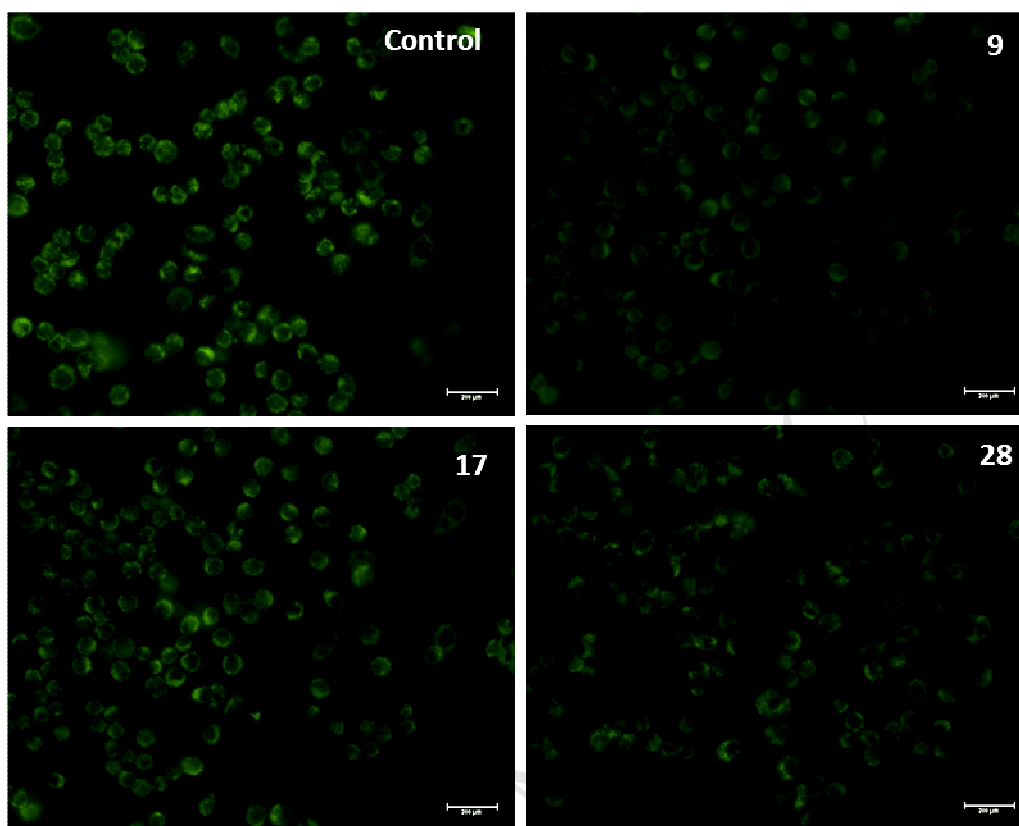


Figure. 8 DNA ladder assay. MCF-7 cells were treated with IC_{50} concentrations of compounds **9**, **17** and **28** for 24 h. Genomic DNA was extracted, and resolved on 1.5 % agarose gels. Lanes 1-3 are DNA from compound treated cells, lane 4 from control cells and M the molecular weight marker.

a)



b)

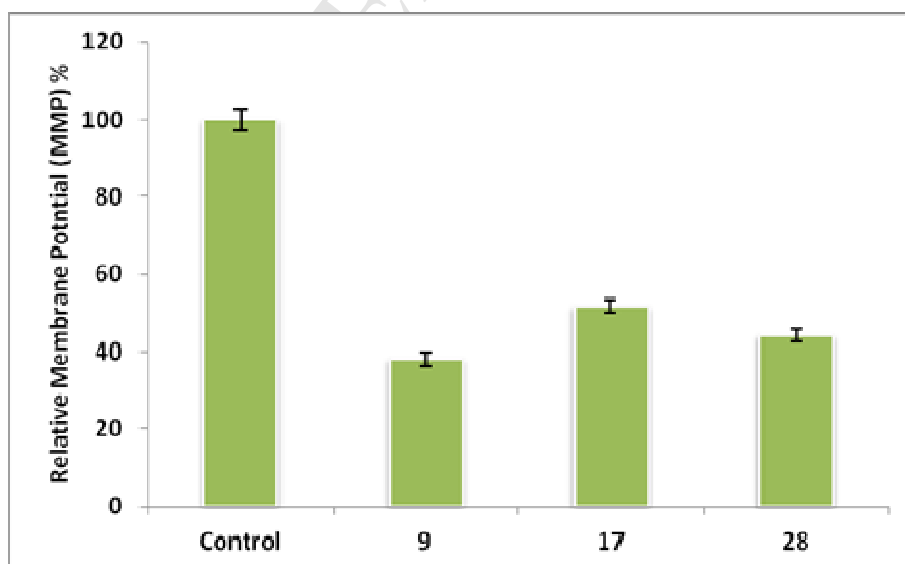
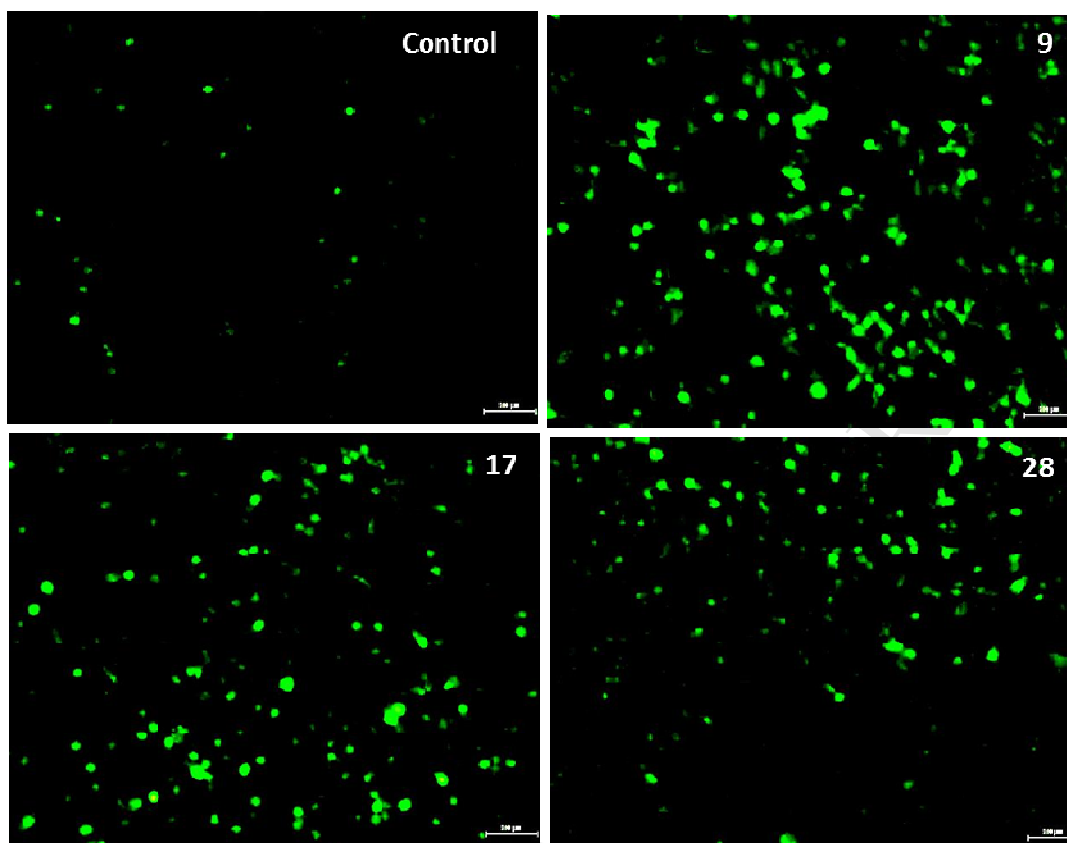


Figure. 9 a) Compounds **9**, **17** and **28** induced loss of mitochondrial membrane potential in MCF-7 cells as demonstrated with rhodamine 123 staining. b) The quantitative determination of loss in fluorescence intensity was measured by spectrofluorometry.

a)



b)

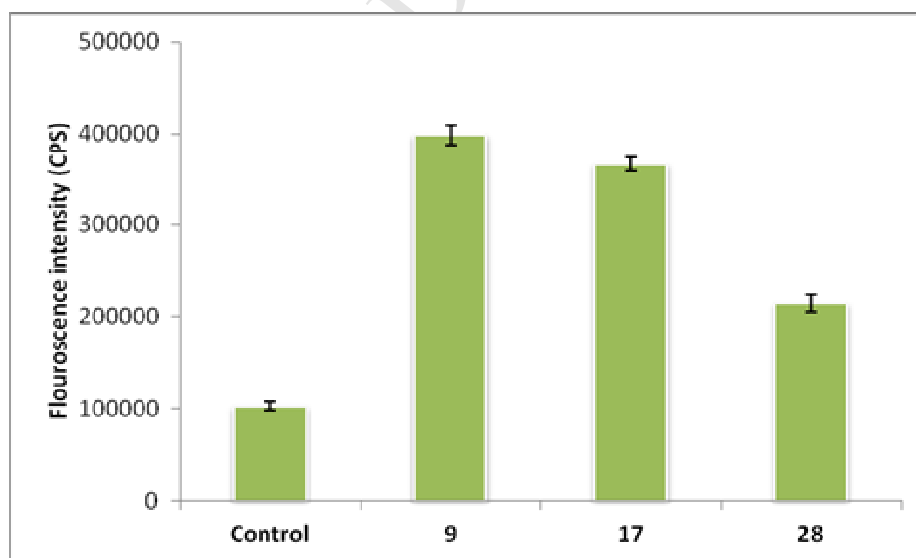


Figure. 10 Effect of compounds on reactive oxygen species levels. **a)** MCF-7 cells were treated with compounds **9**, **17**, and **28**, incubated with carboxy-DCFDA. The cells were observed for Carboxy-DCF fluorescence under fluorescence microscope. **b)** Quantitative

estimation of ROS was done fluorimetrically, using an excitation wavelength of 485 nm and an emission wavelength of 535 nm.

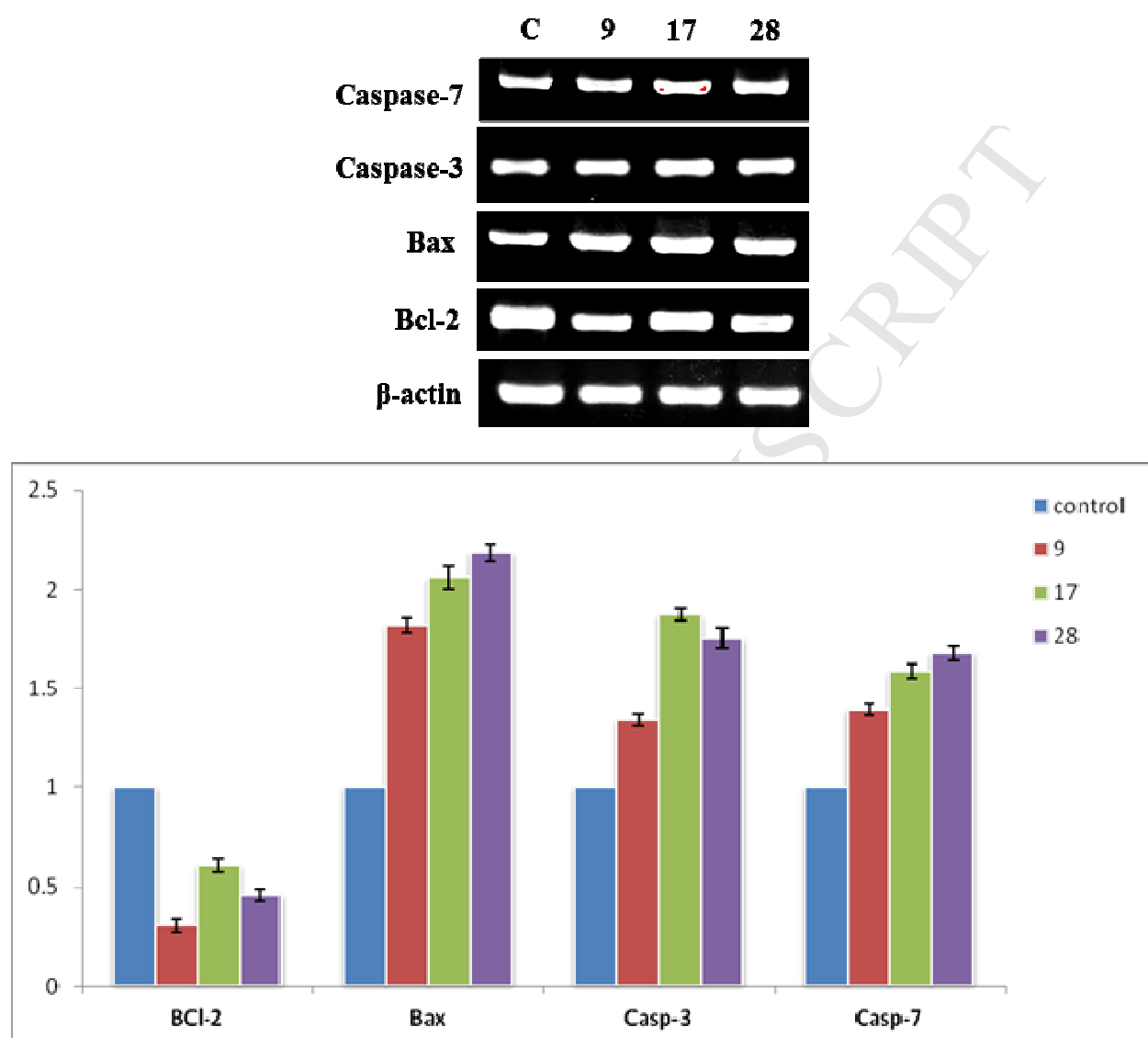
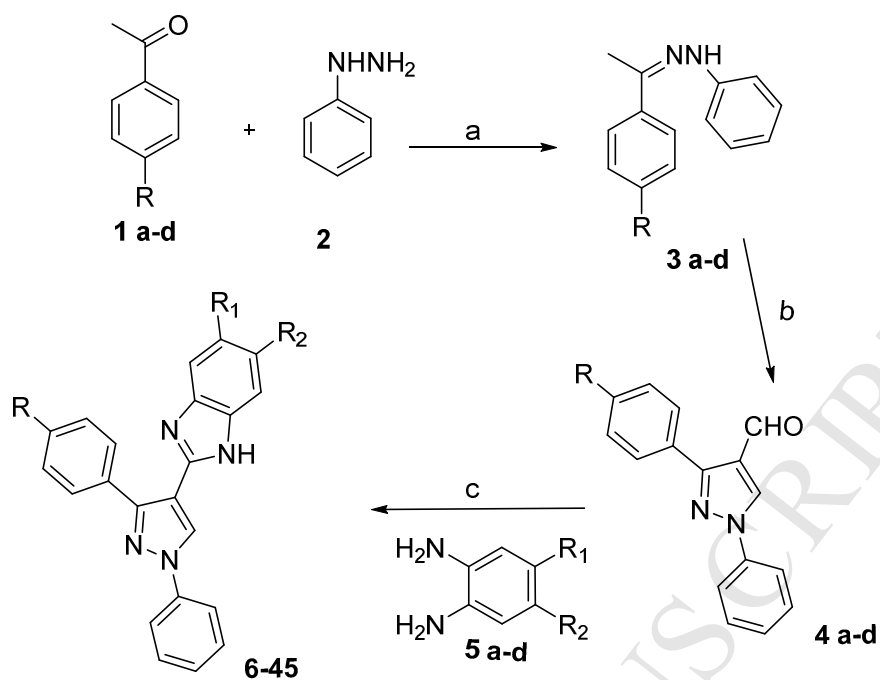


Figure. 11 Effect of compounds **9**, **17** and **28** on the mRNA expression levels of apoptotic signaling molecules in MCF-7 cells. Agarose gel show bax, Bcl-2, caspase-3 and caspase-7 amplification with respect to β -actin (house keeping gene). The relative mRNA expression levels were analyzed by real-time PCR. Each histogram represents the mean values \pm standard deviation of three dependent experiments



Scheme. 1 General synthesis of 2-(1,3-diphenyl-1H-pyrazol-4-yl)-1H-benzo[d]imidazole derivatives (**6-45**). Reagents and conditions: (a) ethanol, 50–60 °C, 3 h; (b) DMF, POCl₃, 50–60 °C, 5 h; (c) ethanol, Na₂S₂O₅, 50–60 °C, 5 h.

- A series of forty pyrazole-benzimidazole hybrids were synthesized.
- All compounds were screened for their anticancer activity
- Three compounds **9**, **17** and **28** displayed promising activity
- These compounds induce cell cycle arrest and apoptosis in MCF-7 cells.

ACCEPTED MANUSCRIPT

Supplementary Material**Design, synthesis and biological evaluation of 1,3-diphenyl-1H-pyrazole derivatives containing benzimidazole skeleton as potential anticancer and apoptosis inducing agents**

T. Srinivasa Reddy,^{a,b,c,d} Hitesh Kulhari,^{a,b,c,d} V. Ganga Reddy,^a Vipul Bansal^{c,d} Ahmed Kamal,^{a,b} * Ravi Shukla,^{c,d,e} *

^a *Medicinal Chemistry and Pharmacology, CSIR-Indian Institute of Chemical Technology, Hyderabad 500 007, India*

^b *IICT - RMIT Research Centre, CSIR-Indian Institute of Chemical Technology, Hyderabad 500 007, India*

^c *Ian Potter NanoBioSensing Facility, NanoBiotechnology Research Laboratory, School of Applied Sciences, RMIT University, Melbourne 3000, Australia*

^d *Health Innovations Research Institute, RMIT University, Melbourne 3083, Australia*

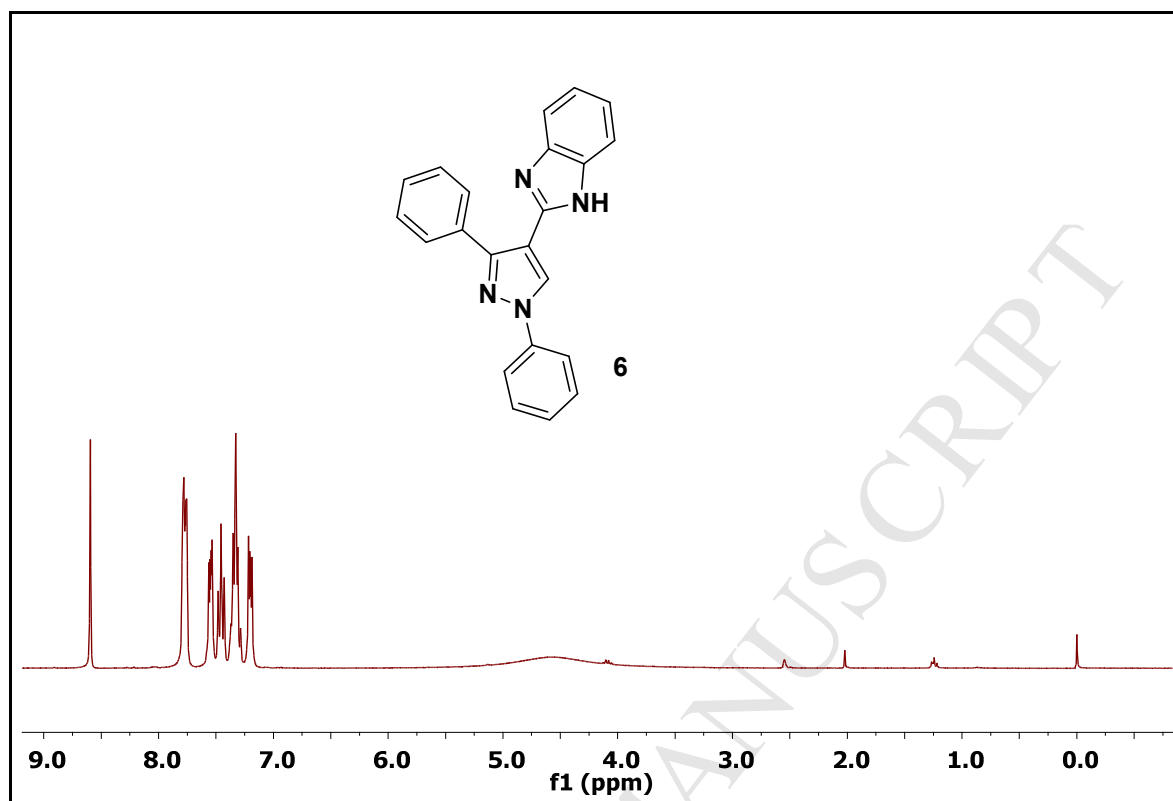
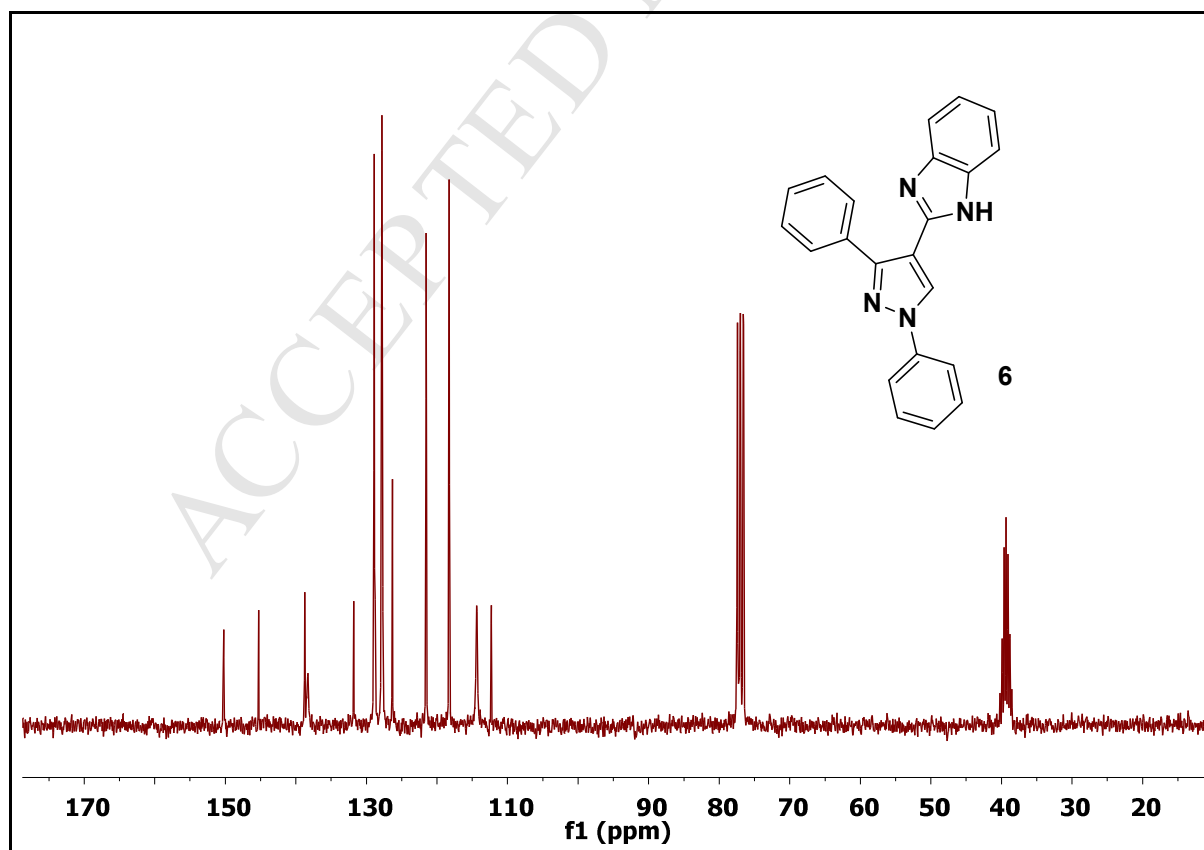
^e *Centre for Advanced Materials and Industrial Chemistry, RMIT University, Melbourne 3000, Australia*

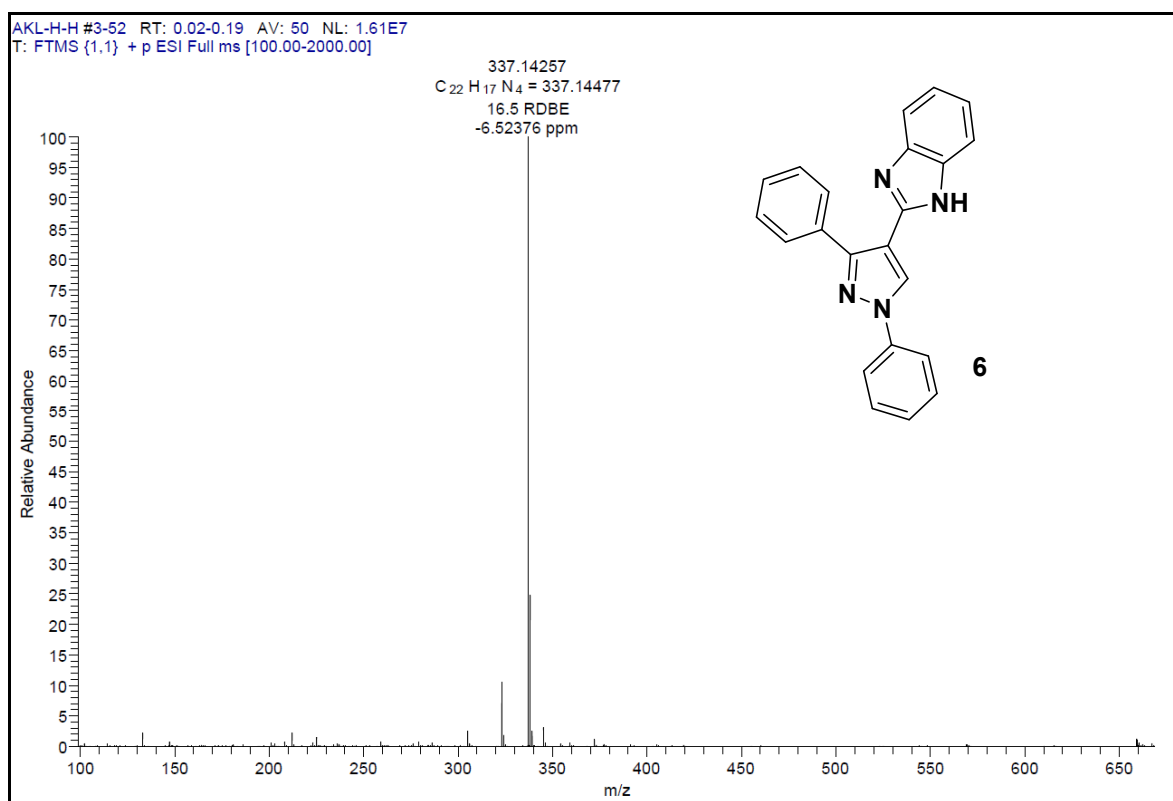
Table. S1 Calculated ADME and drug-like properties of compounds **6-45^a**

Compound	% ABS	Lipinski's Parameters				No. of violations	#metab
		nHBA	nHBD	MW	log <i>P</i>		
6	100	2	1	336.395	5.624	1	0
7	100	2	1	354.386	5.862	1	0
8	100	2	1	370.84	6.246	1	0
9	100	2	1	415.291	6.324	1	0
10	100	2	1	350.422	5.941	1	1
11	100	3	1	366.421	5.843	1	1
12	100	2	1	404.394	6.606	1	0
13	100	2	1	364.449	6.218	1	2
14	100	2	1	405.285	6.558	1	0
15	100	2	1	386.455	6.589	1	1
16	100	2	1	354.386	5.863	1	0
17	100	2	1	372.376	6.1	1	0
18	100	2	1	388.831	6.362	1	0
19	100	2	1	433.282	6.419	1	0
20	100	3	1	384.412	5.961	1	1
21	100	2	1	368.412	6.159	1	1
22	100	2	1	422.384	6.845	1	0
23	100	2	1	382.439	6.457	1	2
24	100	2	1	423.276	6.797	1	0
25	100	2	1	404.445	6.817	1	1
26	100	2	1	370.84	6.104	1	0
27	100	2	1	388.831	6.362	1	0
28	100	2	1	405.285	6.624	1	0
29	100	2	1	449.736	6.702	1	0
30	100	3	1	400.866	6.201	1	1
31	100	2	1	438.839	7.107	1	0

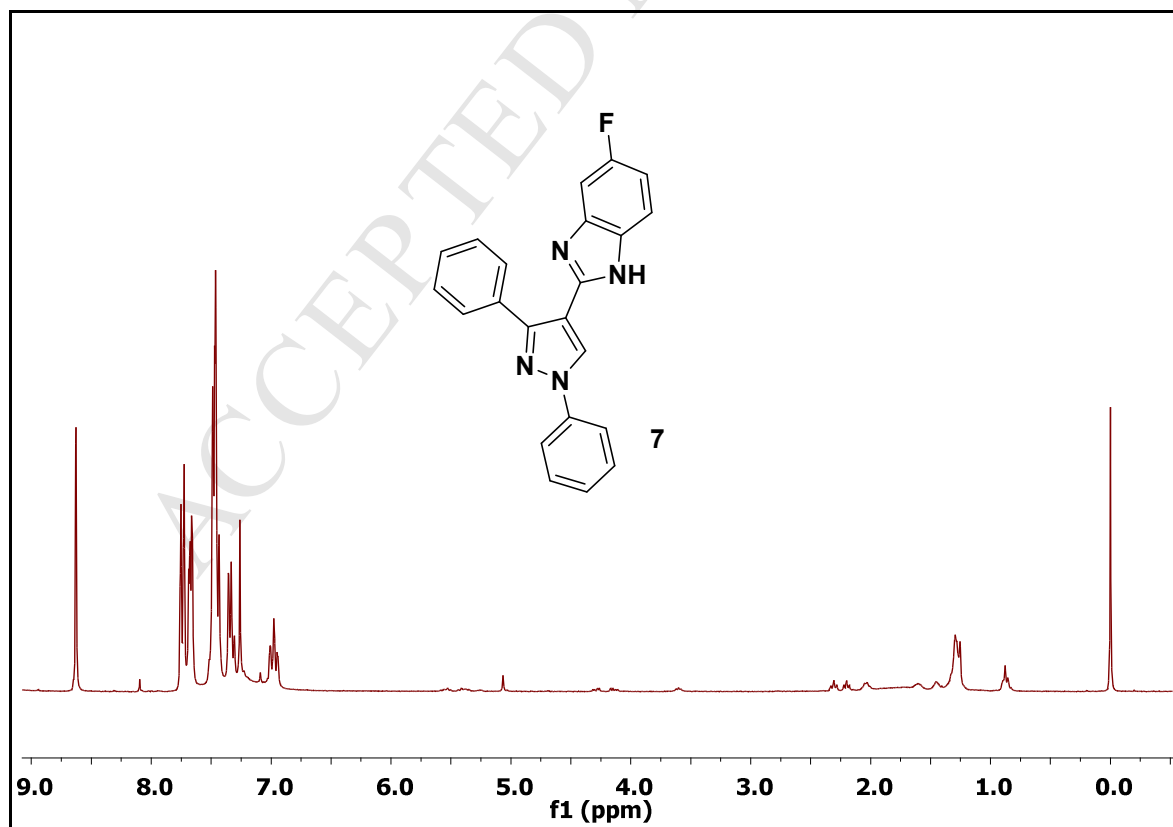
32	100	2	1	384.867	6.421	1	1
33	100	2	1	398.894	6.698	1	2
34	100	2	1	439.73	7.038	1	0
35	100	2	1	420.9	7.059	1	1
36	100	3	1	366.421	5.722	1	1
37	100	3	1	384.412	5.938	1	1
38	100	3	1	400.866	6.198	1	1
39	100	3	1	445.317	6.276	1	1
40	100	4	1	396.448	5.795	1	2
41	100	3	1	434.42	6.701	1	1
42	100	3	1	380.448	6.159	1	2
43	100	3	1	394.475	6.436	1	3
44	100	3	1	435.312	6.653	1	1
45	100	3	1	416.481	6.652	1	2

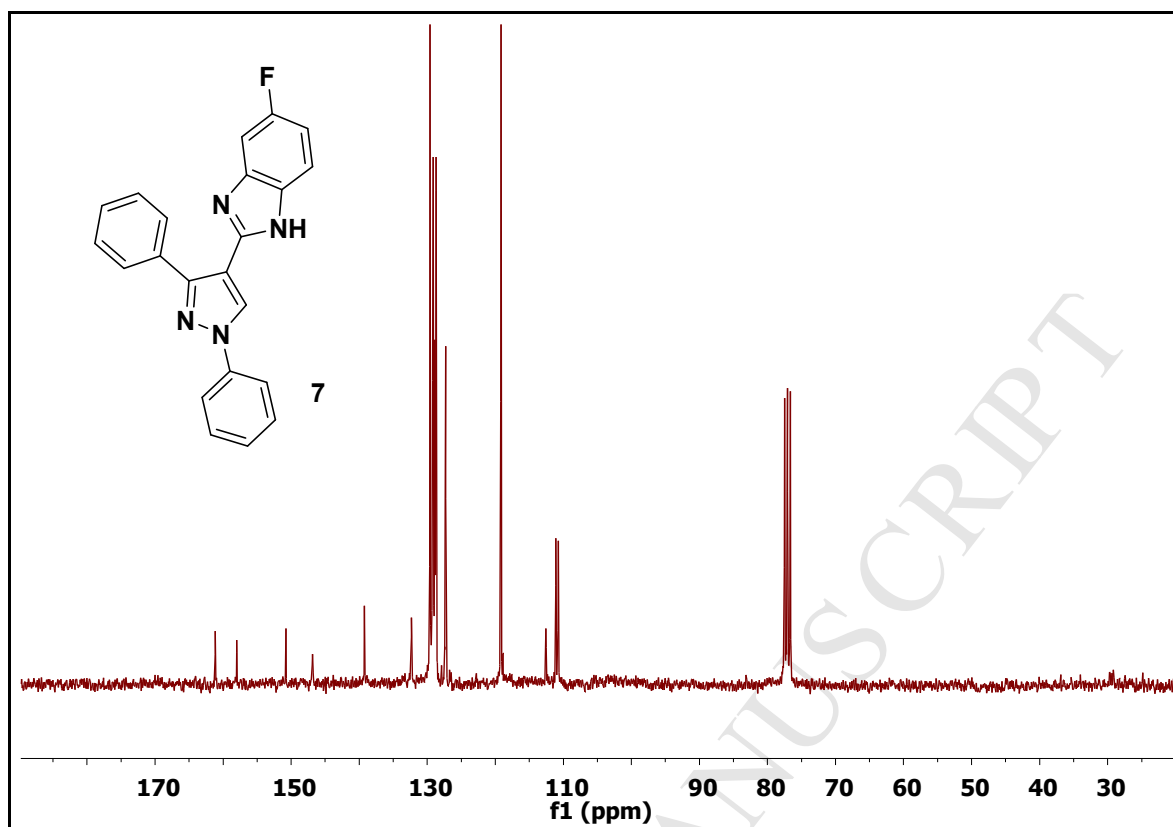
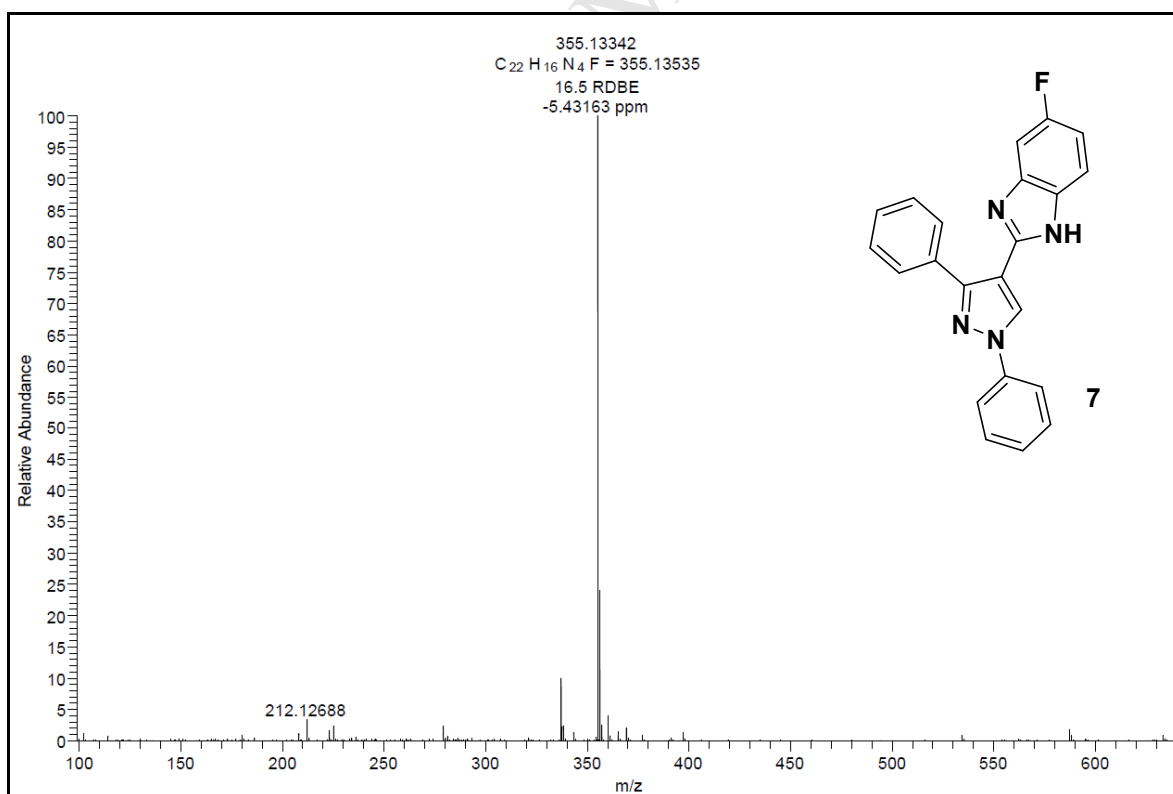
^a Number of hydrogen bond acceptor (NO) = nHBA; Number of hydrogen bond donors (OHNH) = nHBD; molecular weight = MW; Partition coefficient = log *P*; Number of violations of Lipinski's rule of five = No. of violations; Predicted percentage of human oral absorption = % ABS and #metab = Number of likely metabolic reactions (optimum value < 8). The rules are: MW < 500, log *P* < 5, nHBD ≤ 5, nHBA ≤ 10. Compounds that satisfy these rules are considered drug-like.

^1H NMR, ^{13}C NMR and HRMS spectra of new compounds (6-45) ^1H NMR spectra of compound 6 ^{13}C NMR spectra of compound 6

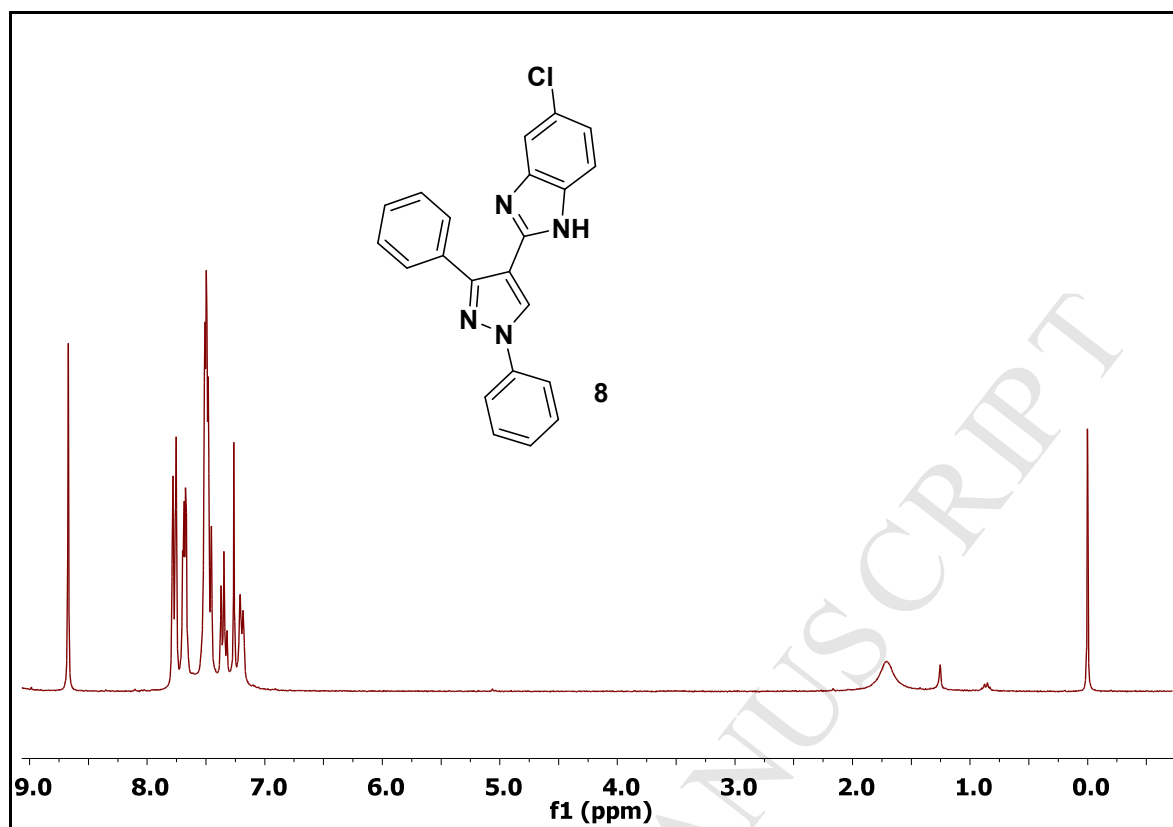
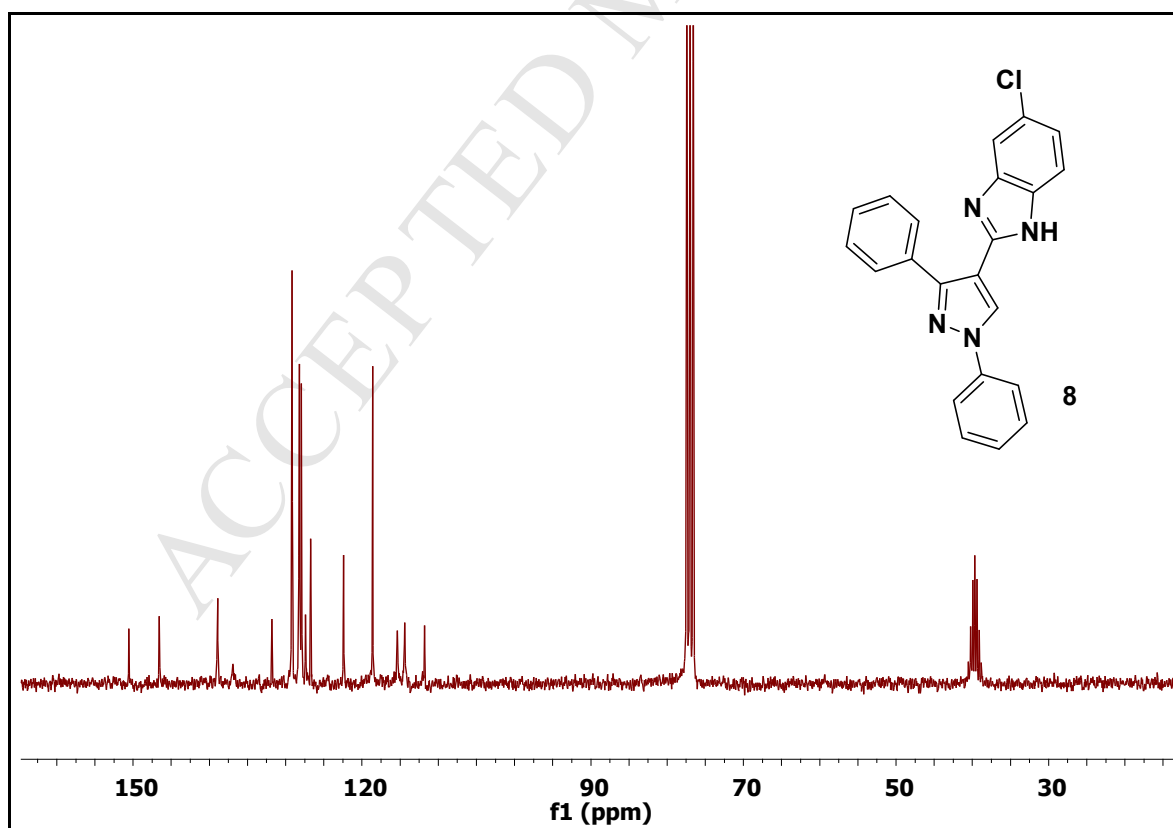


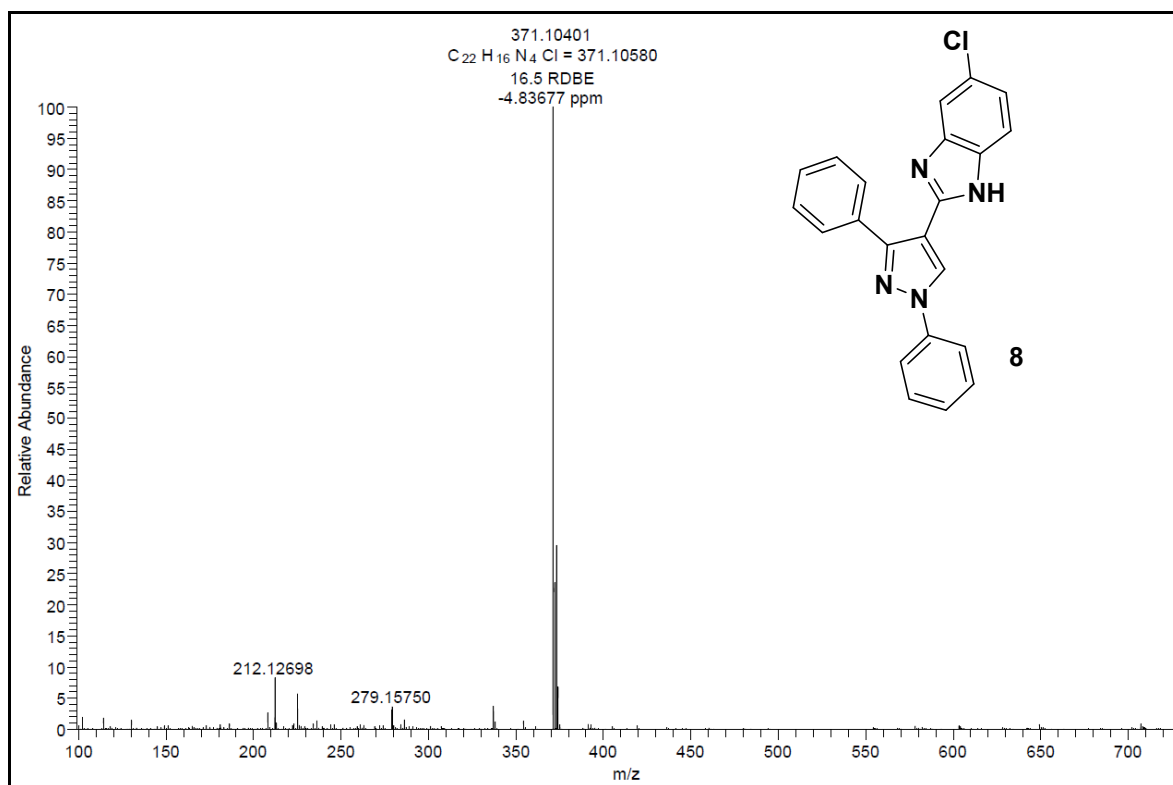
HRMS spectra of compound 6

¹H NMR spectra of compound 7

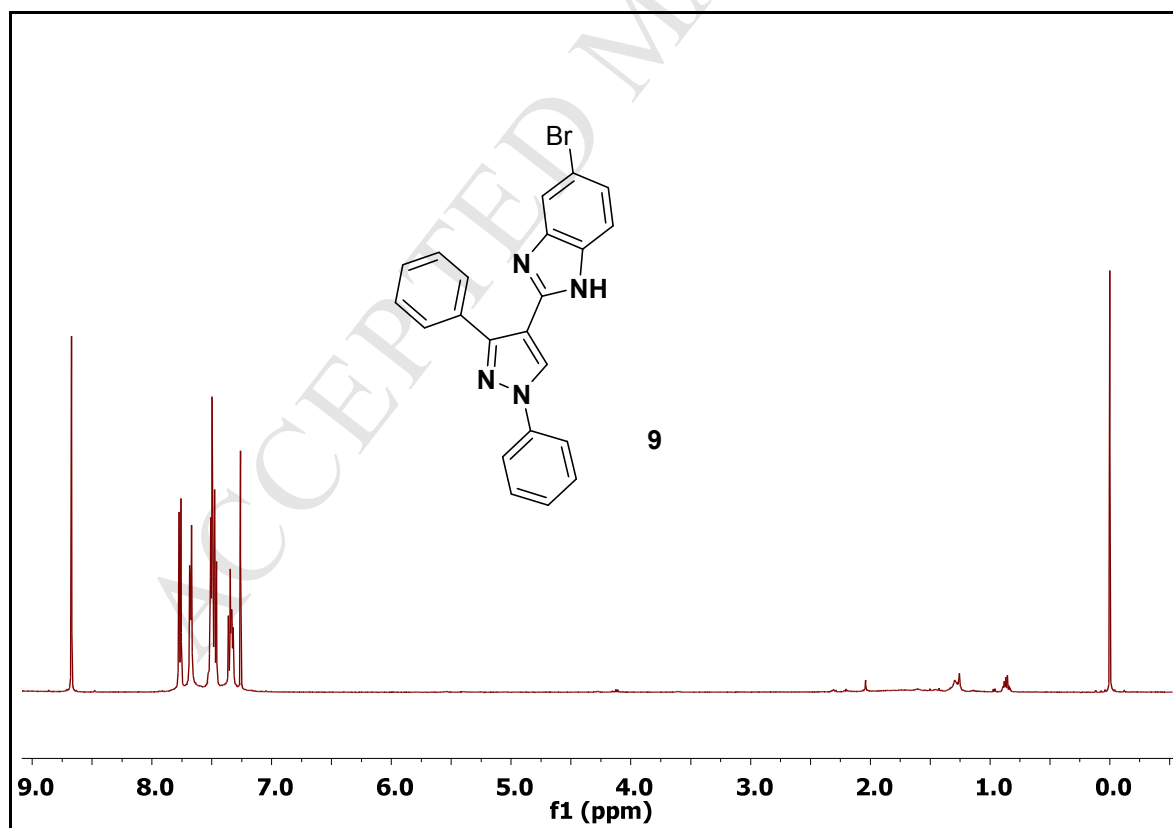
 ^{13}C NMR spectra of compound 7

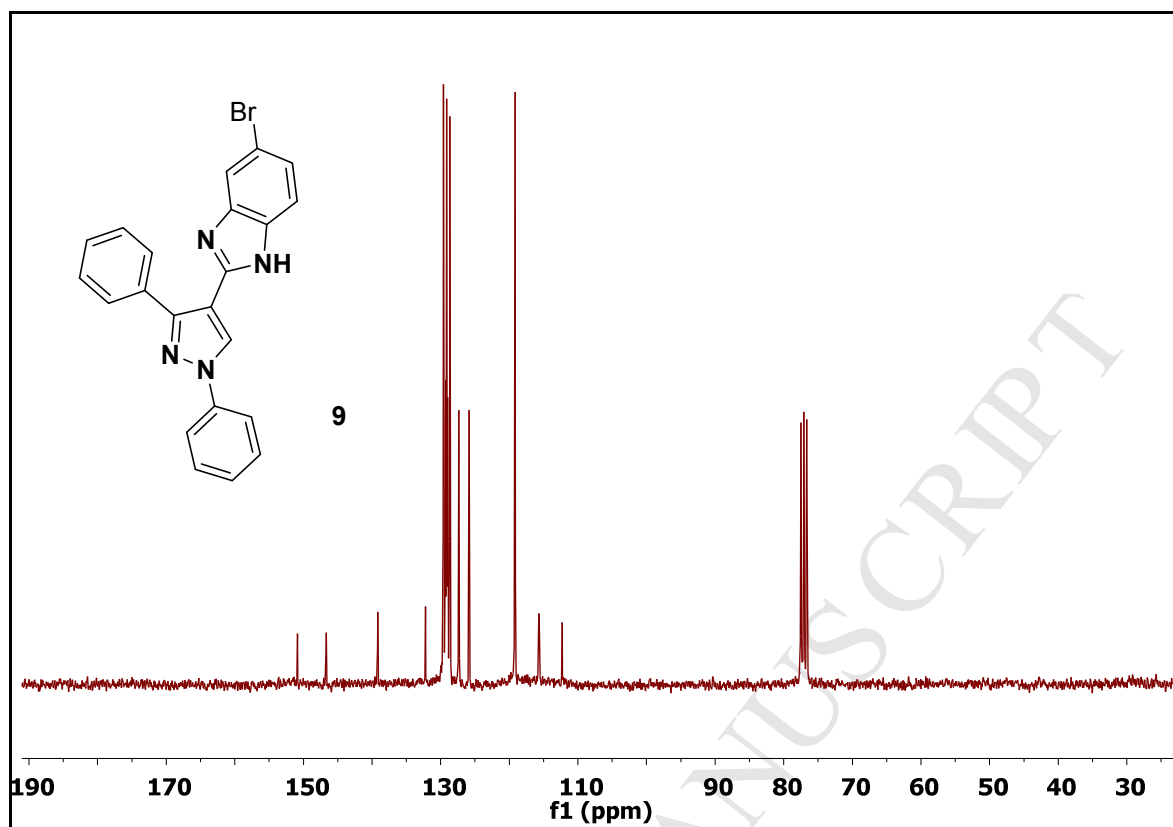
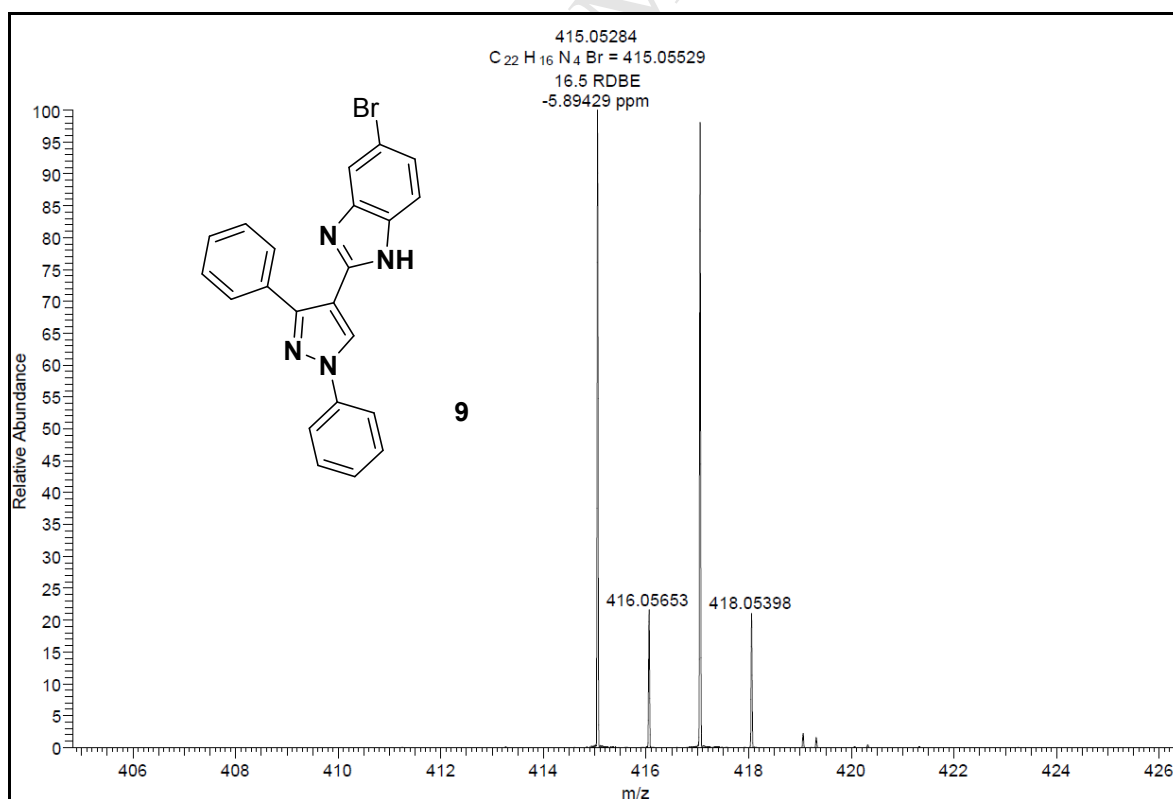
HRMS spectra of compound 7

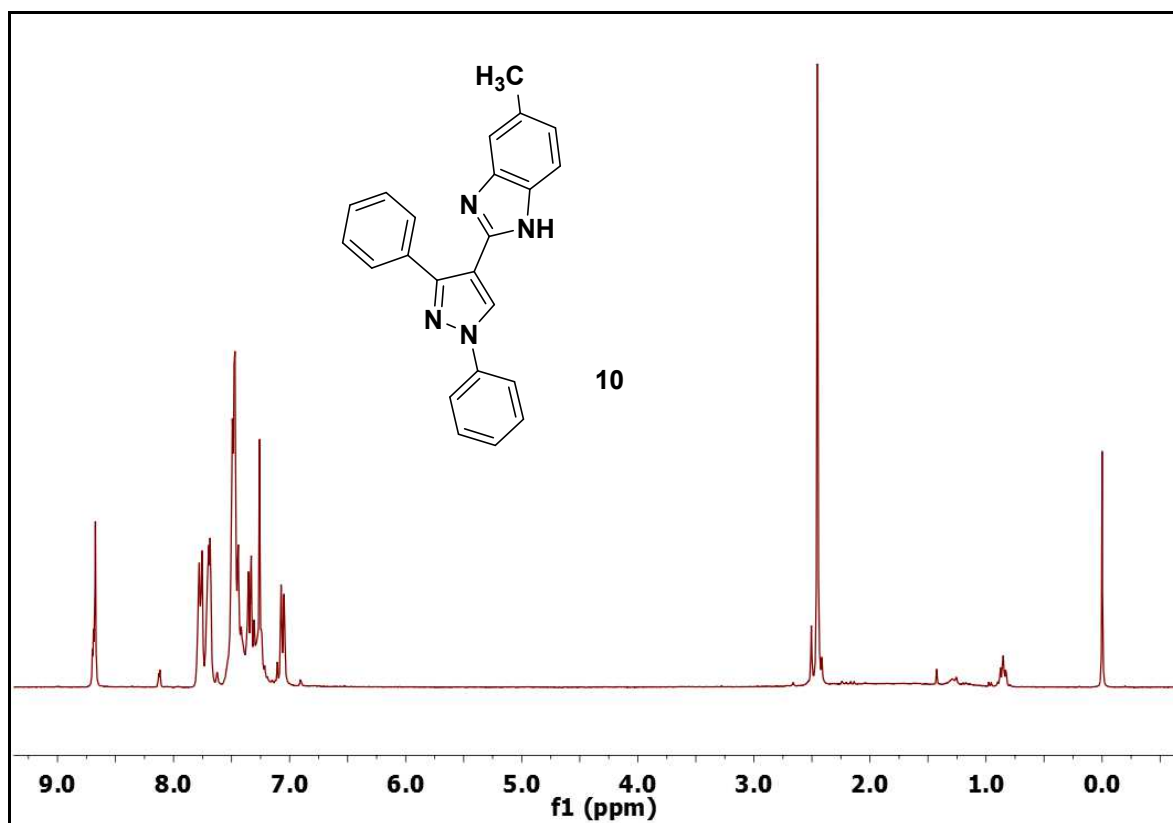
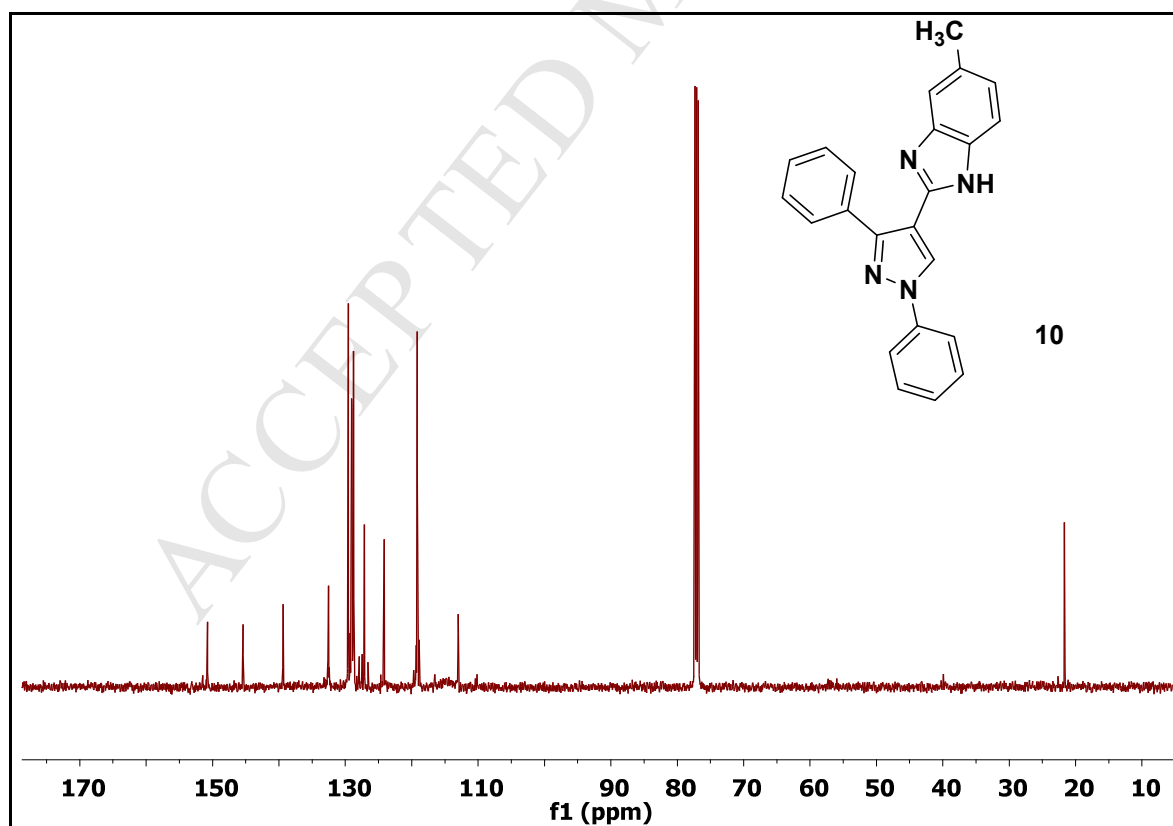
¹H NMR spectra of compound 8¹³C NMR spectra of compound 8

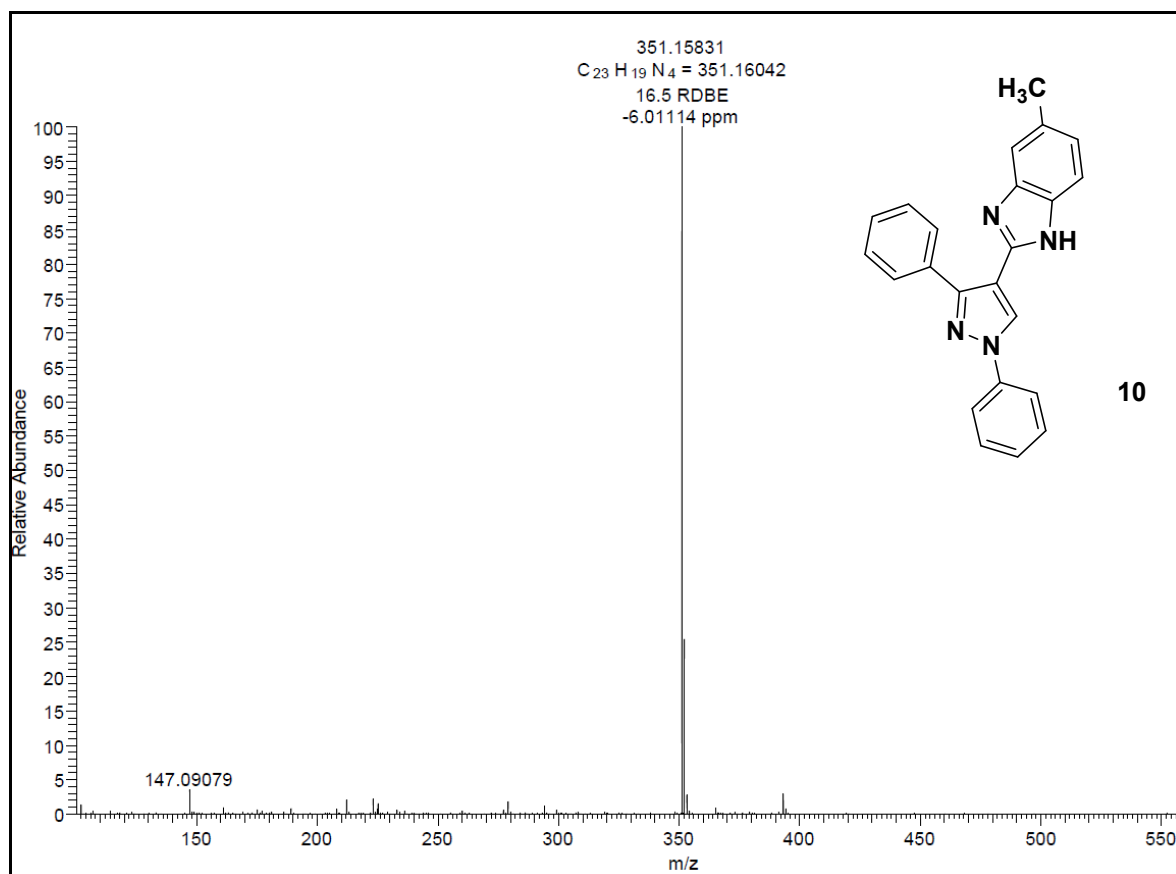
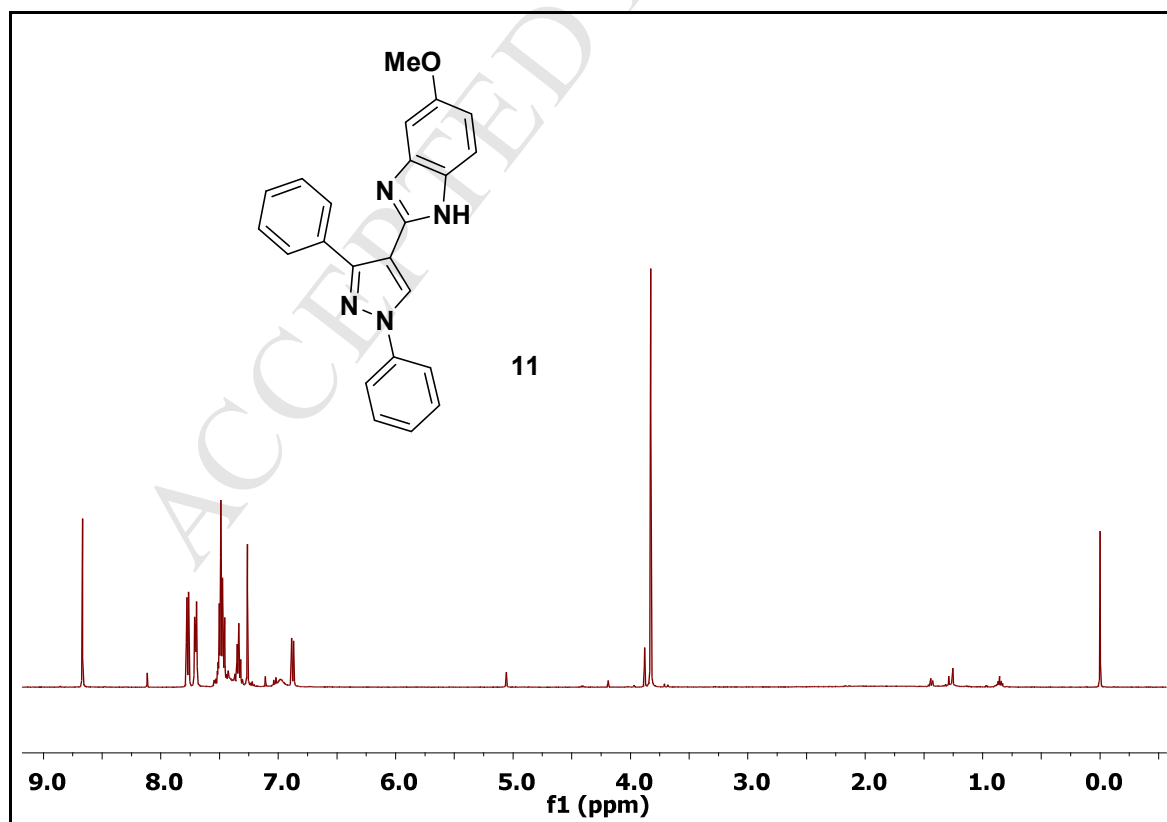


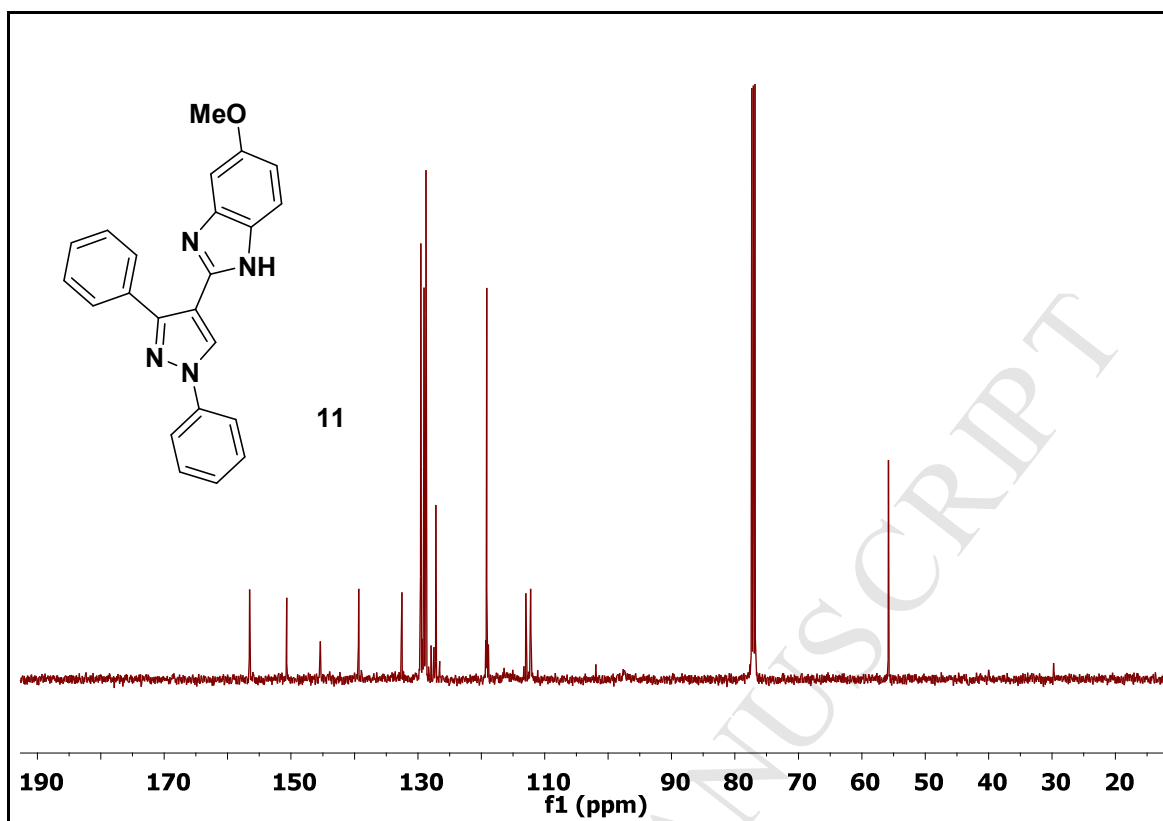
HRMS spectra of compound 8

¹H NMR spectra of compound 9

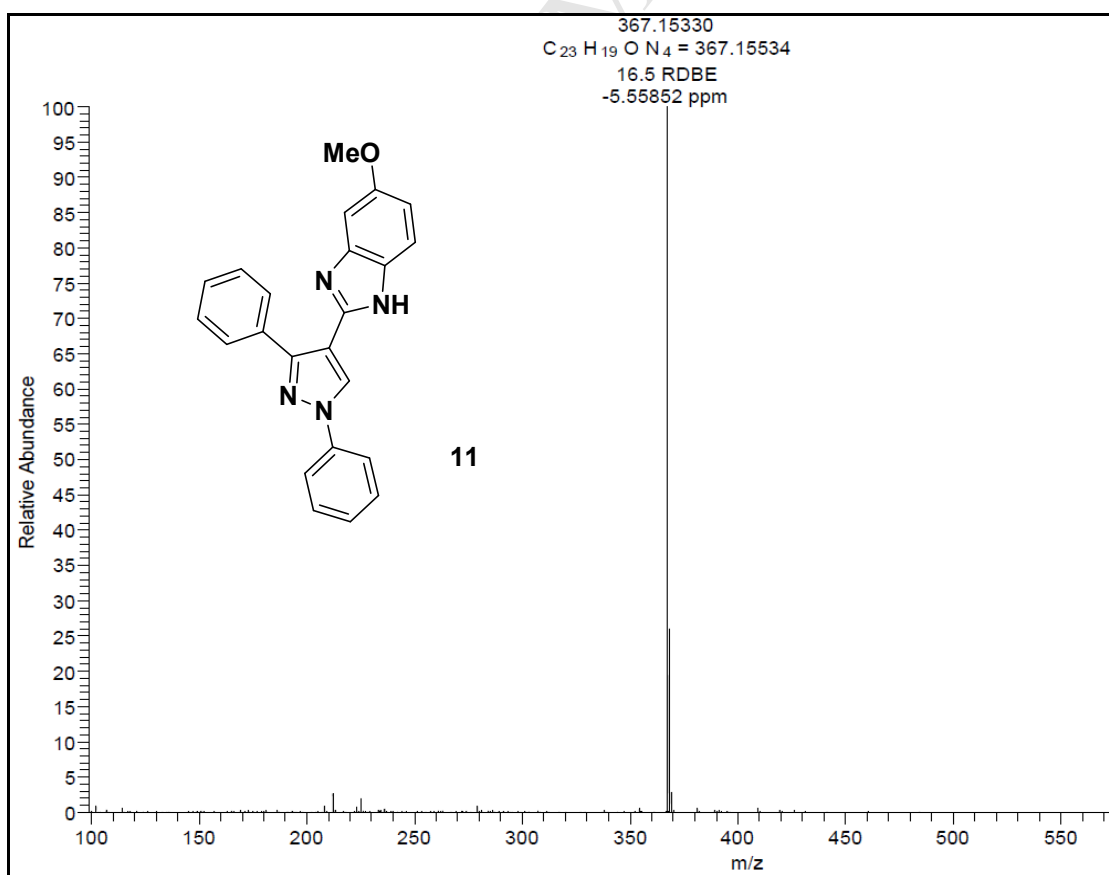
 ^{13}C NMR spectra of compound **9**HRMS spectra of compound **9**

 ^1H NMR spectra of compound 10 ^{13}C NMR spectra of compound 10

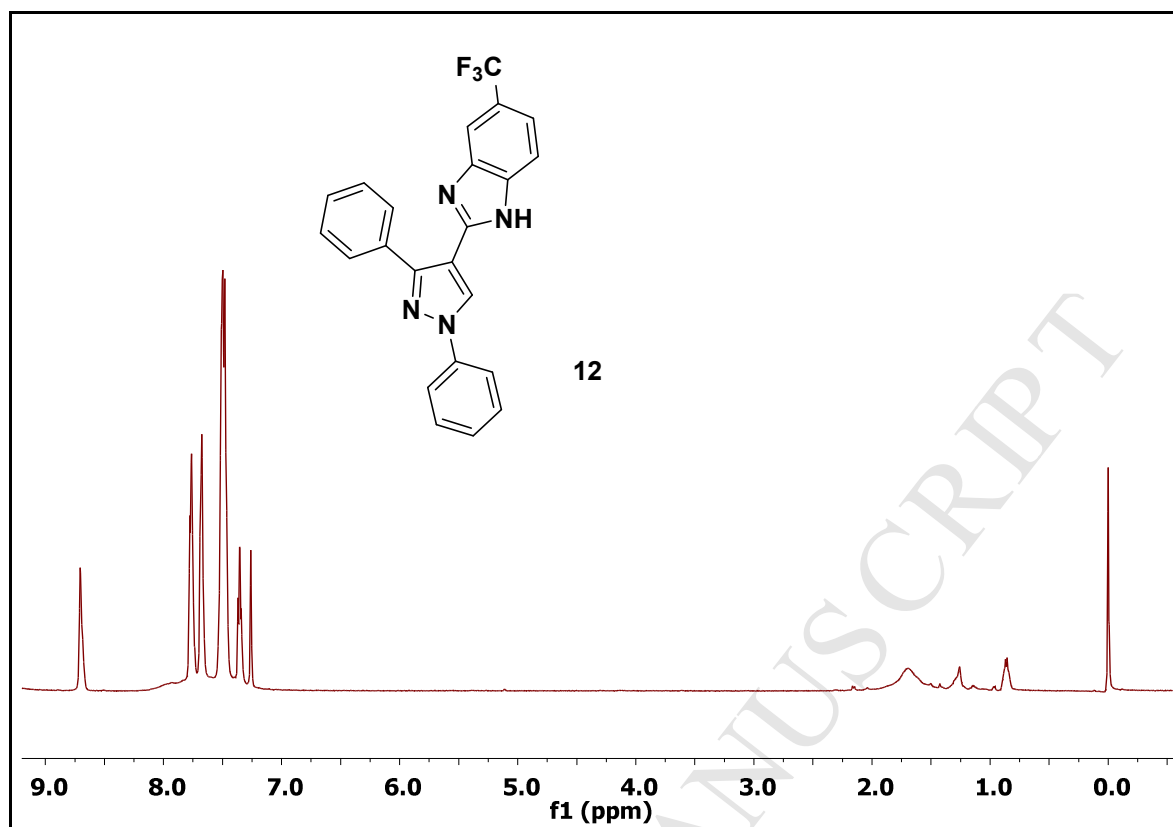
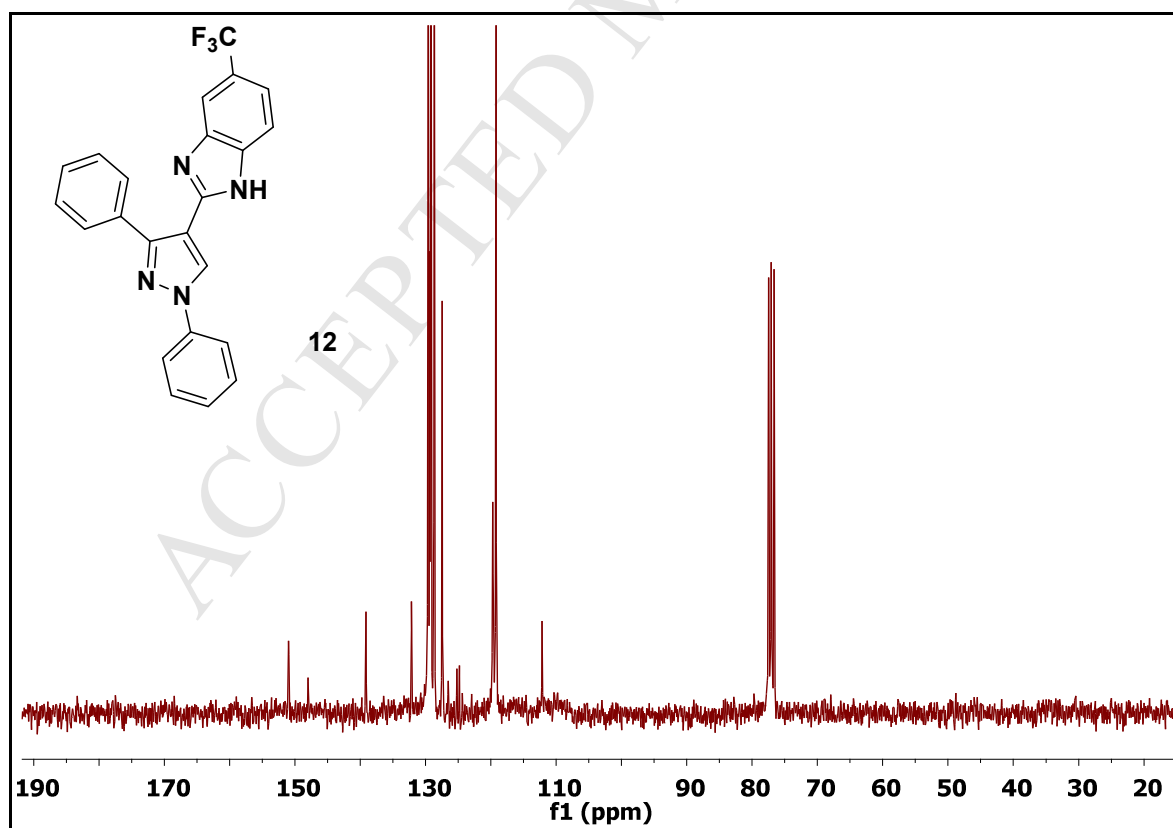
HRMS spectra of compound **10** 1H NMR spectra of compound **11**

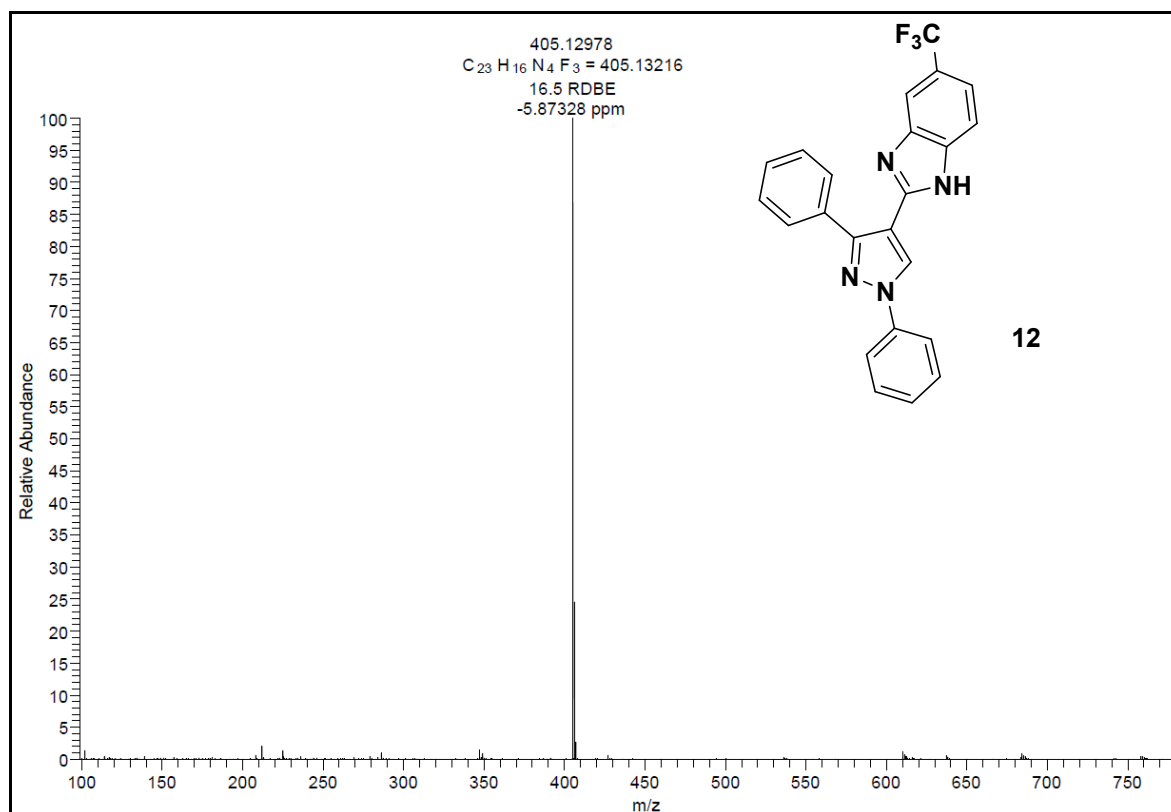


¹³C NMR spectra of compound **11**

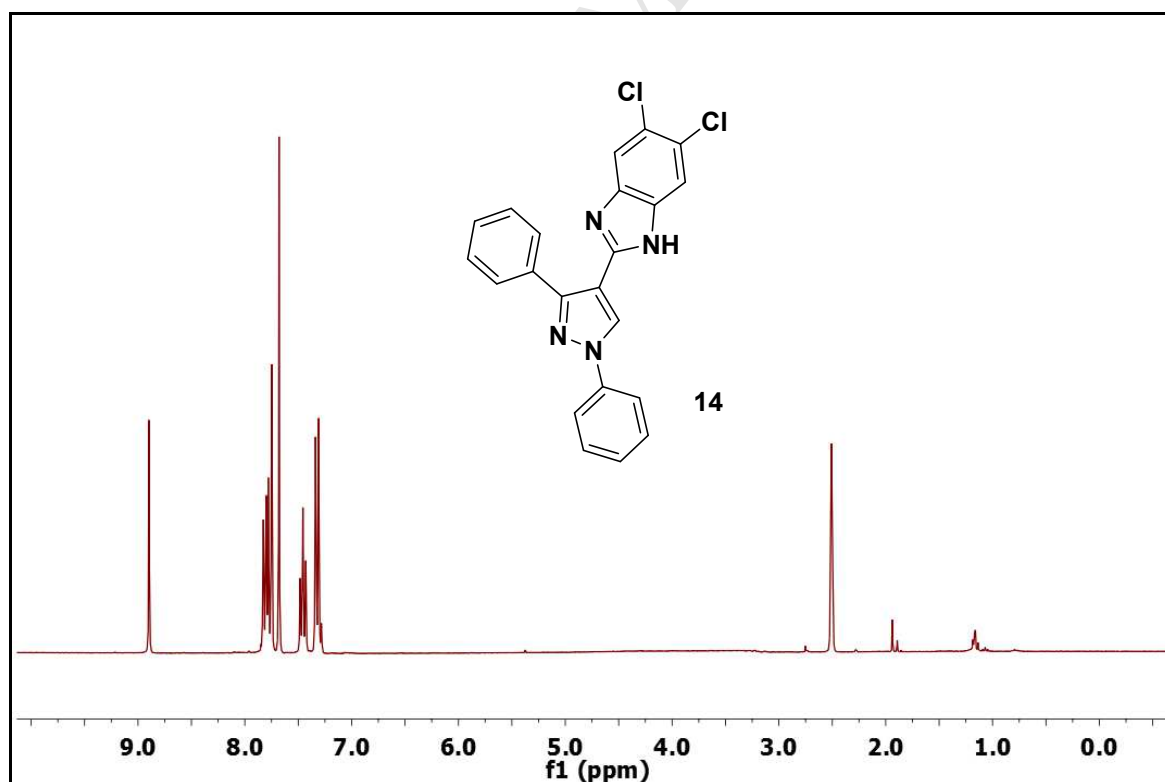


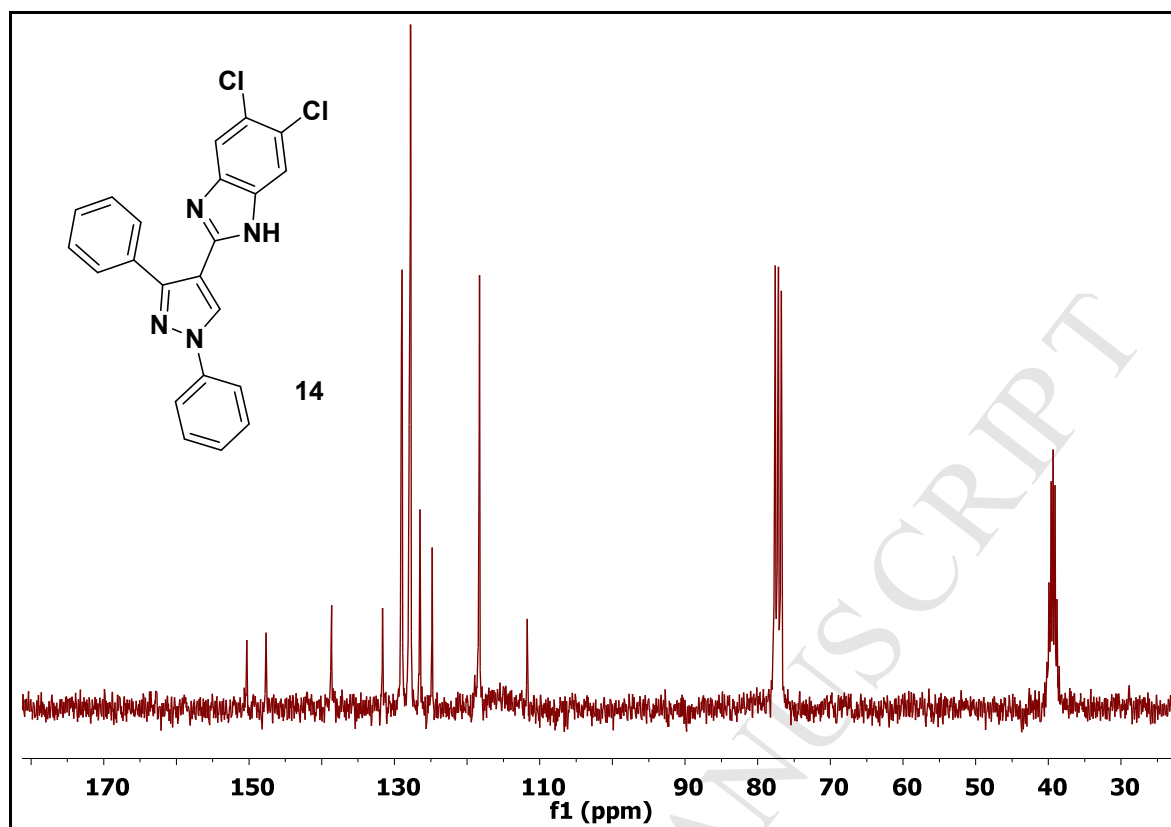
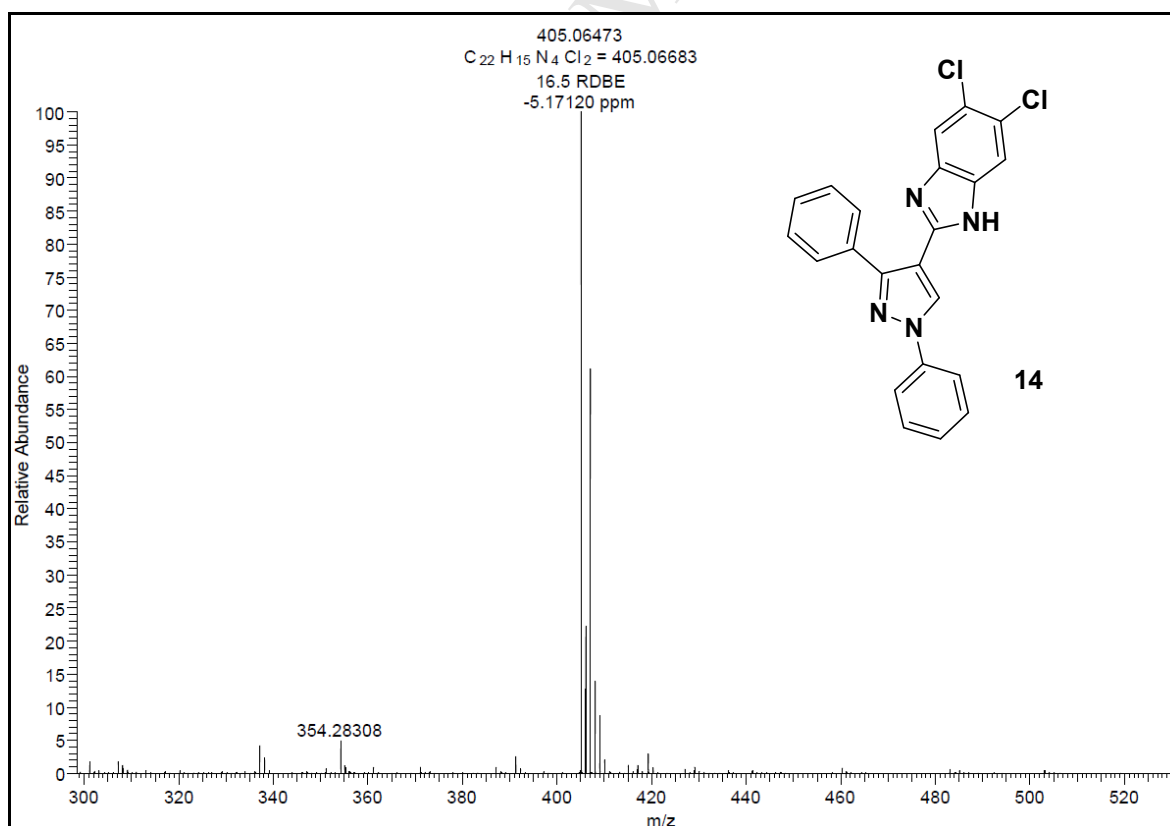
HRMS spectra of compound **11**

 ^1H NMR spectra of compound 12 ^{13}C NMR spectra of compound 12

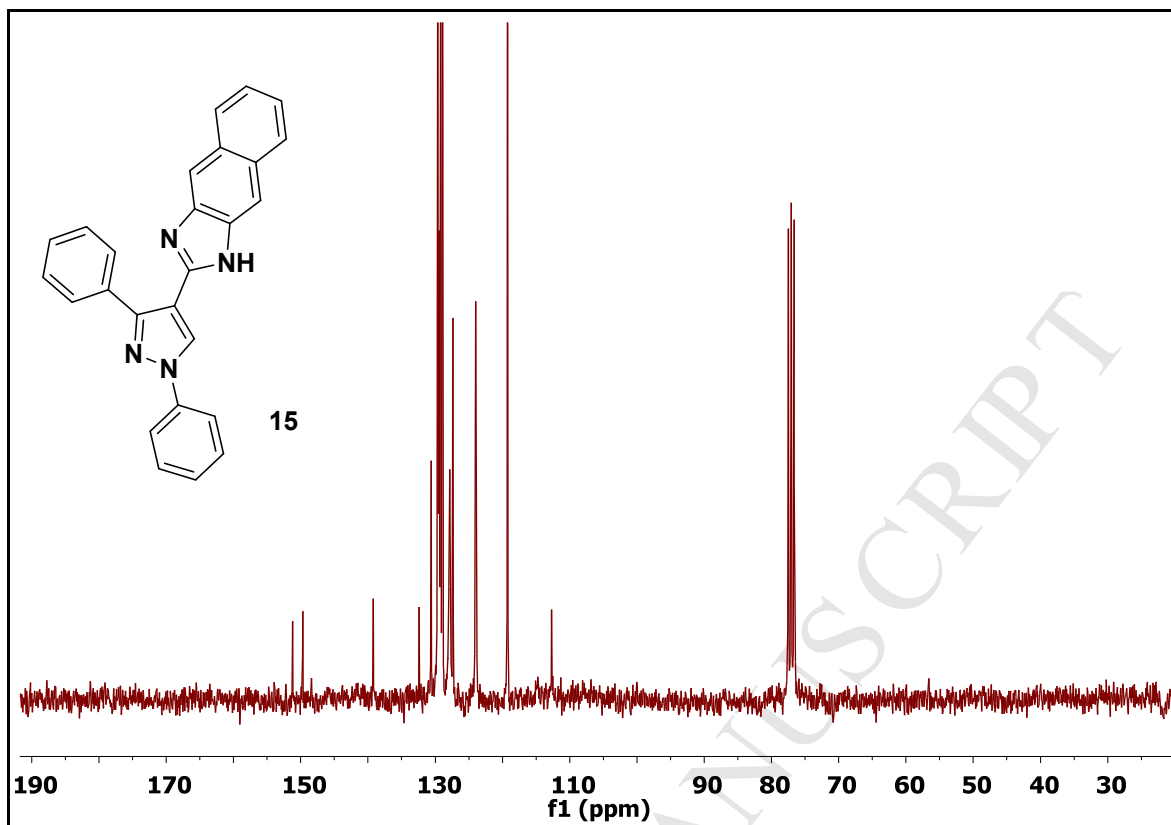
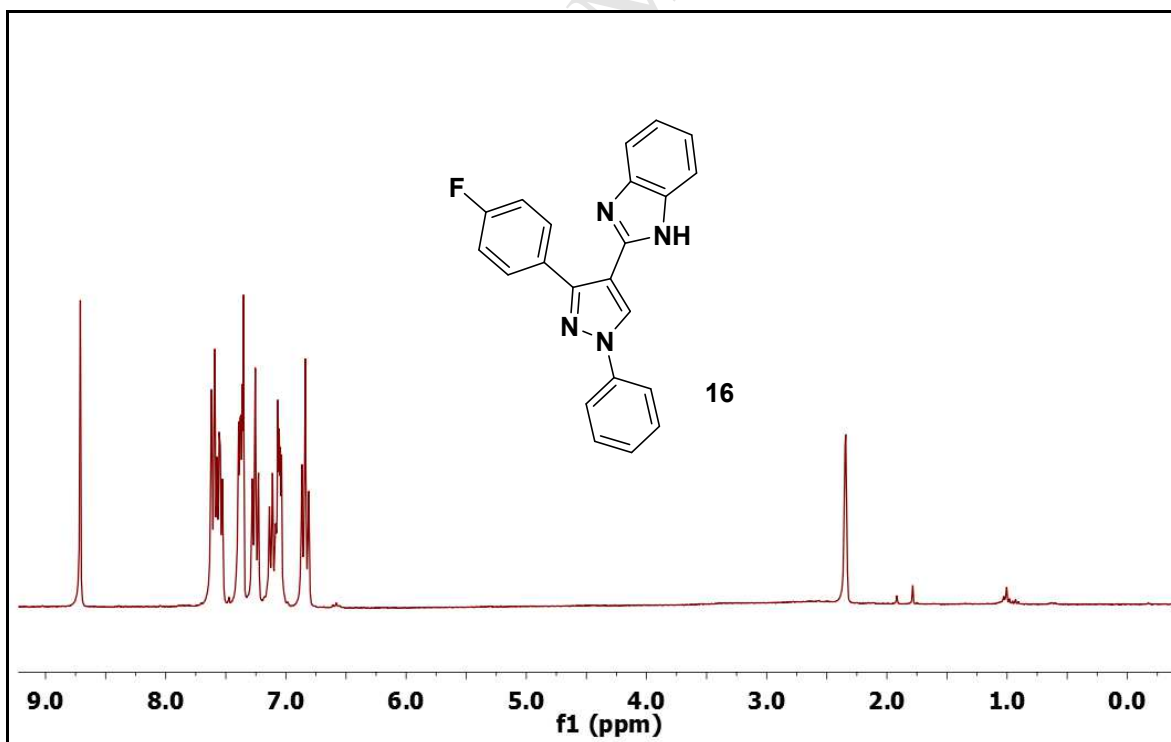


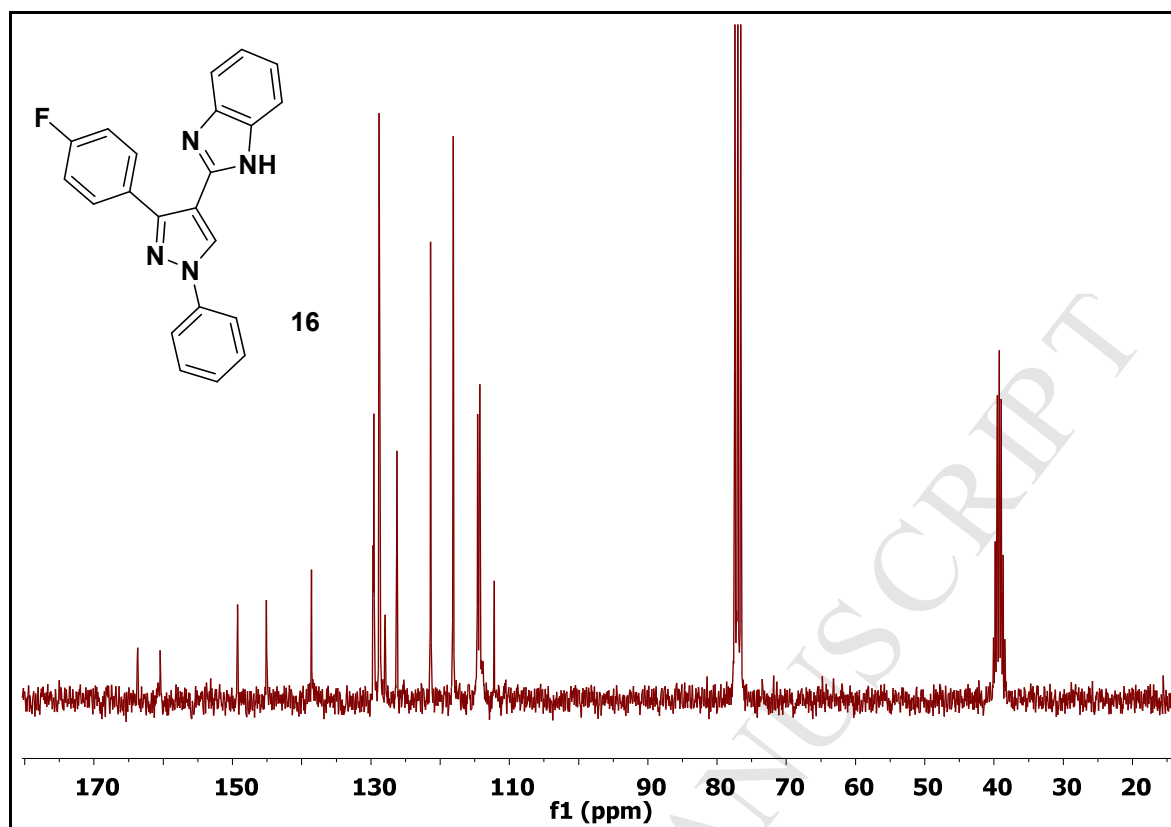
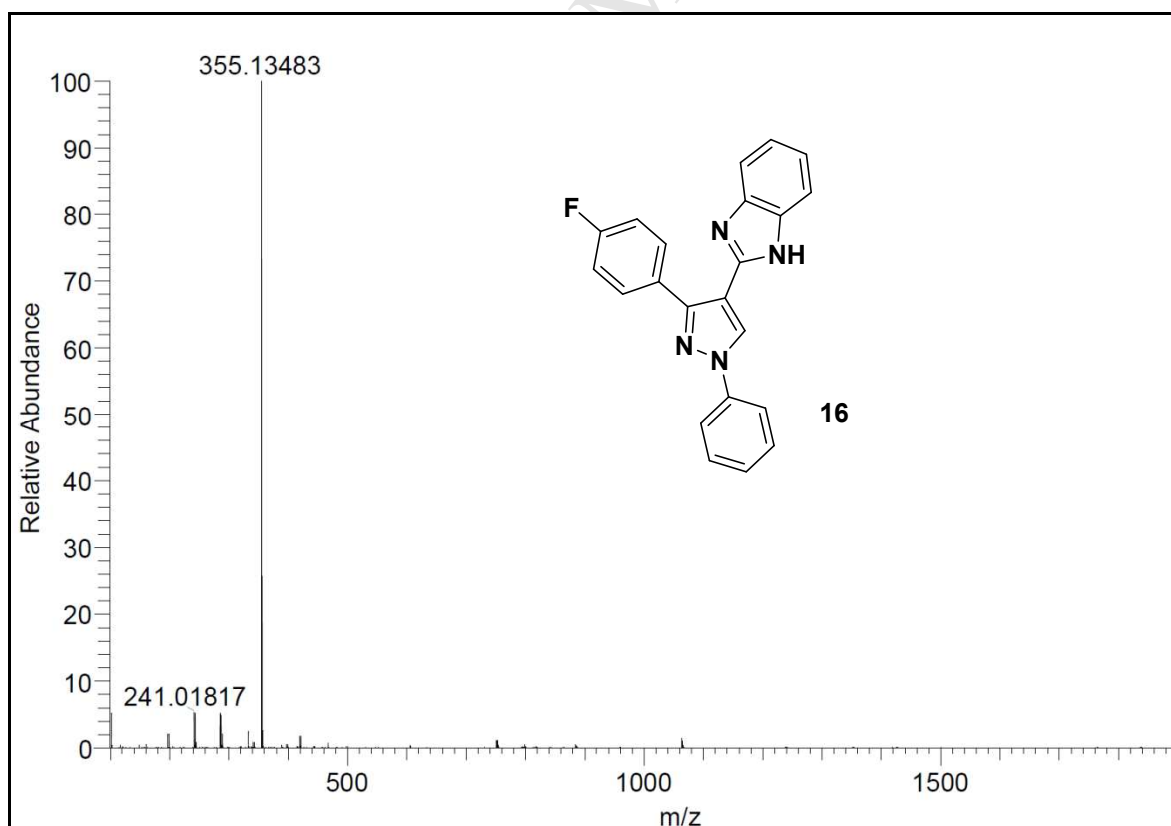
HRMS spectra of compound 12

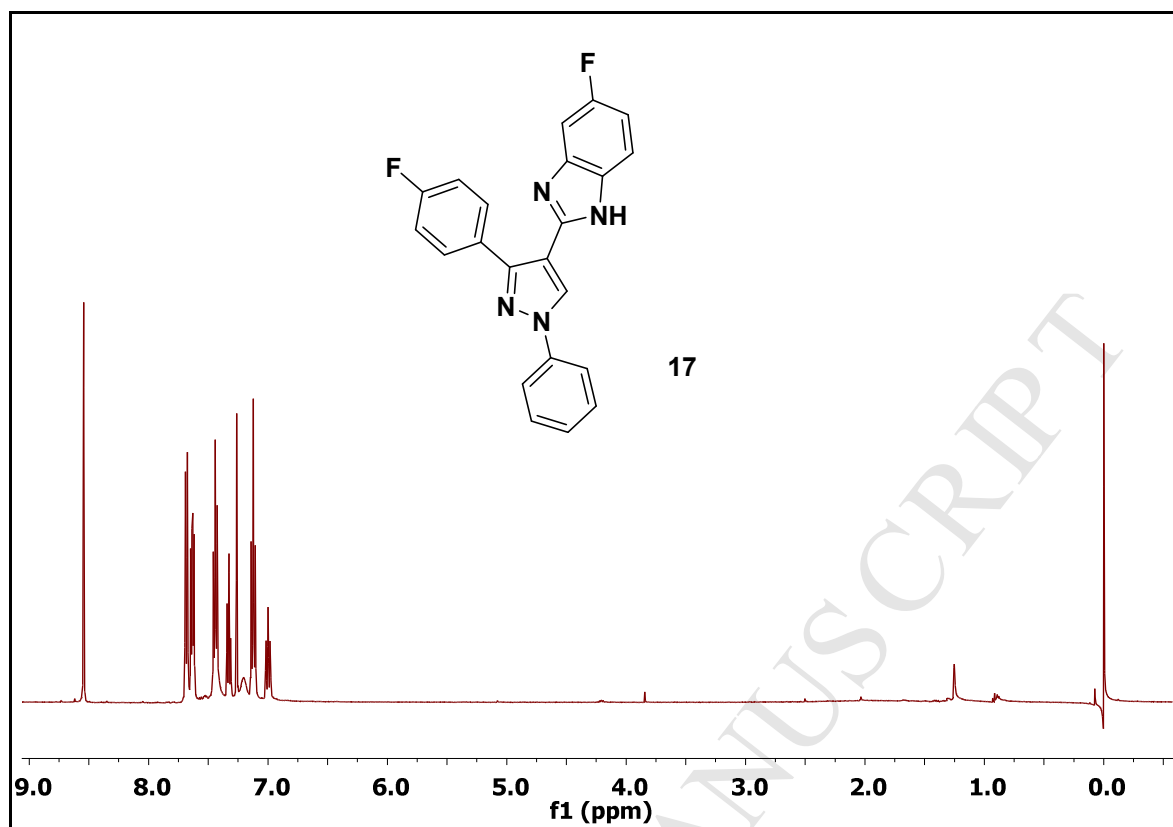
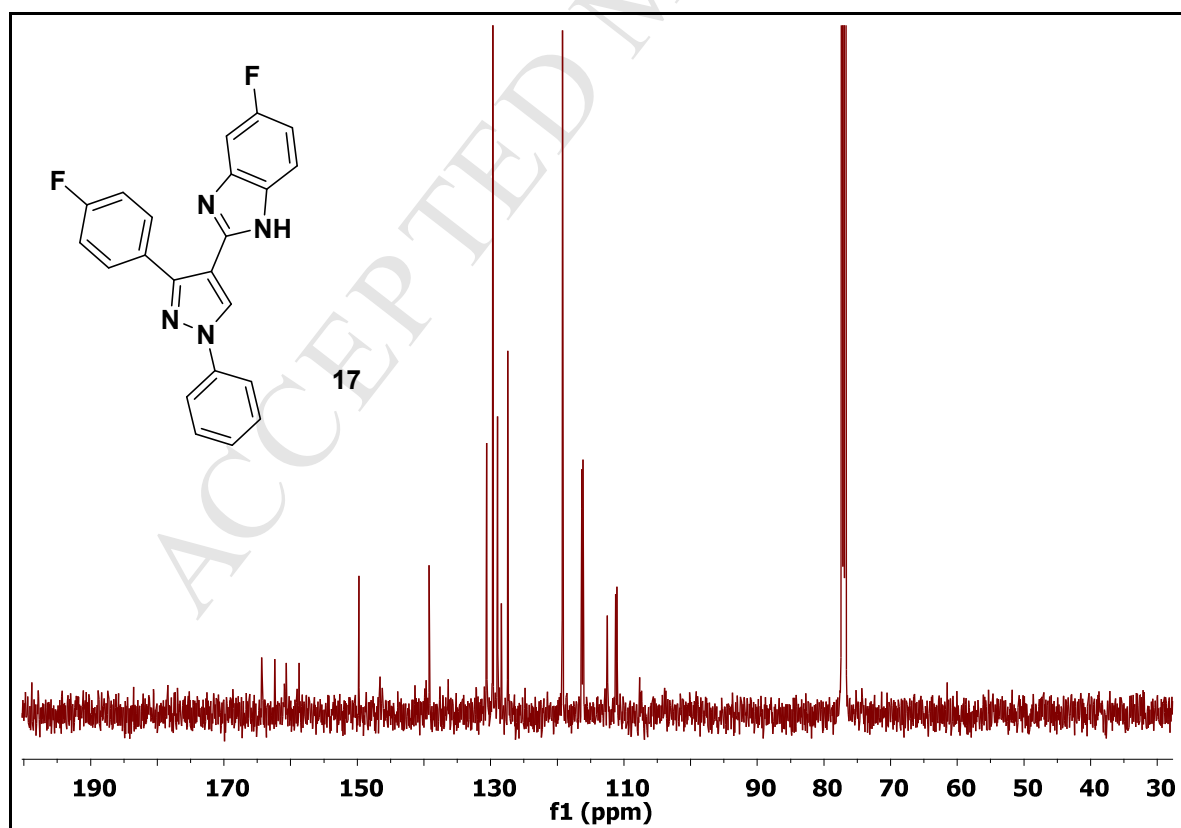
¹H NMR spectra of compound 14

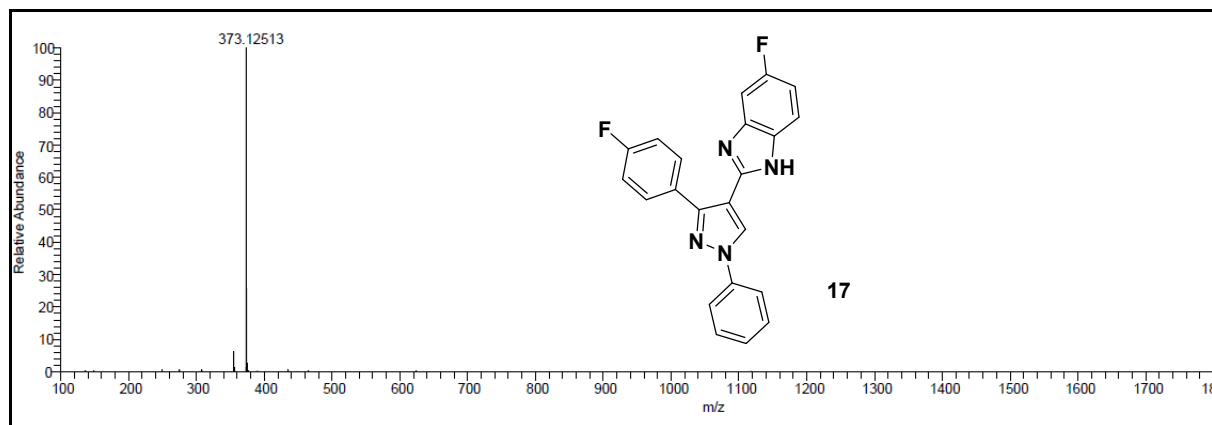
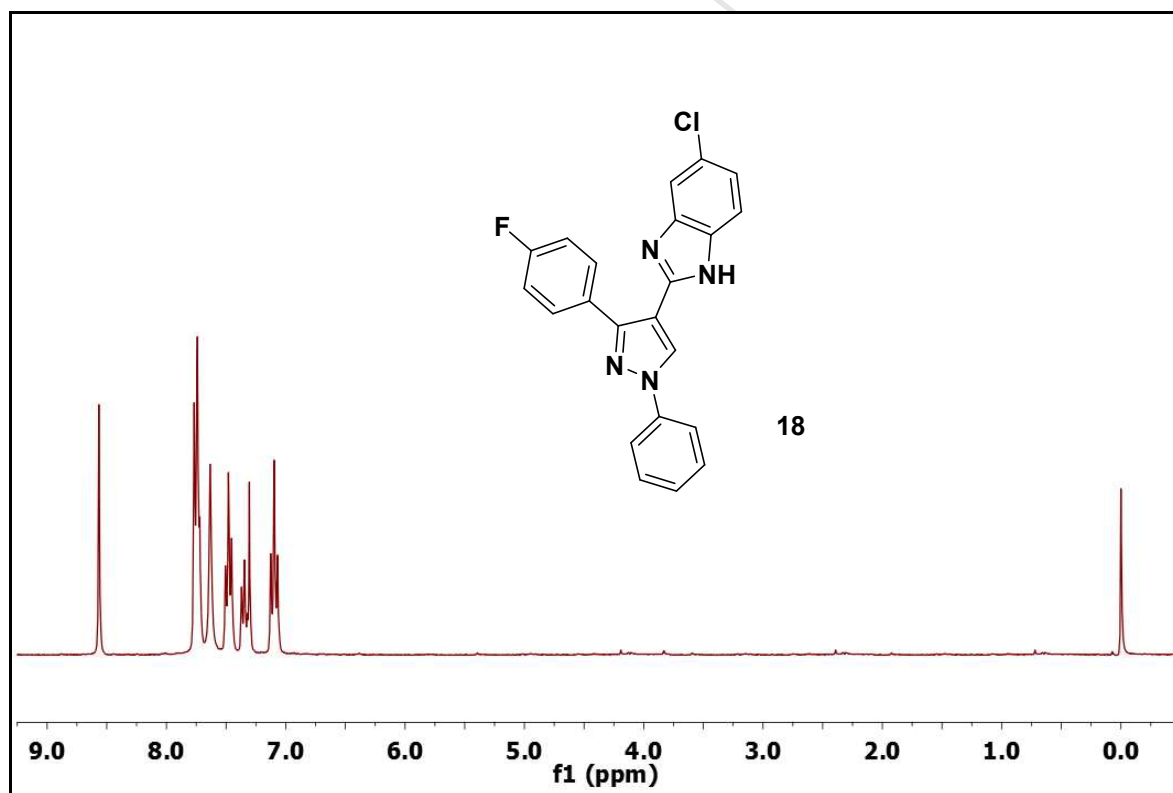
¹³C NMR spectra of compound 14

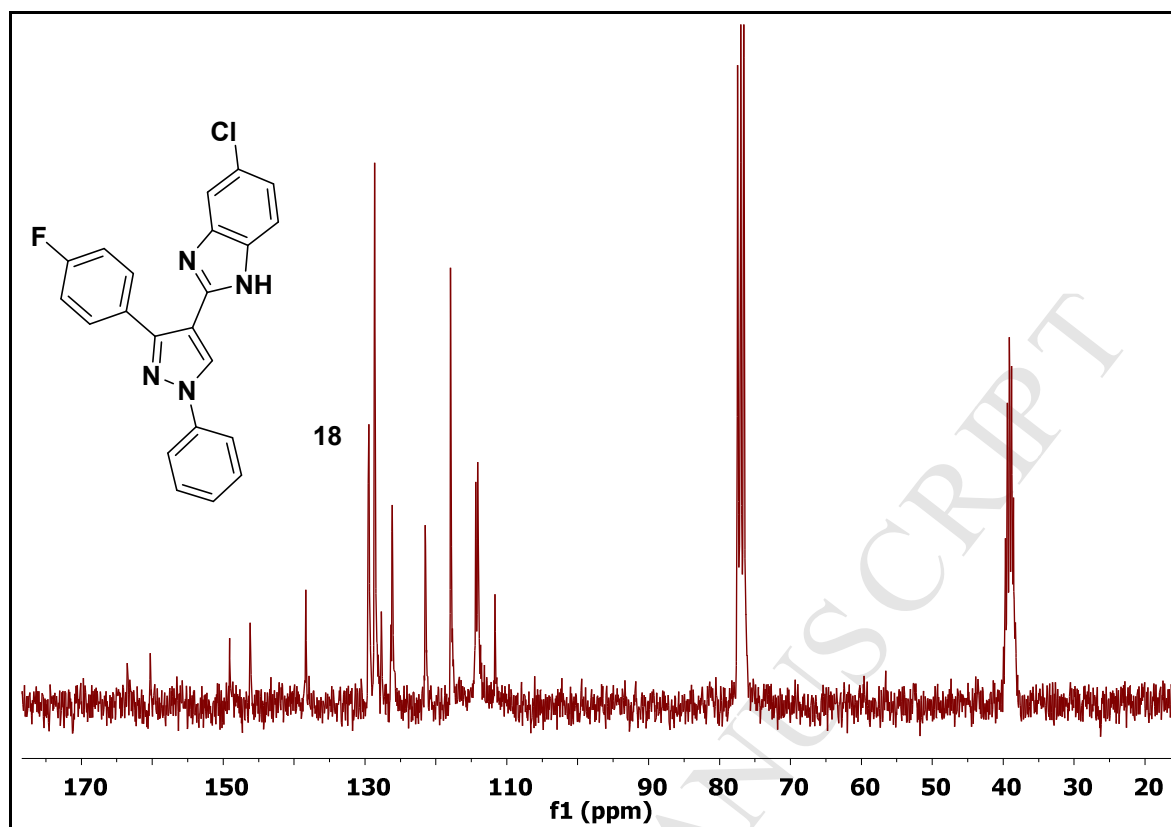
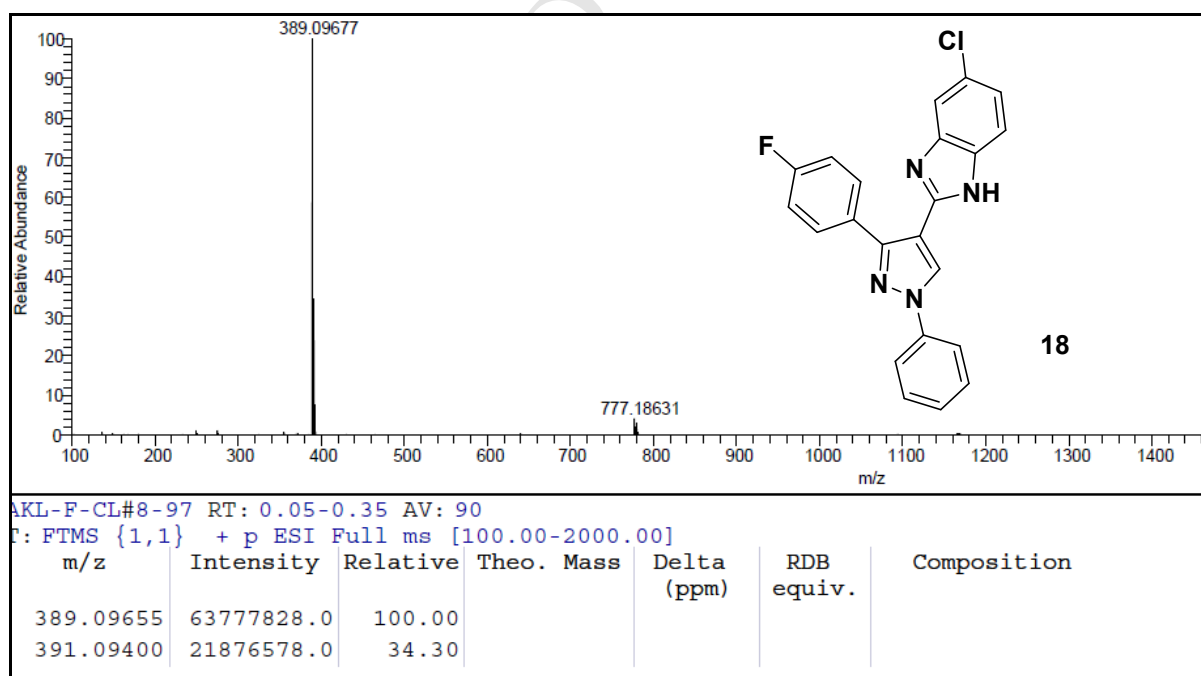
HRMS spectra of compound 14

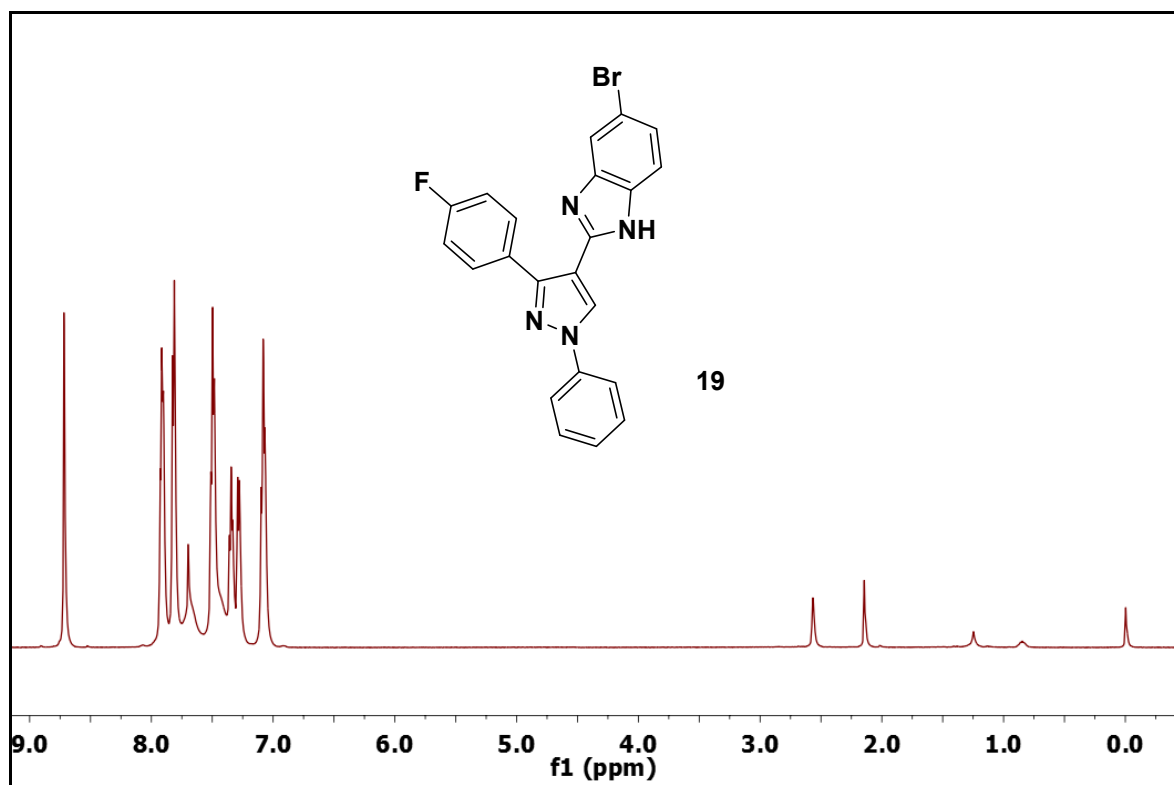
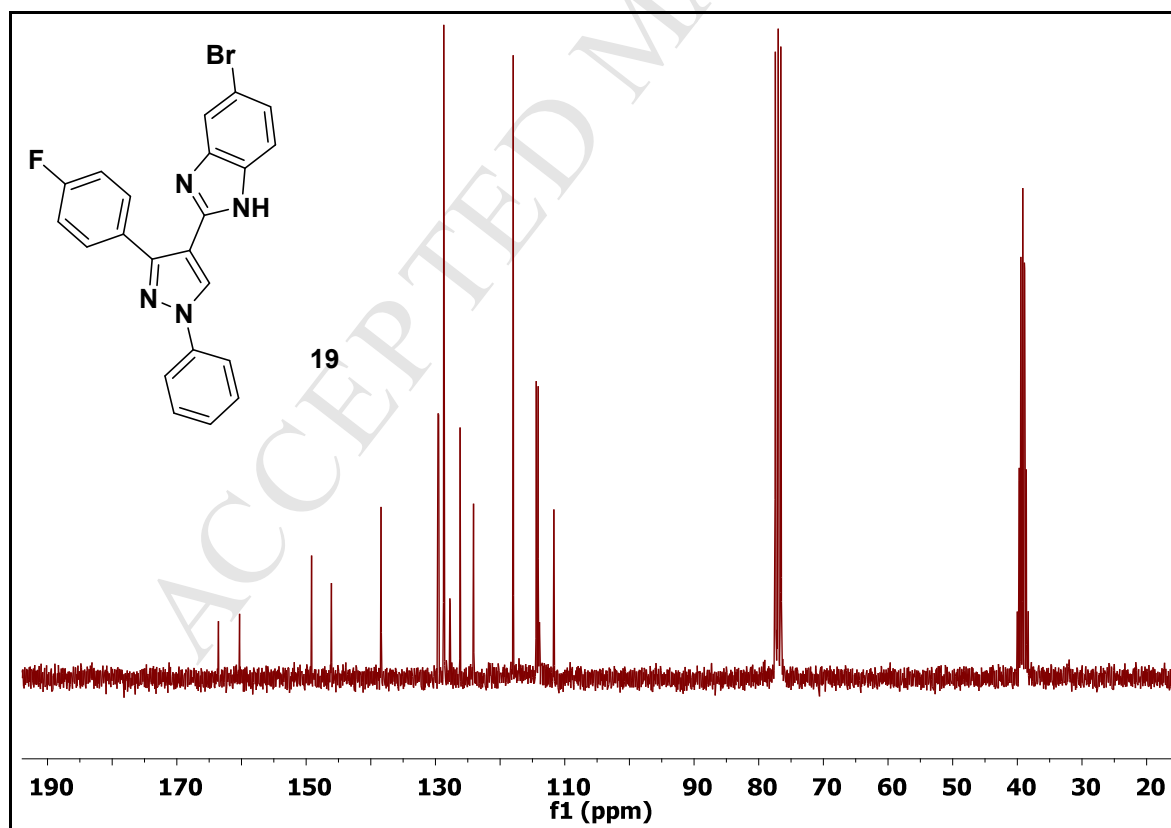
 ^{13}C NMR spectra of compound 15 ^1H NMR spectra of compound 16

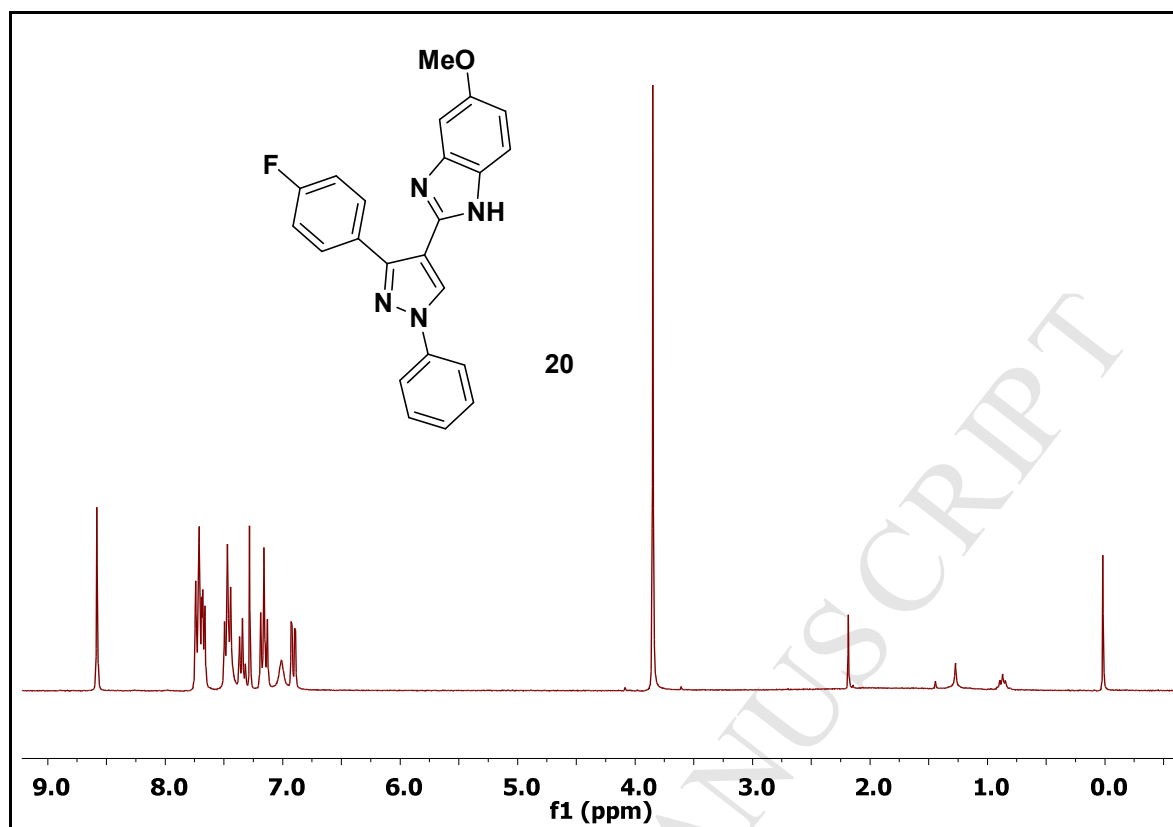
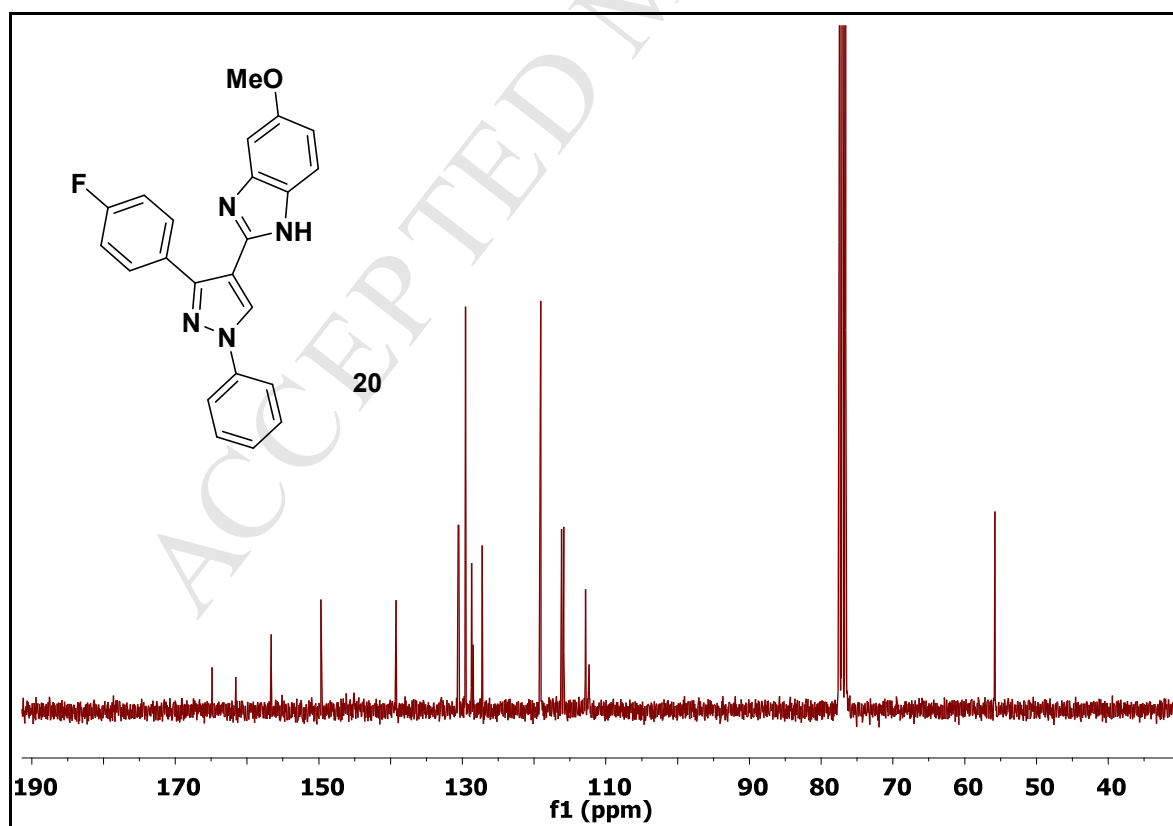
 ^{13}C NMR spectra of compound **16**HRMS spectra of compound **16**

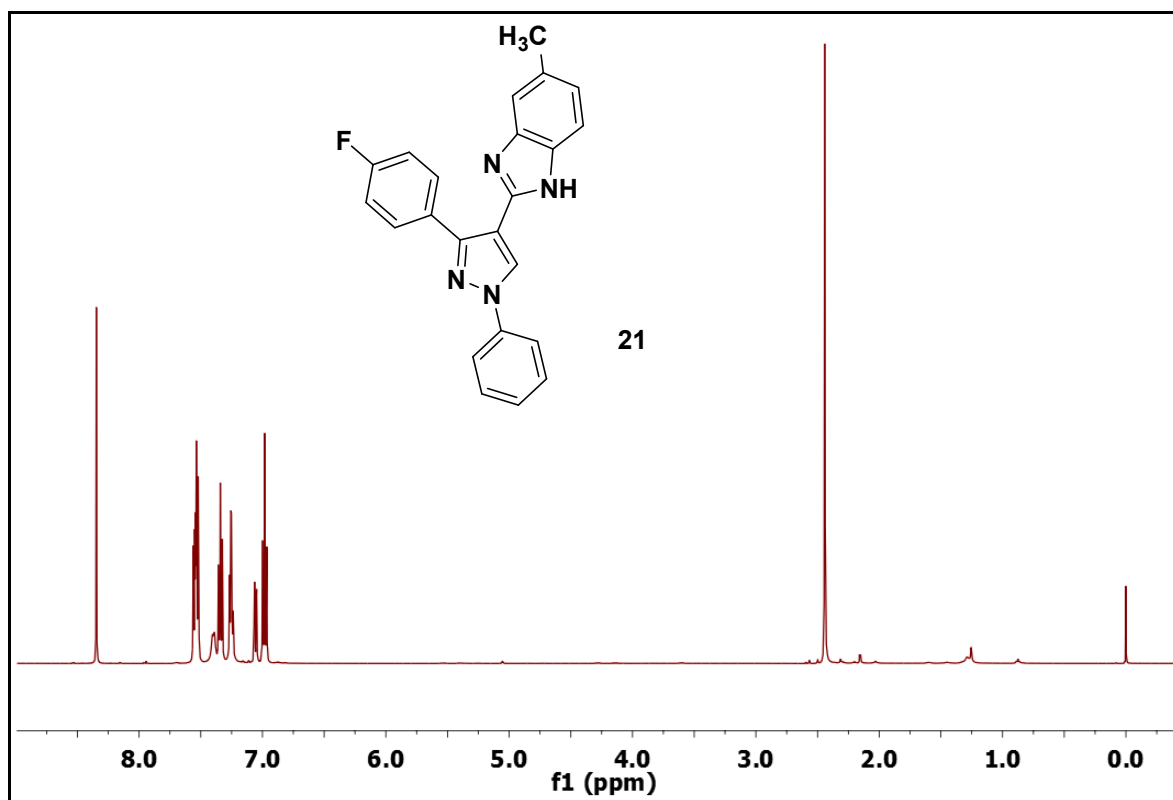
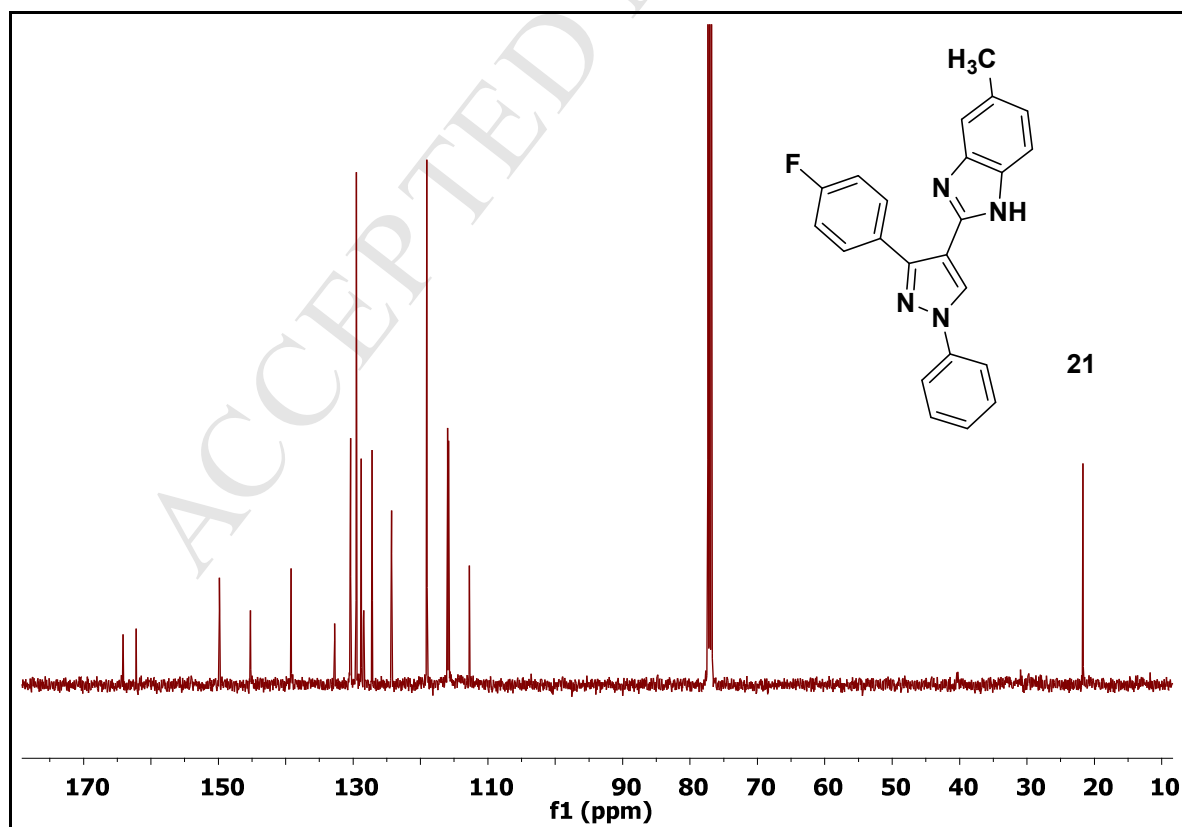
 ^1H NMR spectra of compound 17 ^{13}C NMR spectra of compound 17

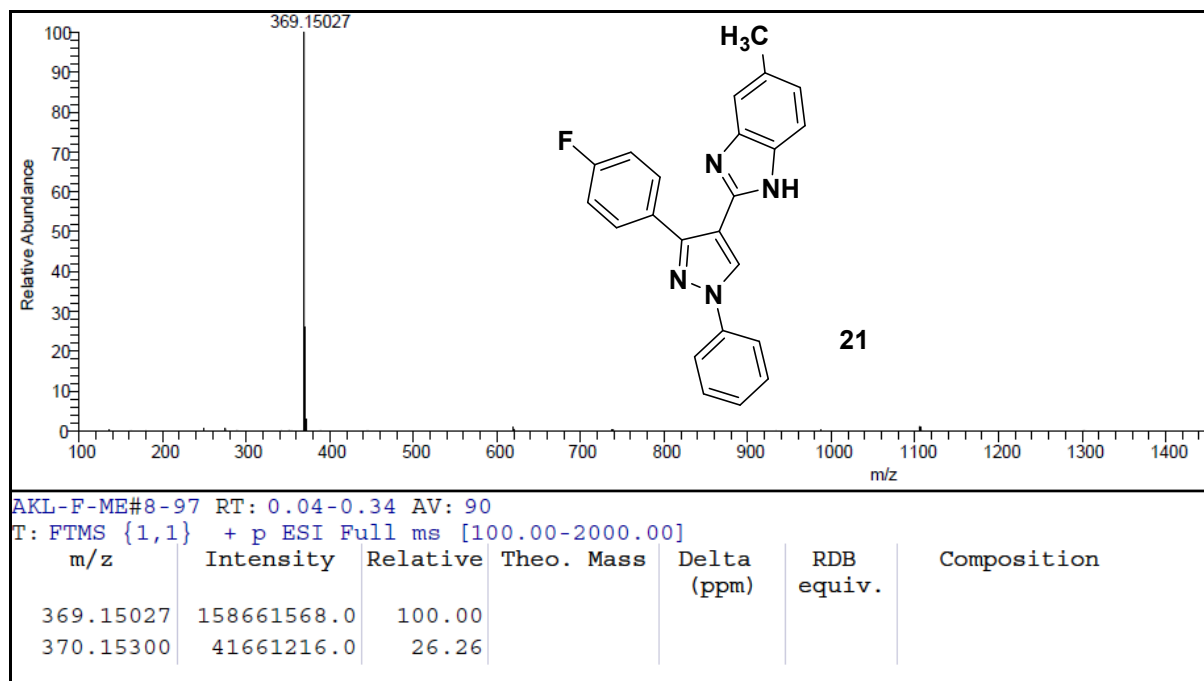
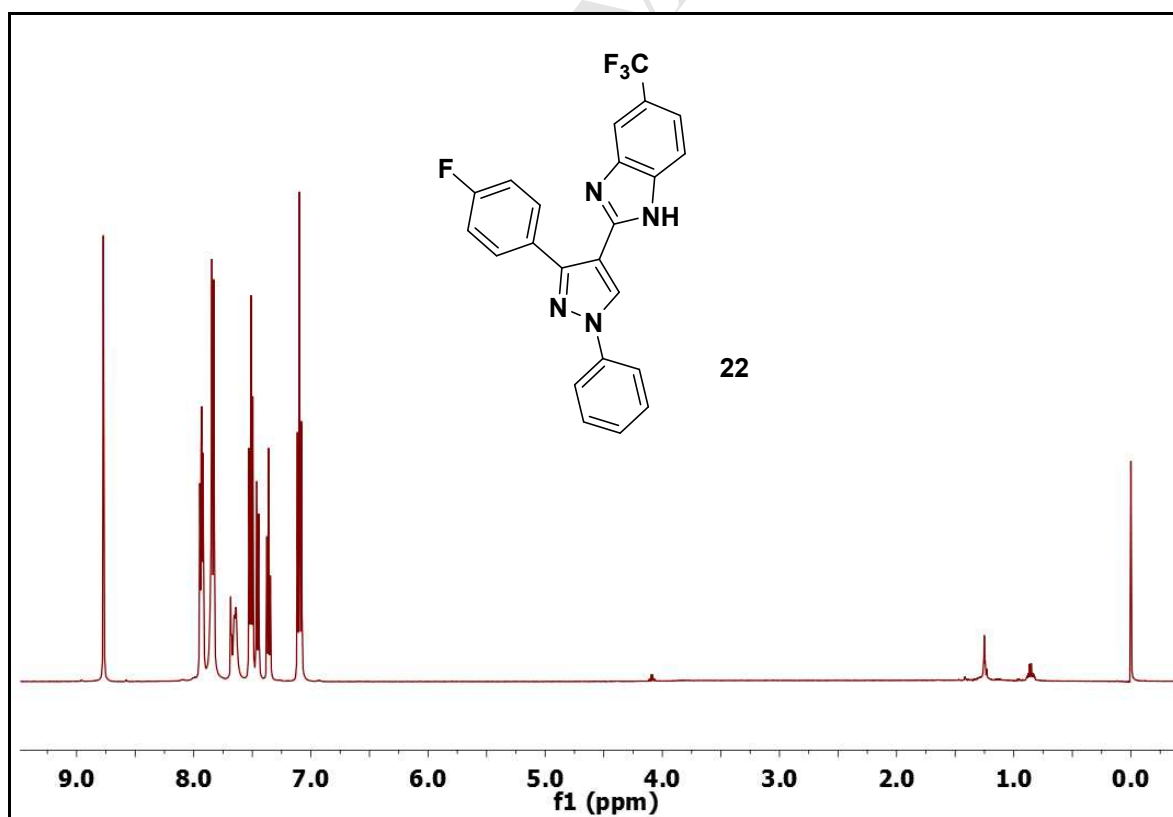
HRMS spectra of compound **17**¹H NMR spectra of compound **18**

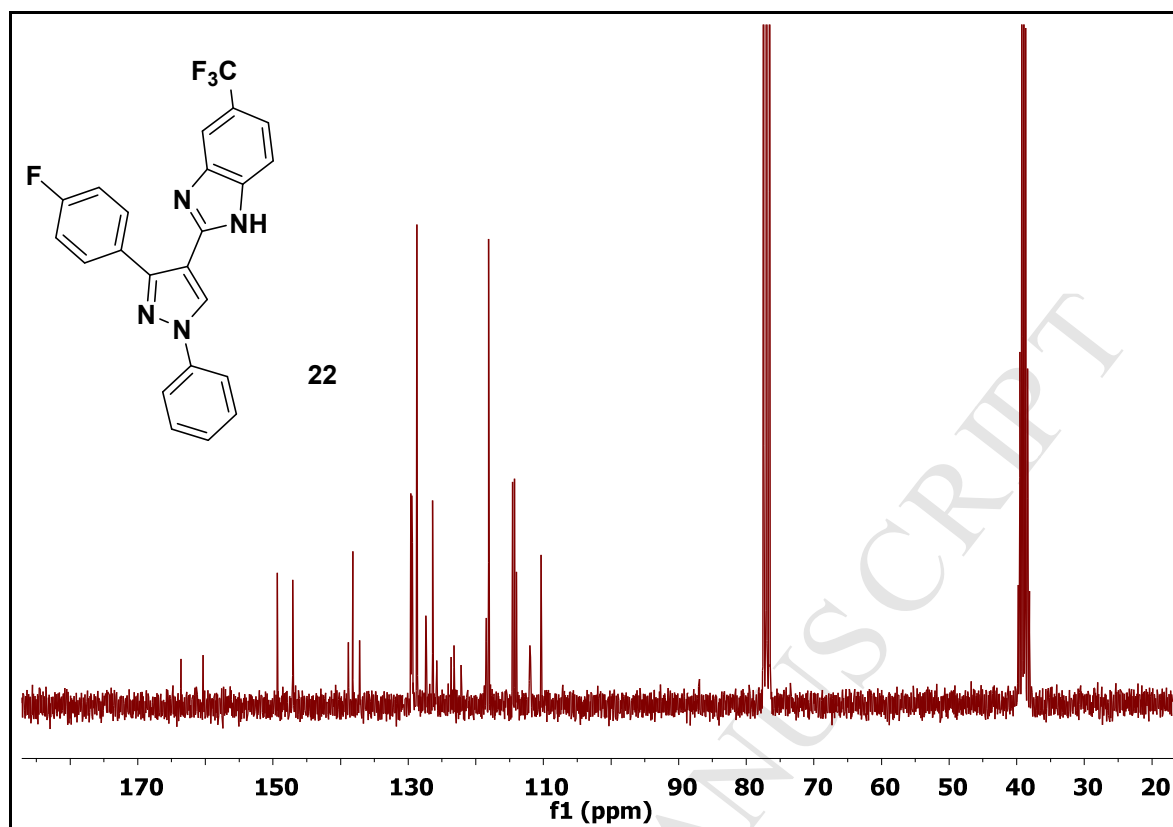
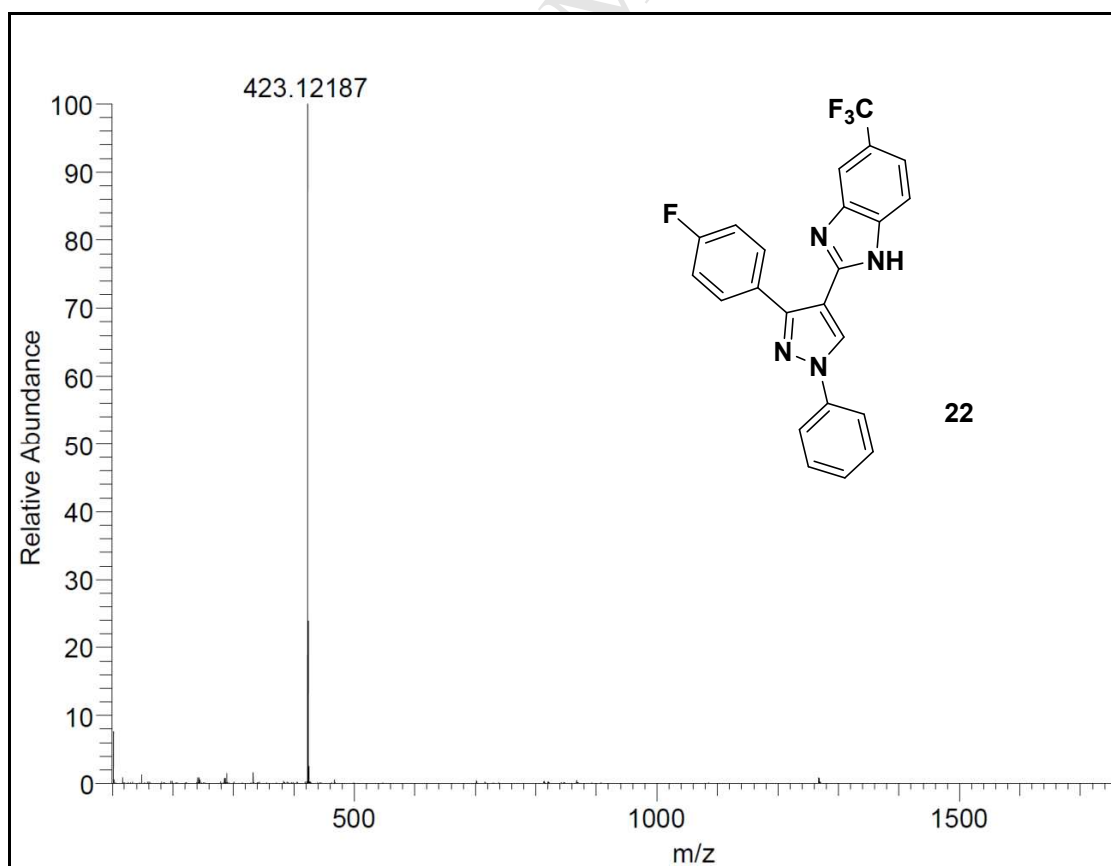
¹³C NMR spectra of compound **18**HRMS spectra of compound **18**

¹H NMR spectra of compound 19¹³C NMR spectra of compound 19

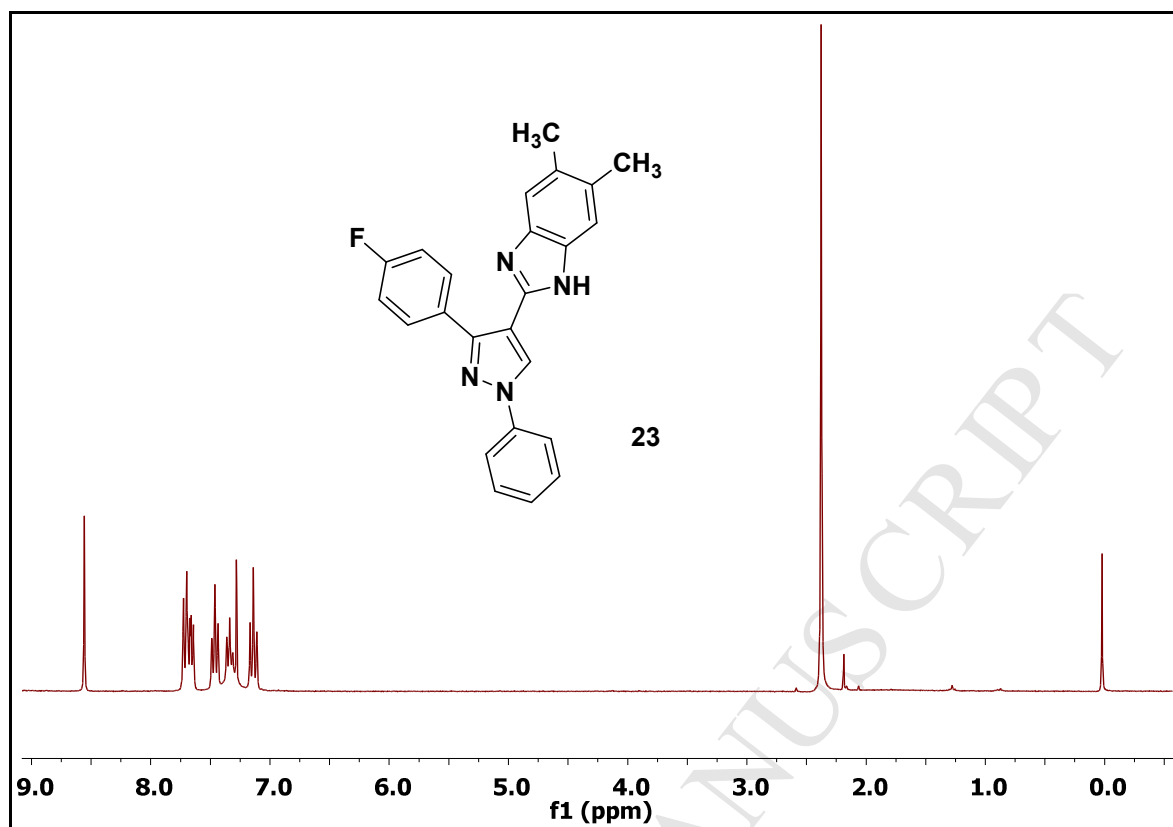
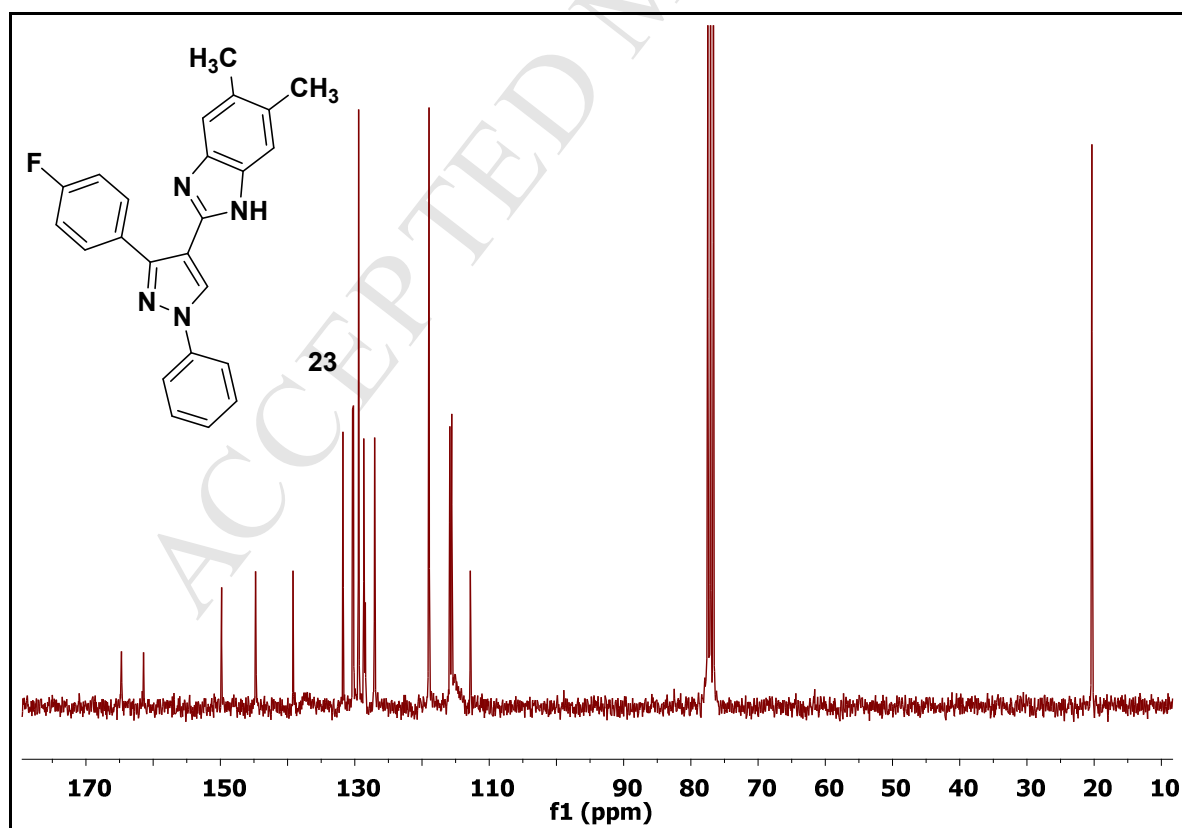
 ^1H NMR spectra of compound 20 ^{13}C NMR spectra of compound 20

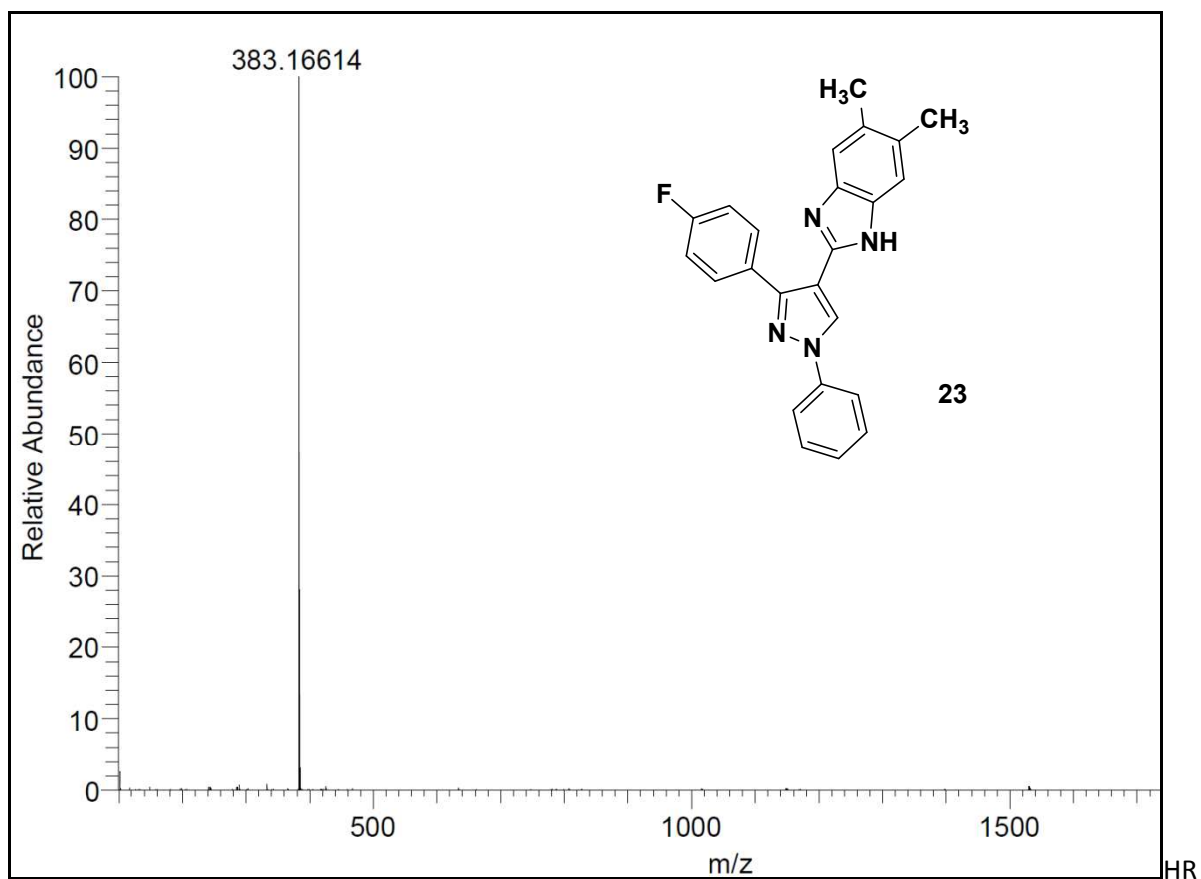
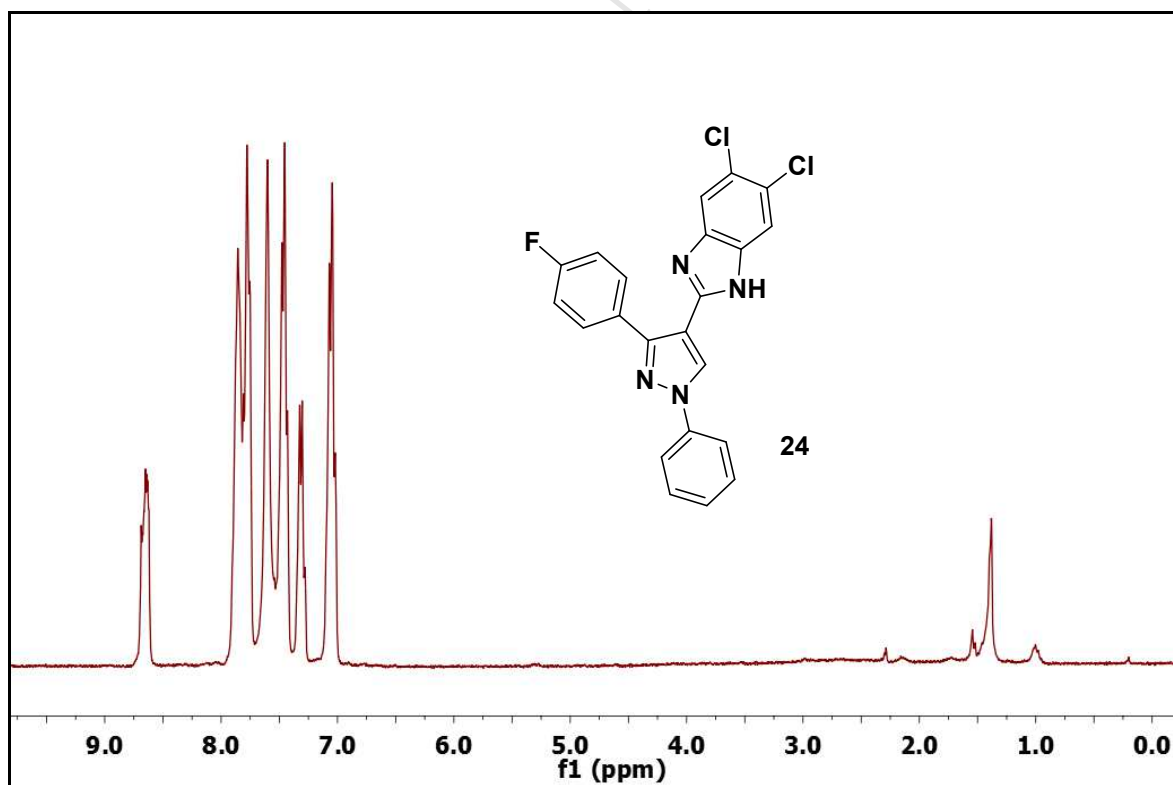
¹H NMR spectra of compound 21¹³C NMR spectra of compound 21

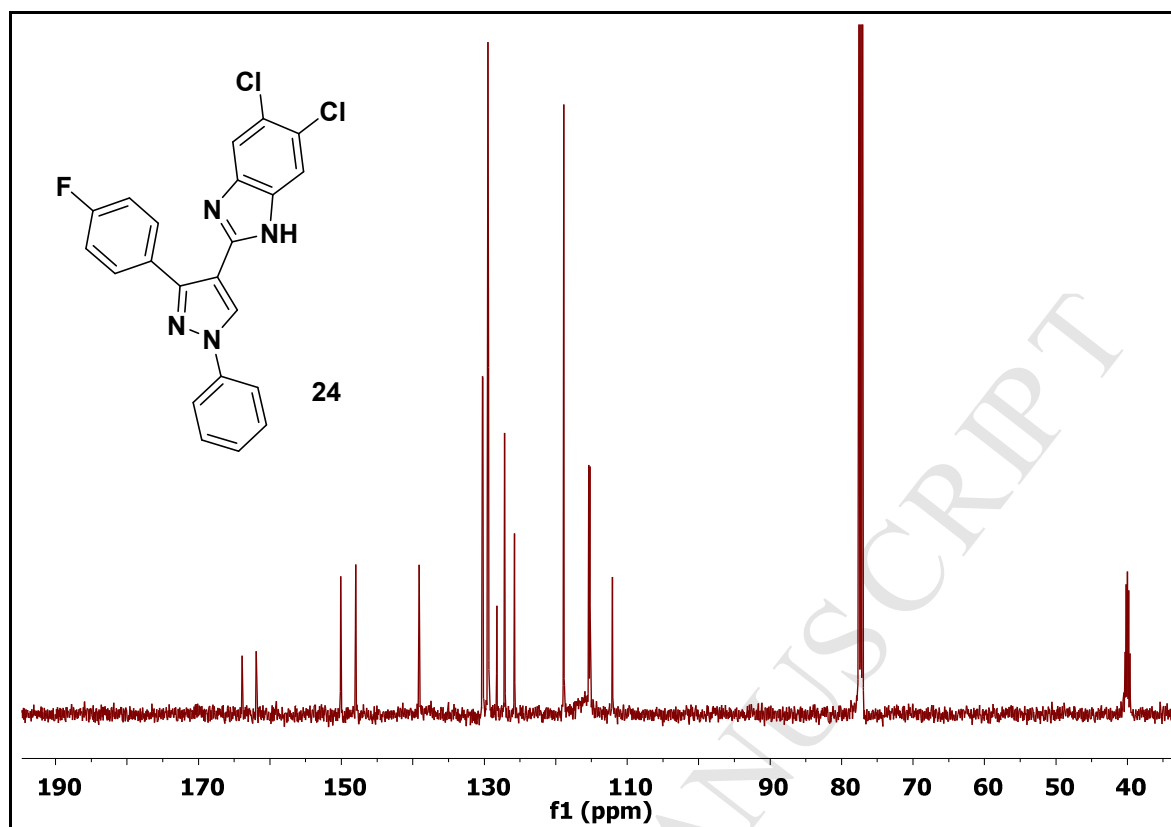
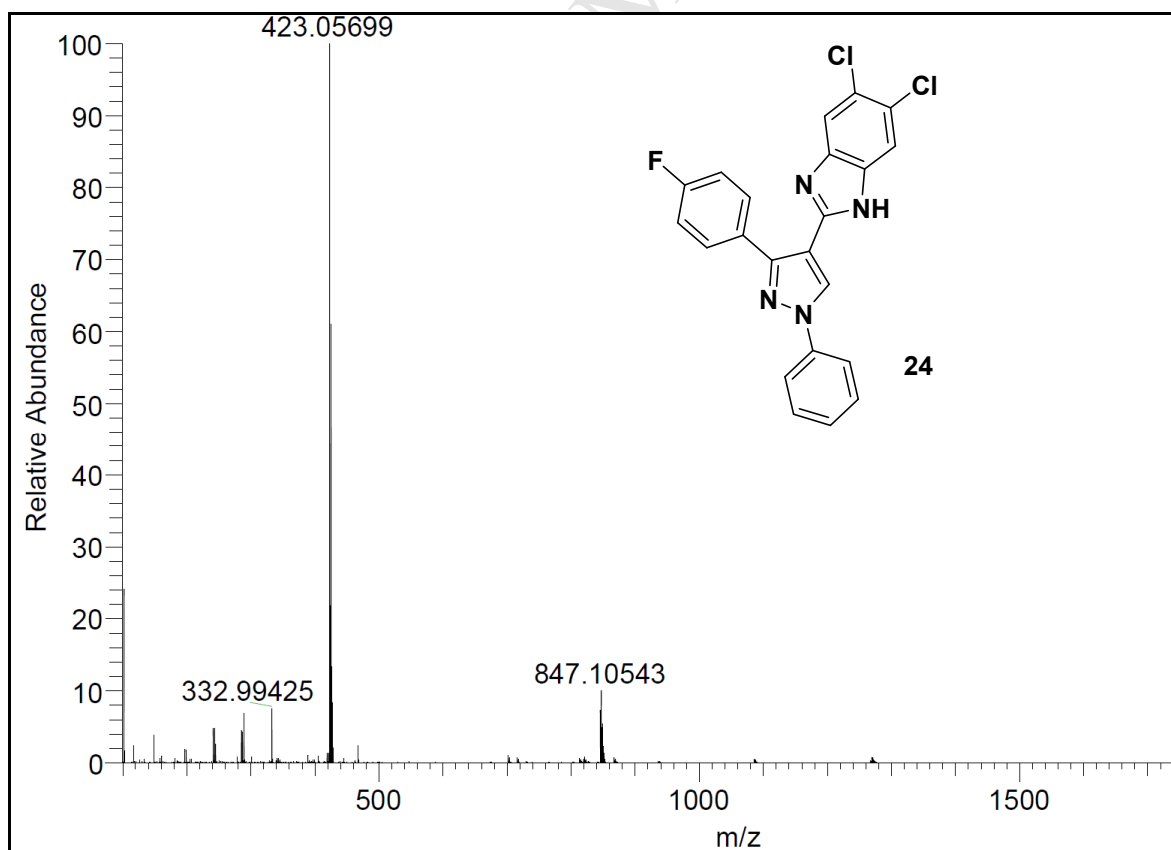
HRMS spectra of compound **21**¹H NMR spectra of compound **22**

 ^{13}C NMR spectra of compound 21

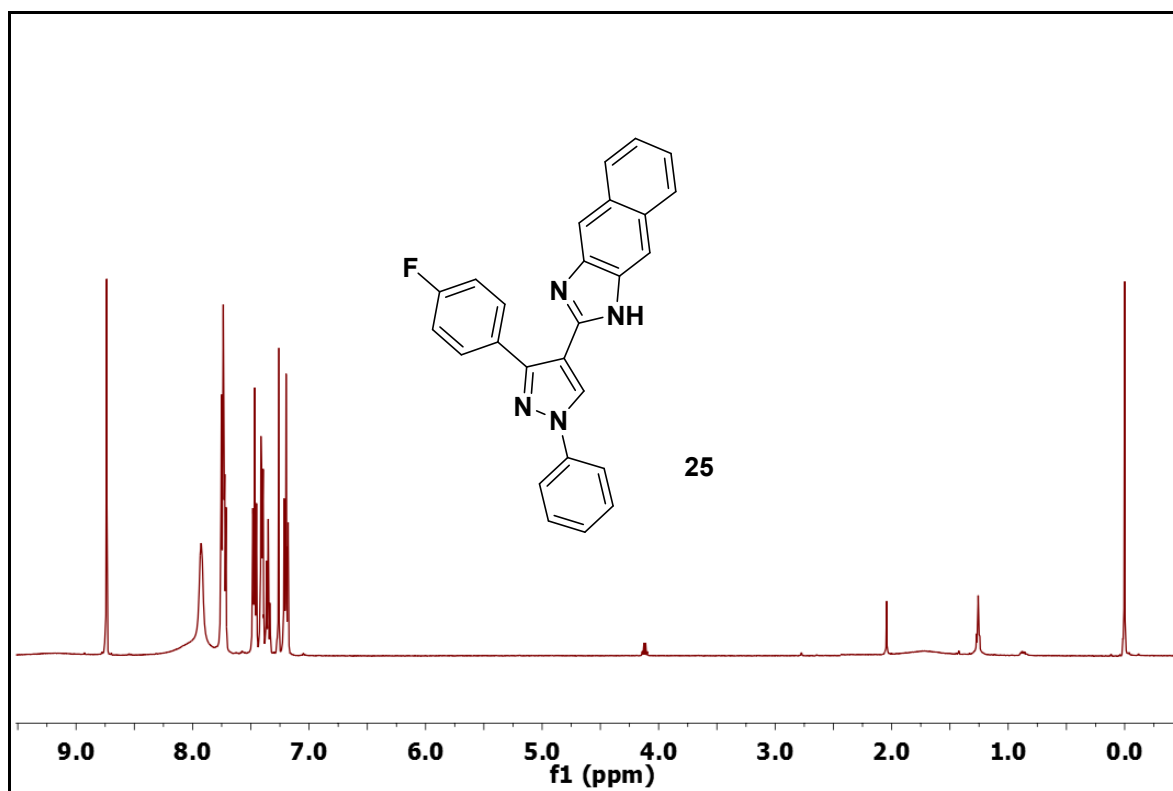
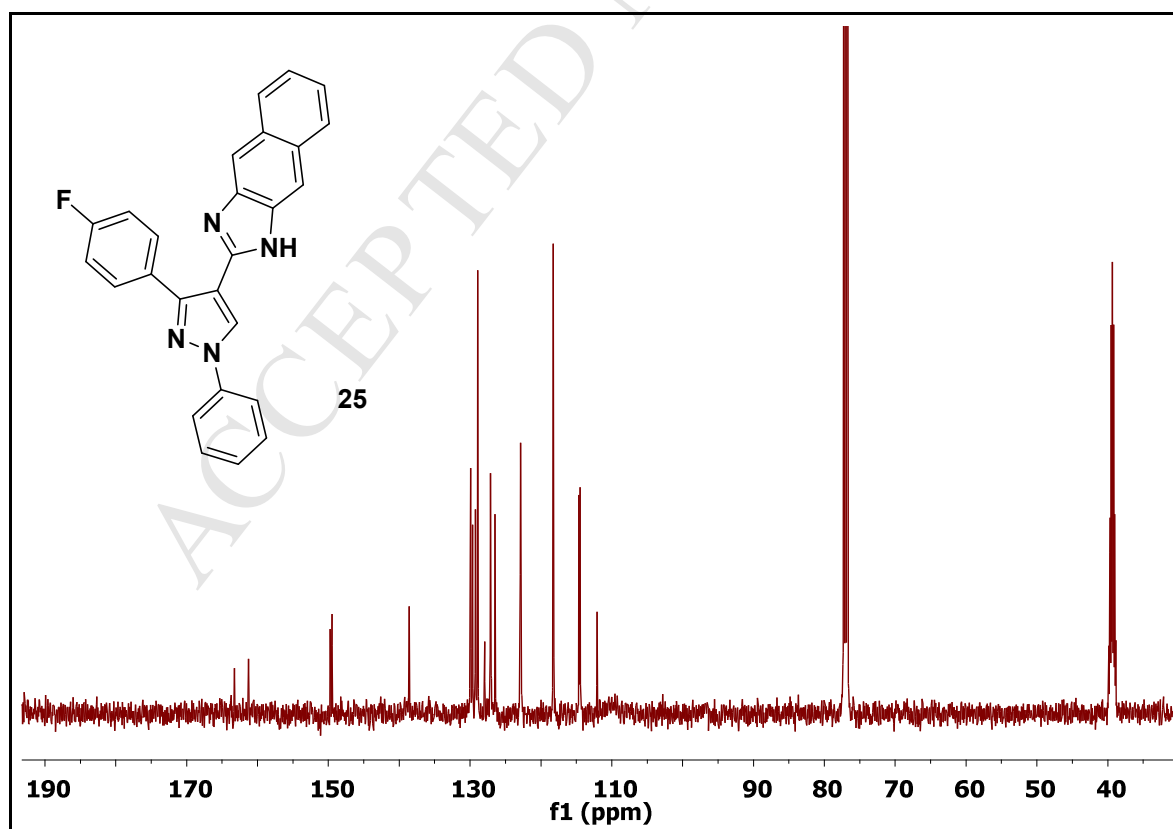
HRMS spectra of compound 22

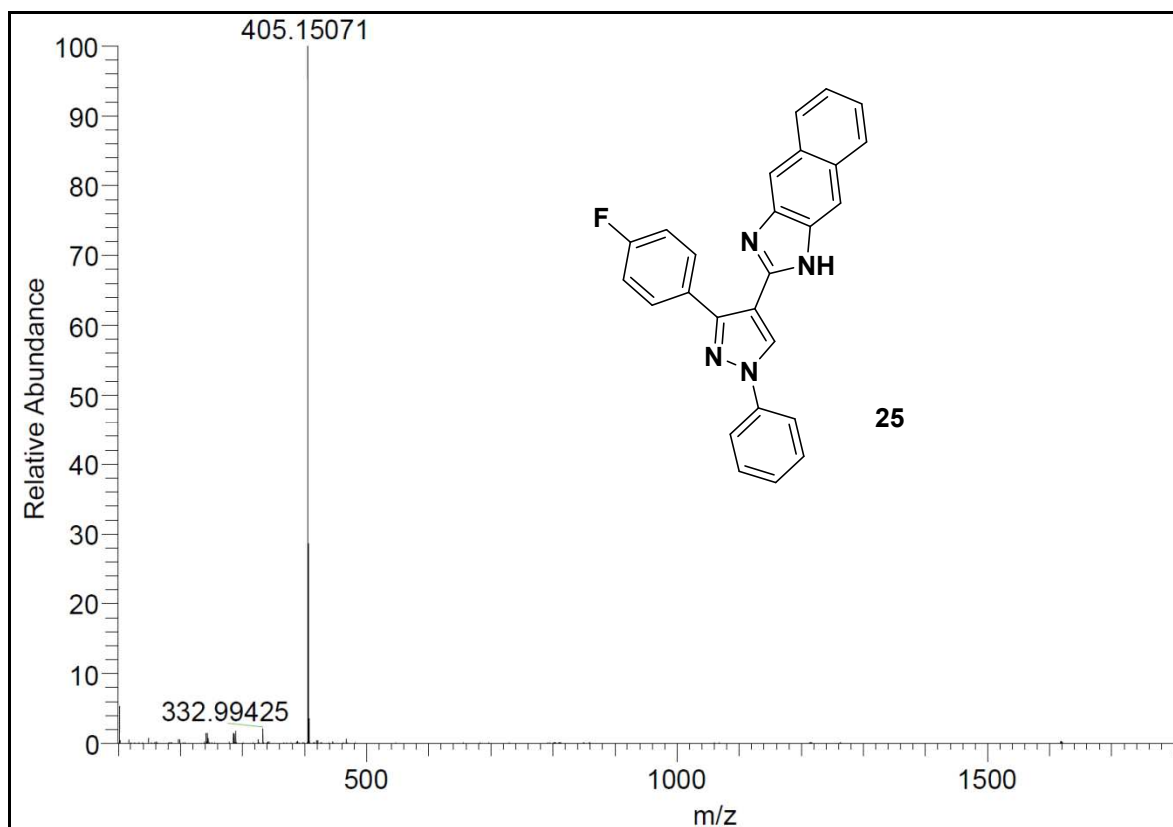
¹H NMR spectra of compound 23¹³C NMR spectra of compound 23

MS spectra of compound **23** ^1H NMR spectra of compound **24**

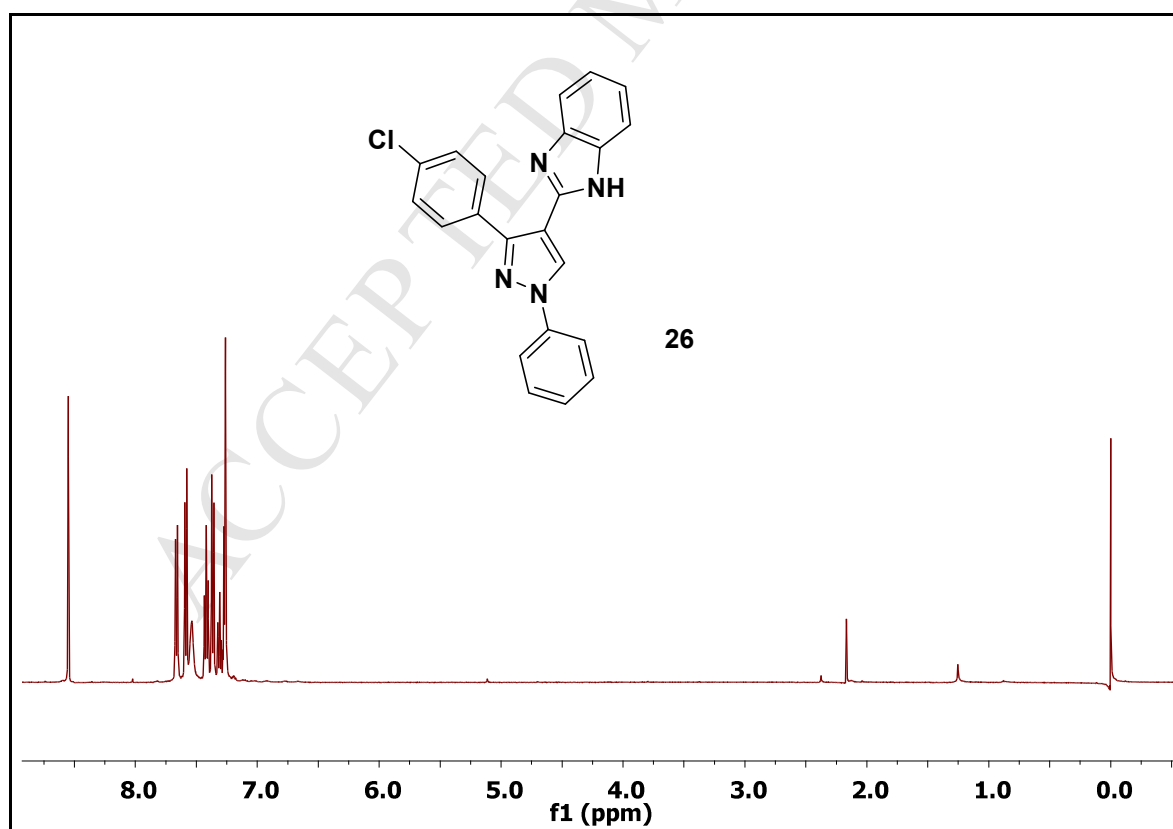
 ^{13}C NMR spectra of compound 24

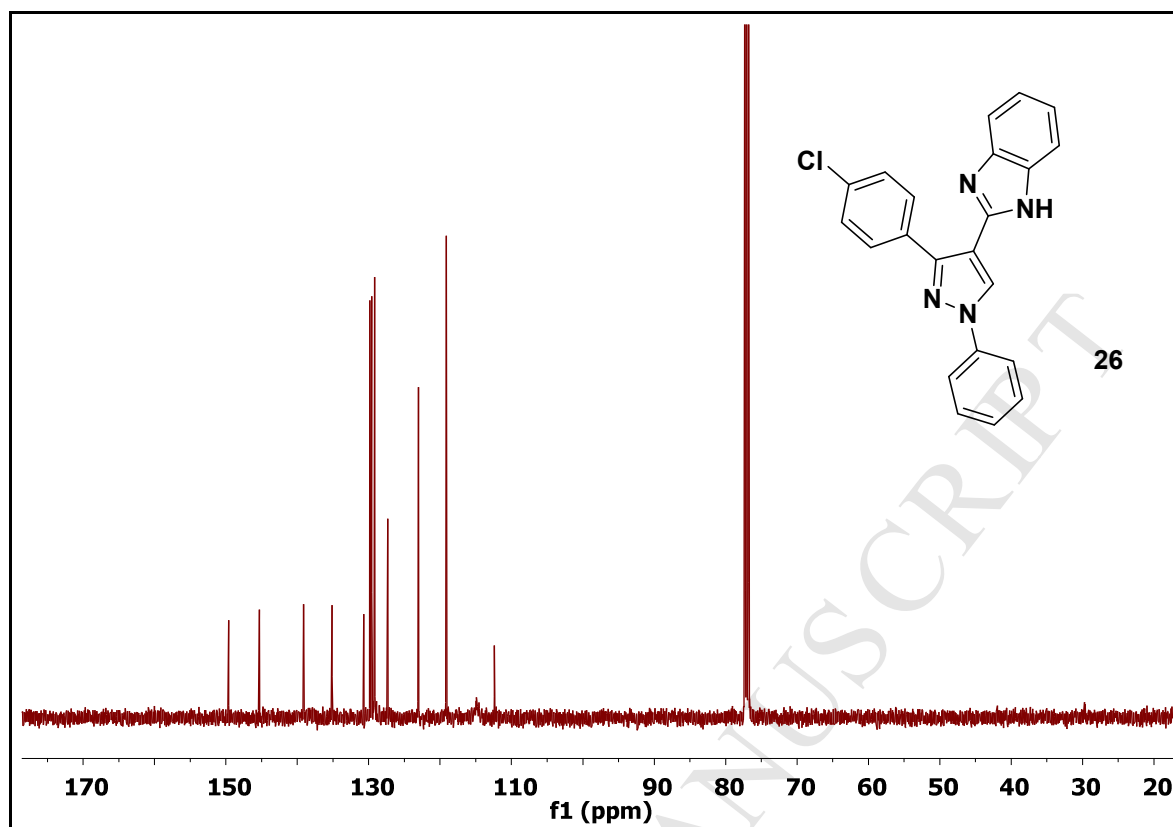
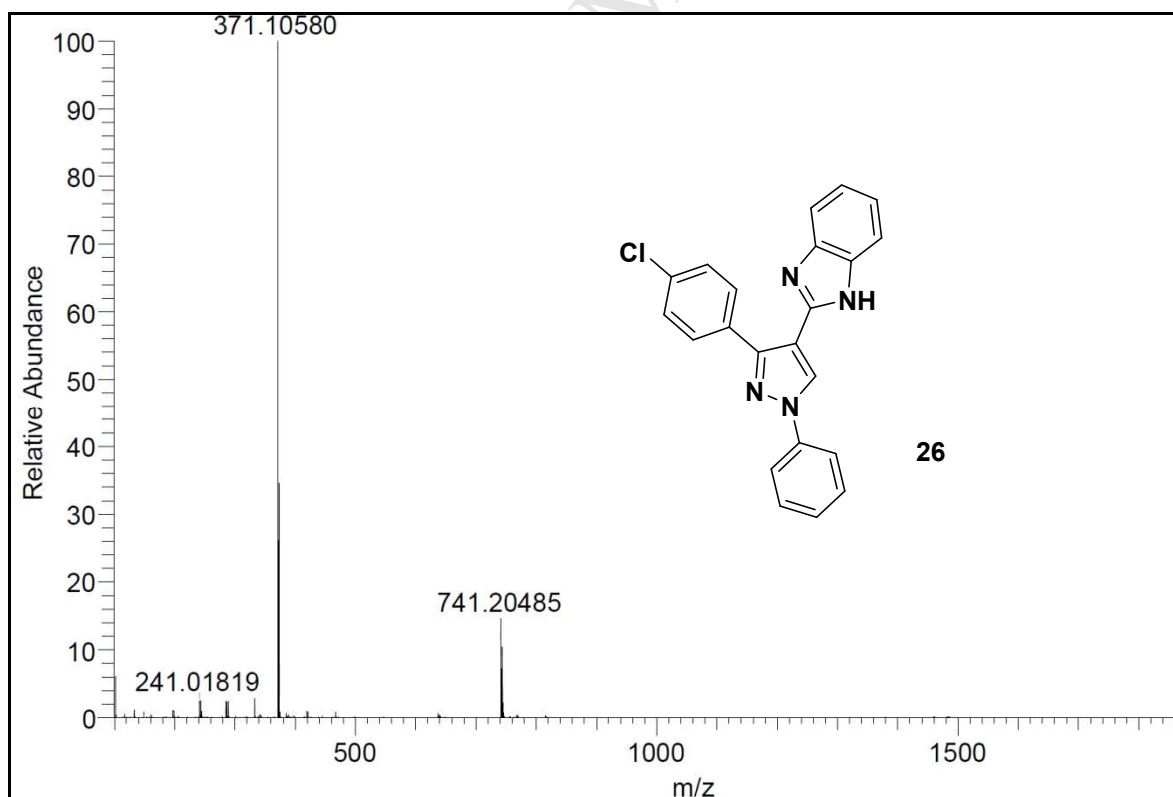
HRMS spectra of compound 24

¹H NMR spectra of compound 25¹³C NMR spectra of compound 25

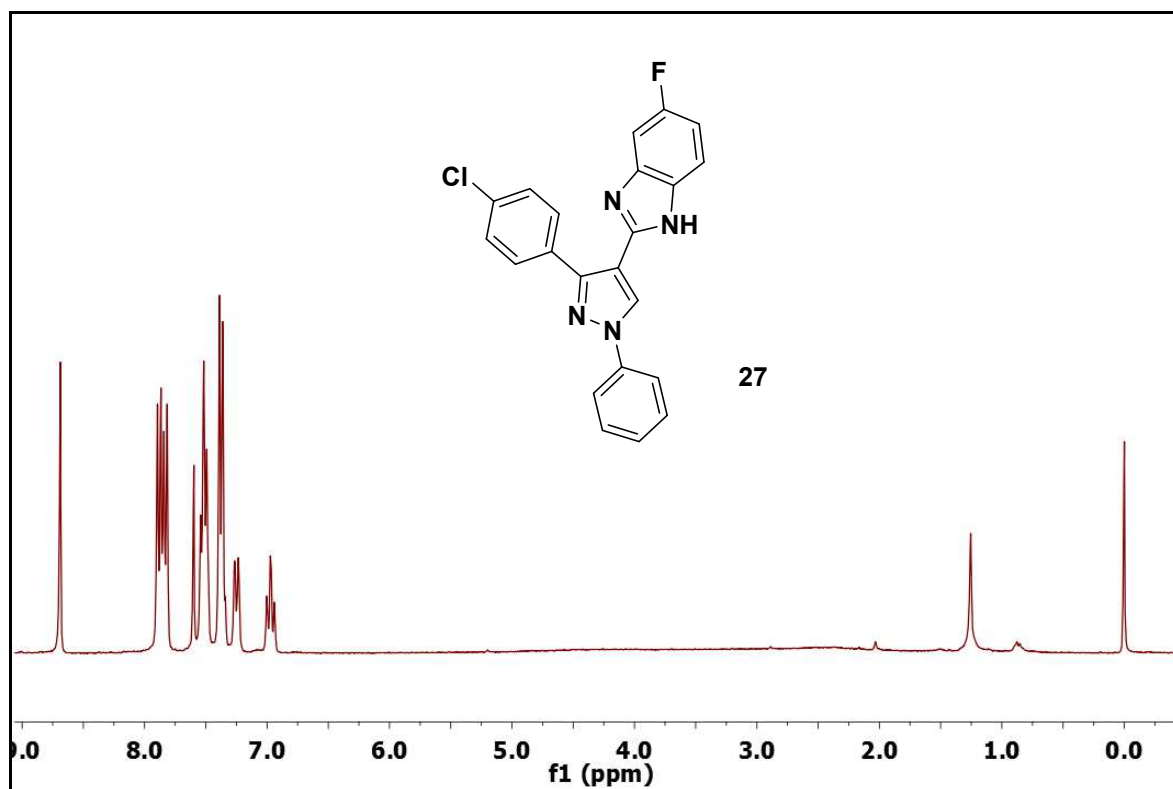
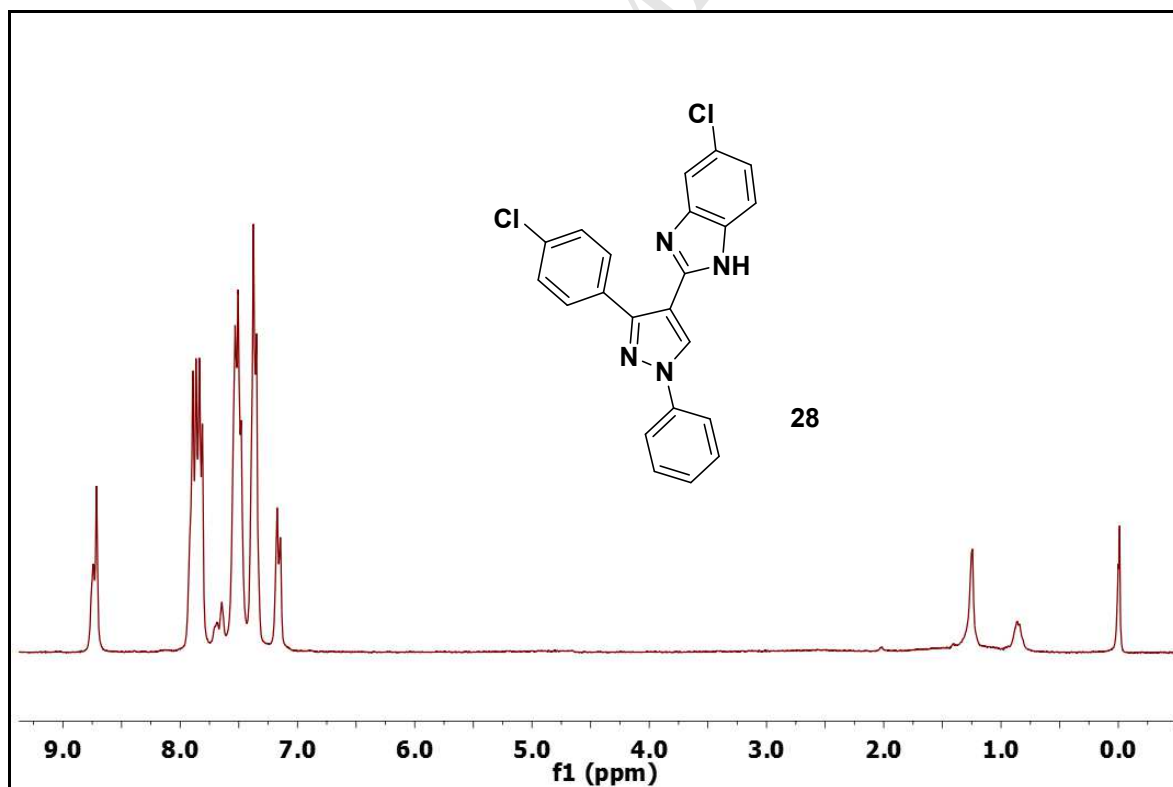


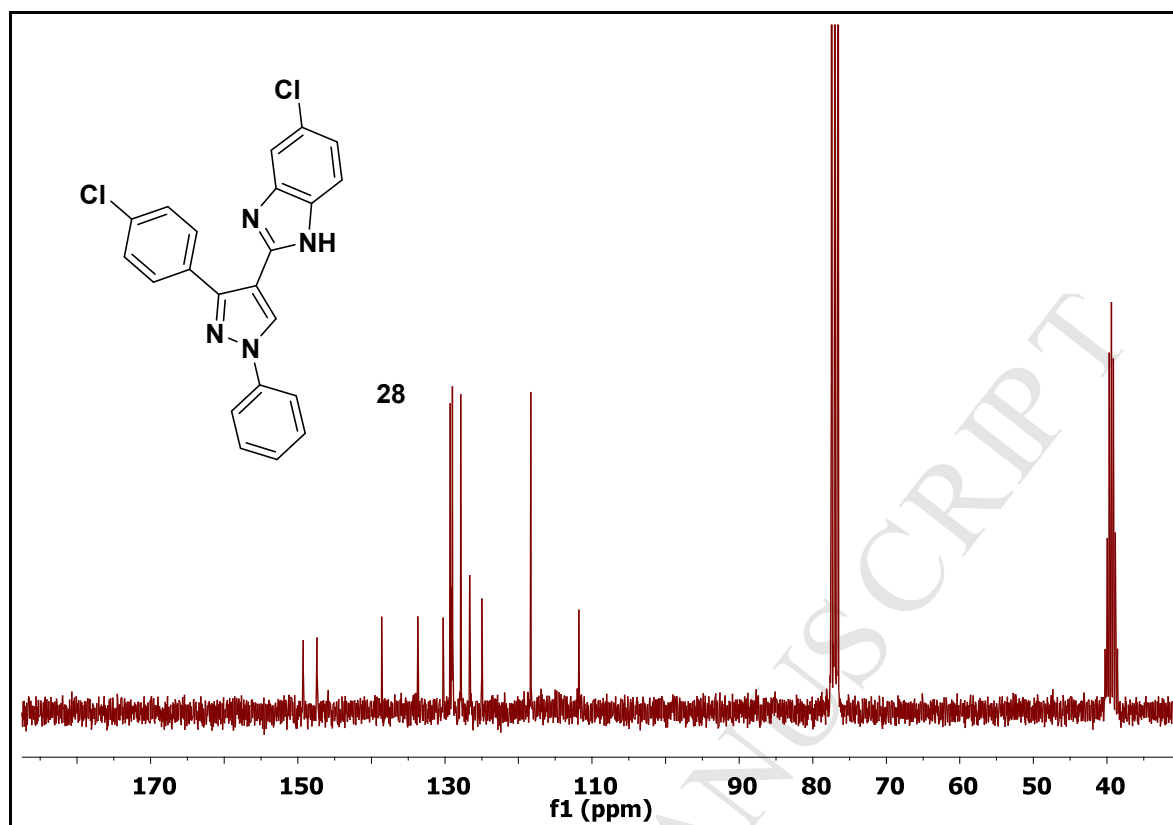
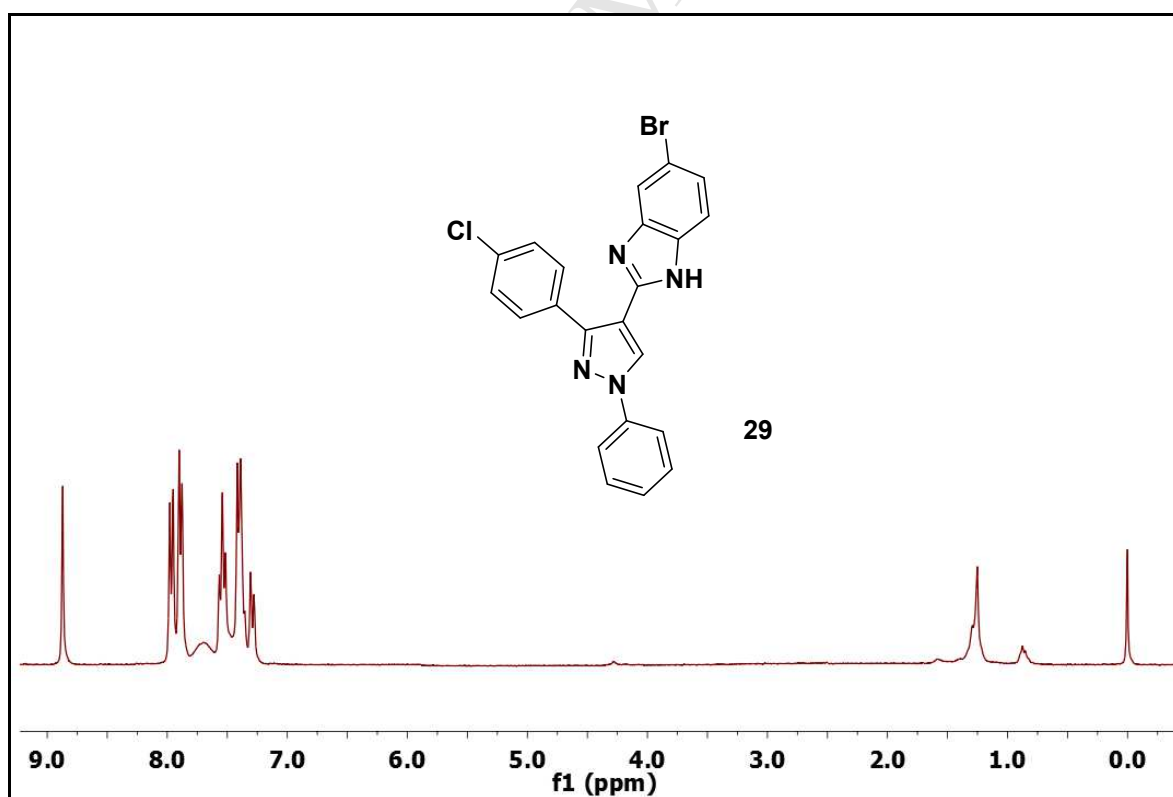
HRMS spectra of compound 25

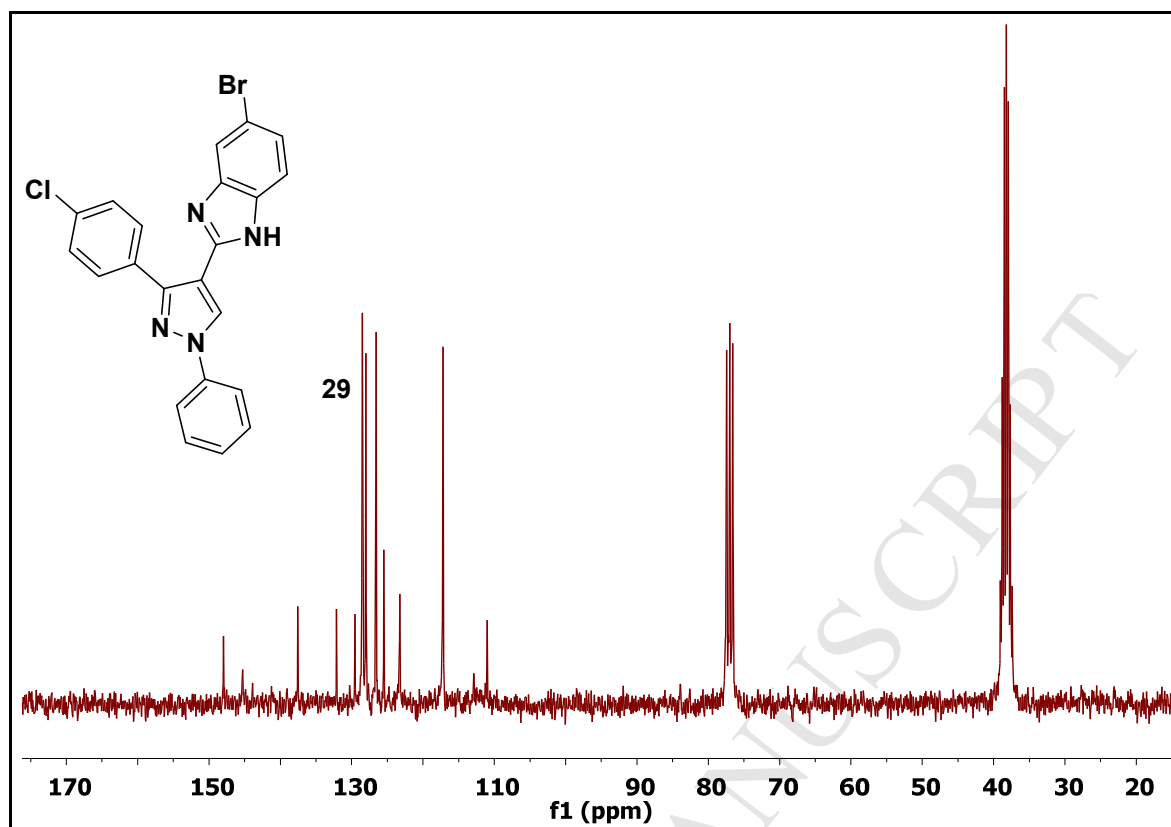
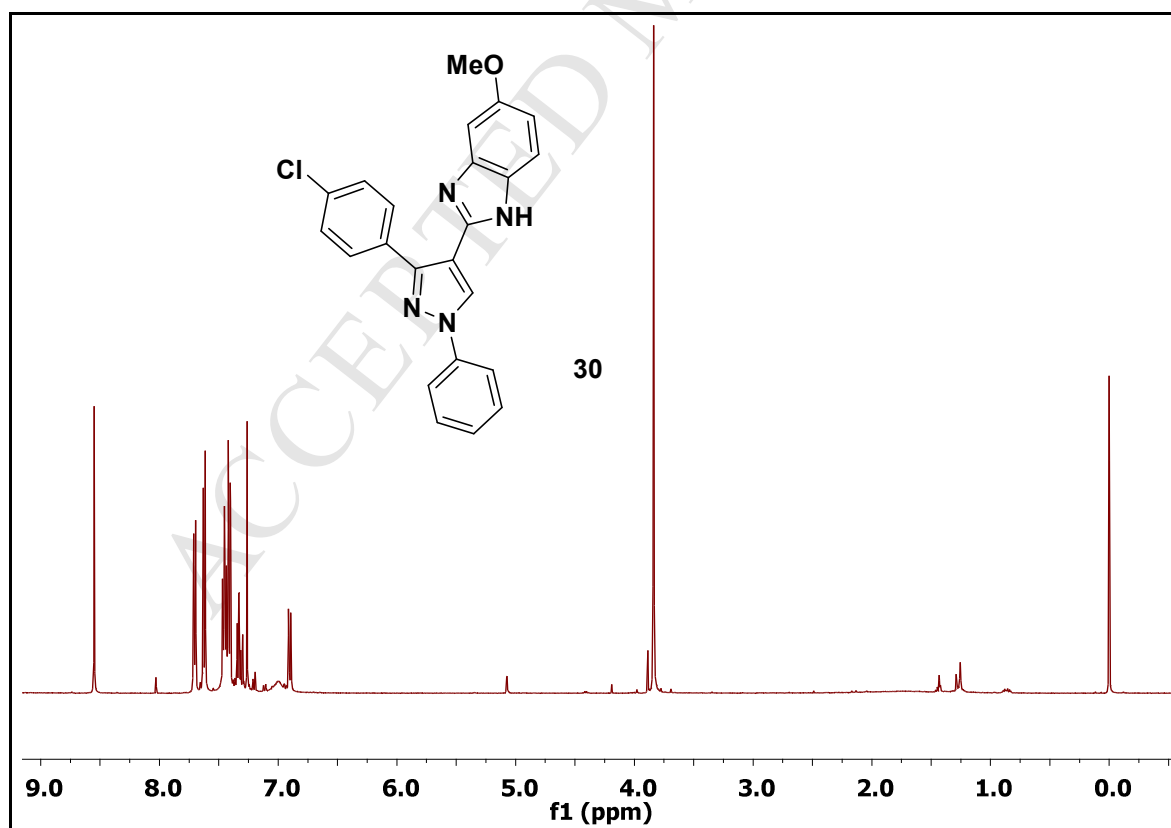
¹H NMR spectra of compound 26

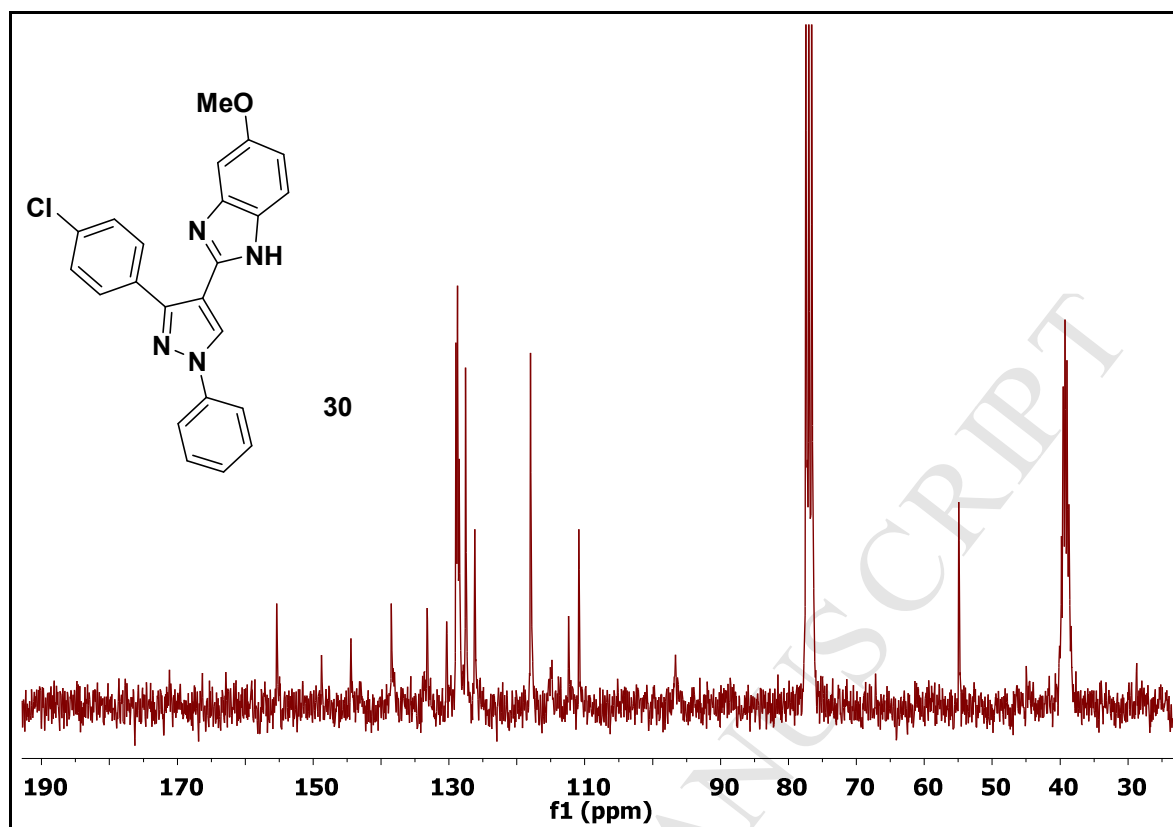
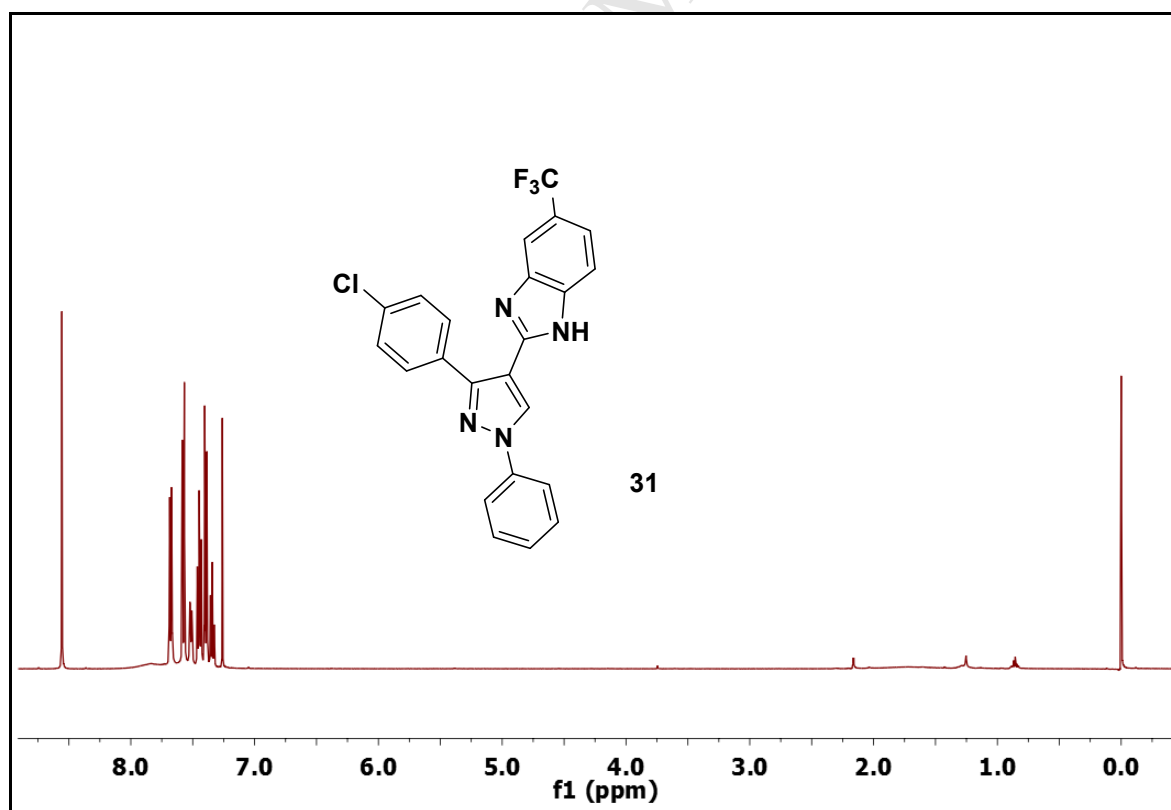
 ^{13}C NMR spectra of compound 26

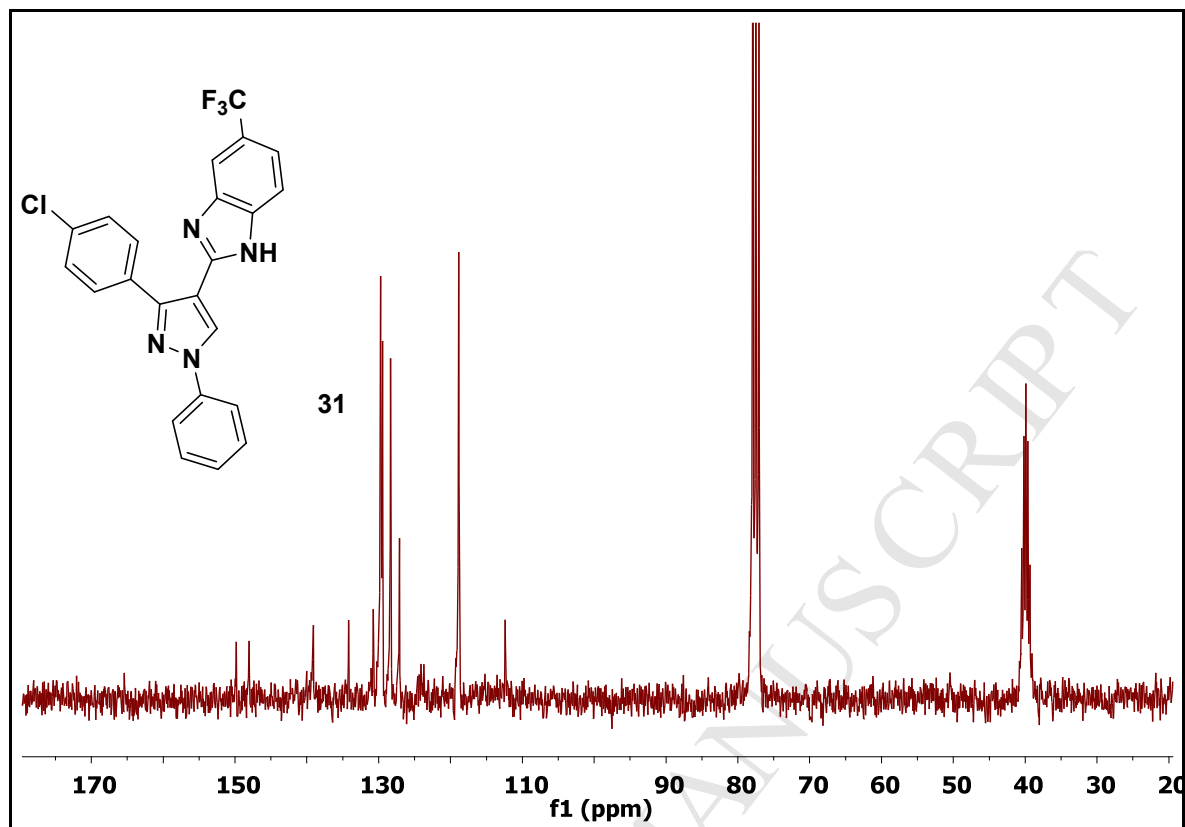
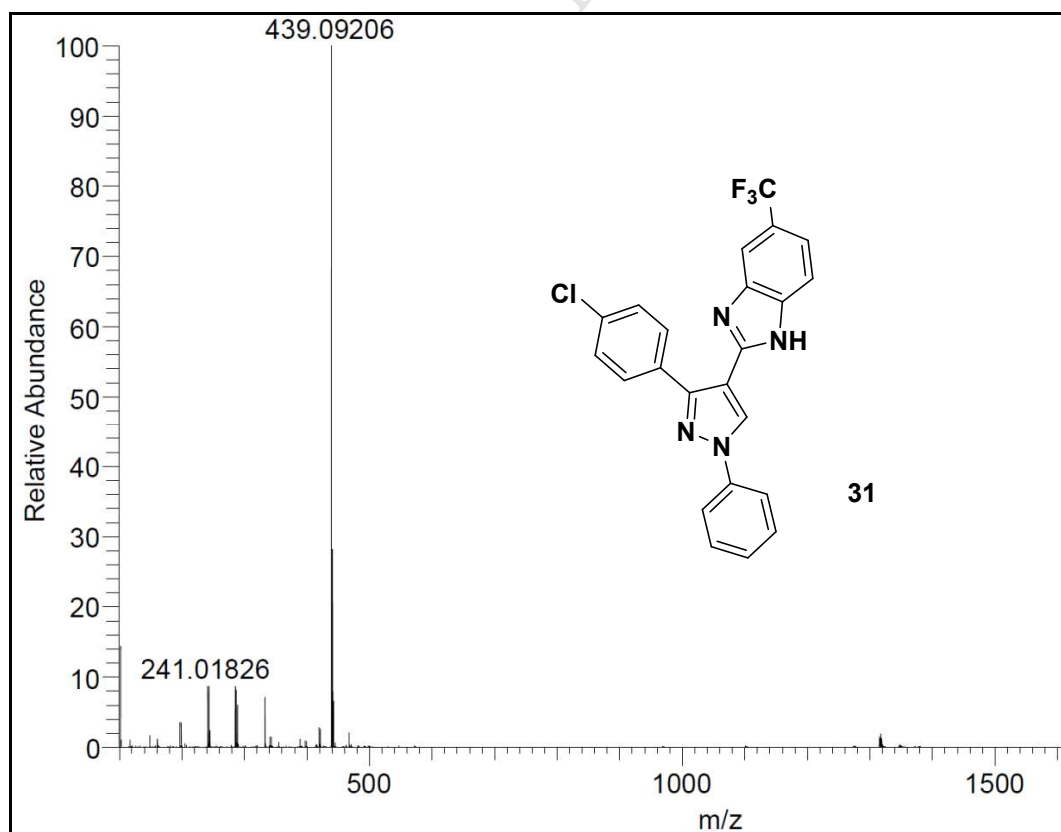
HRMS spectra of compound 26

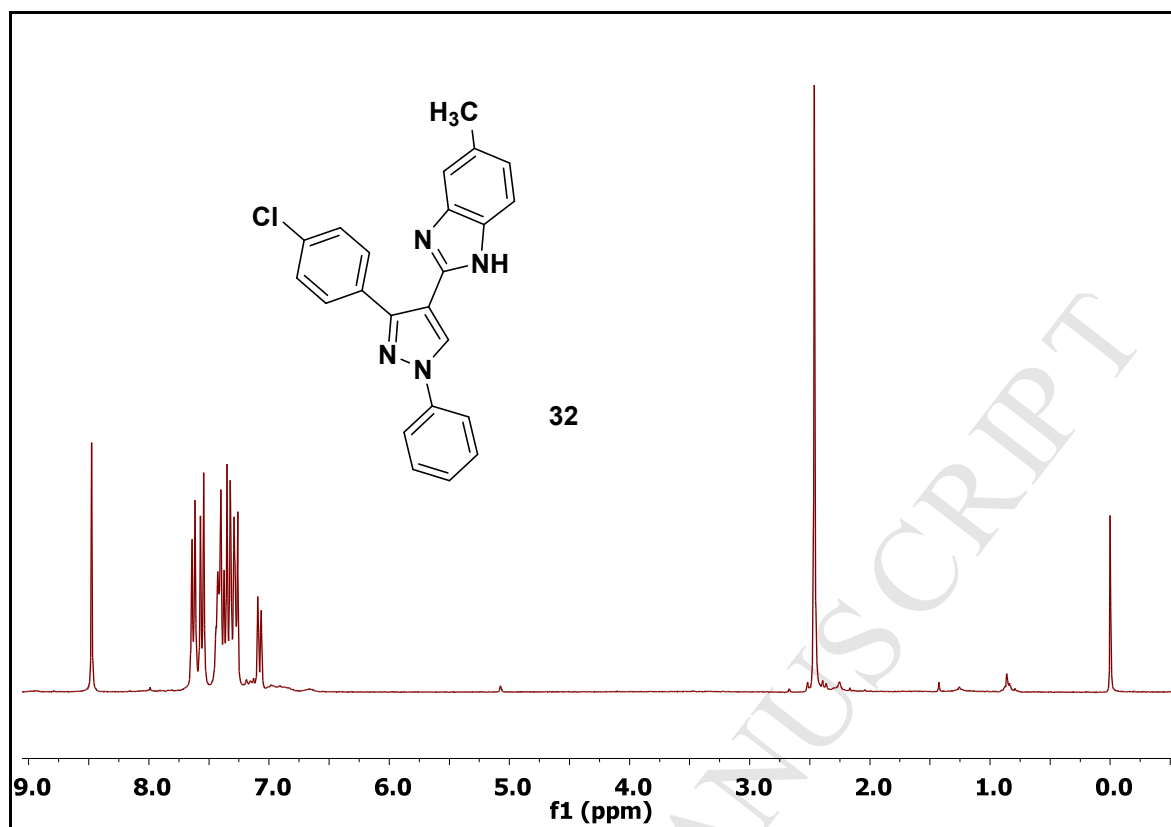
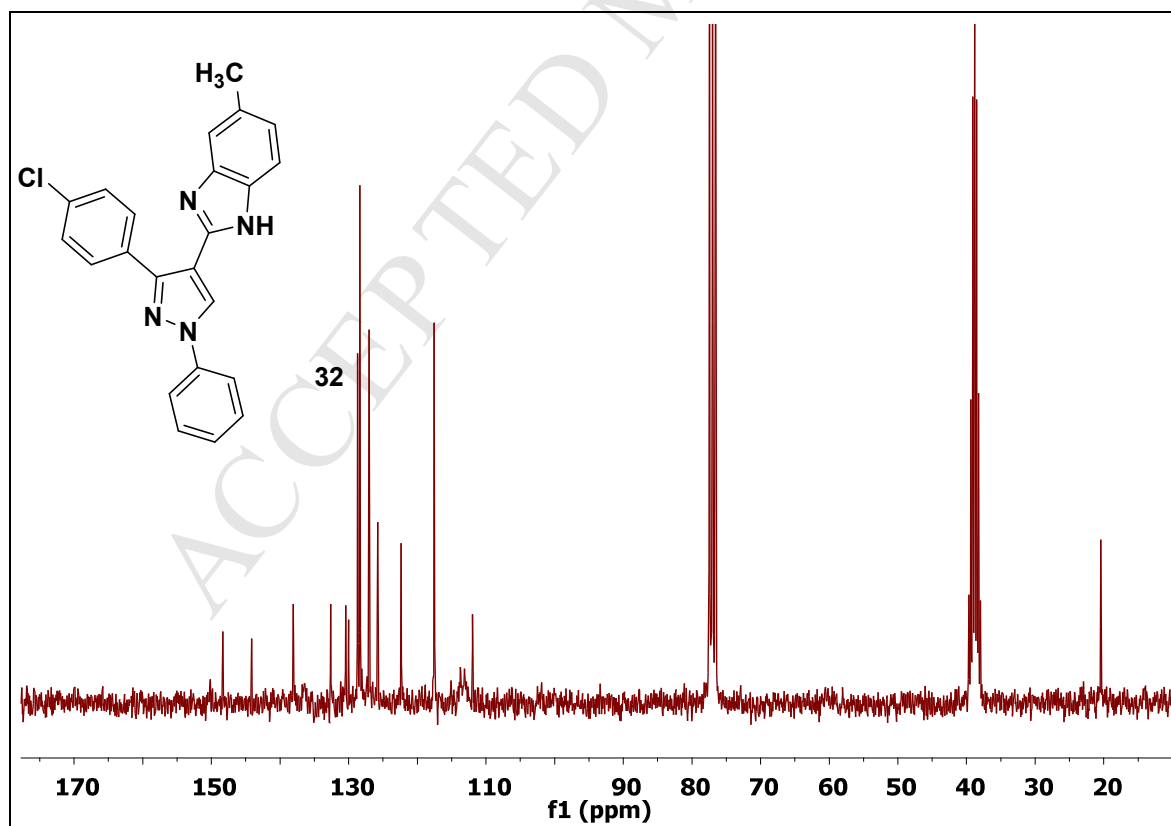
¹H NMR spectra of compound 27¹H NMR spectra of compound 28

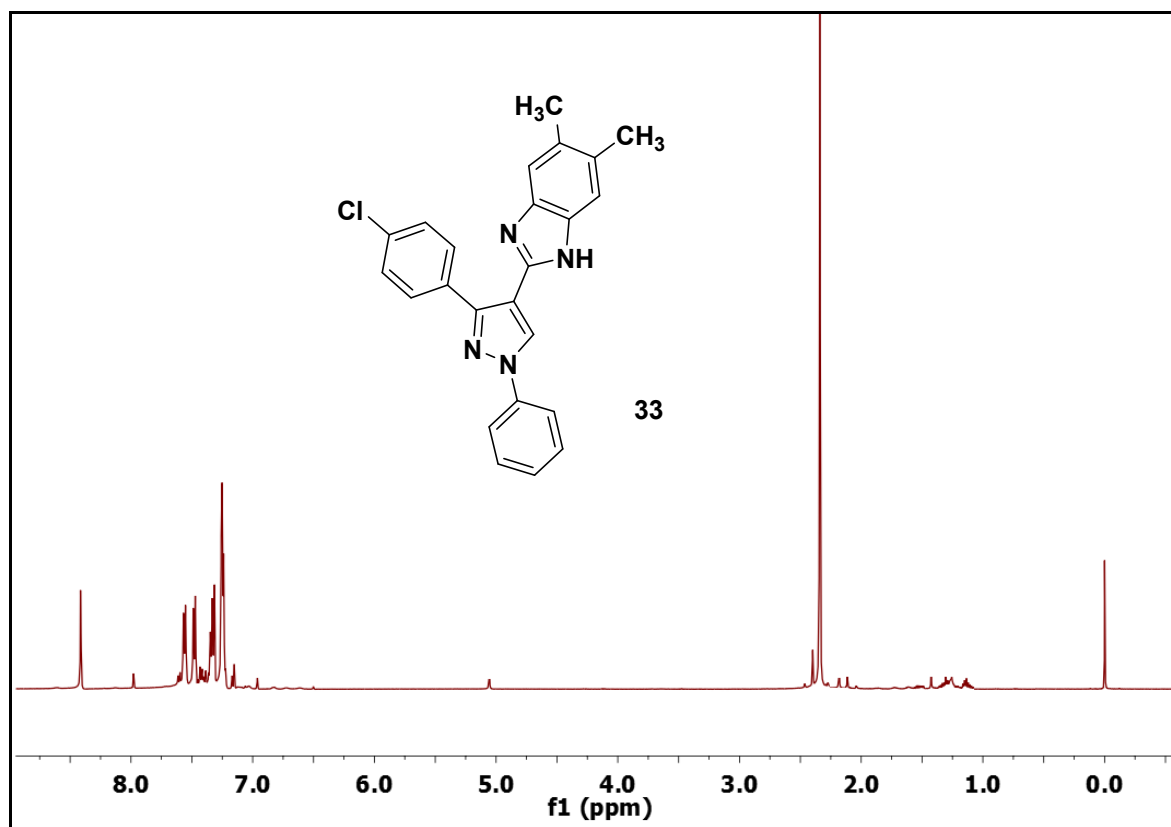
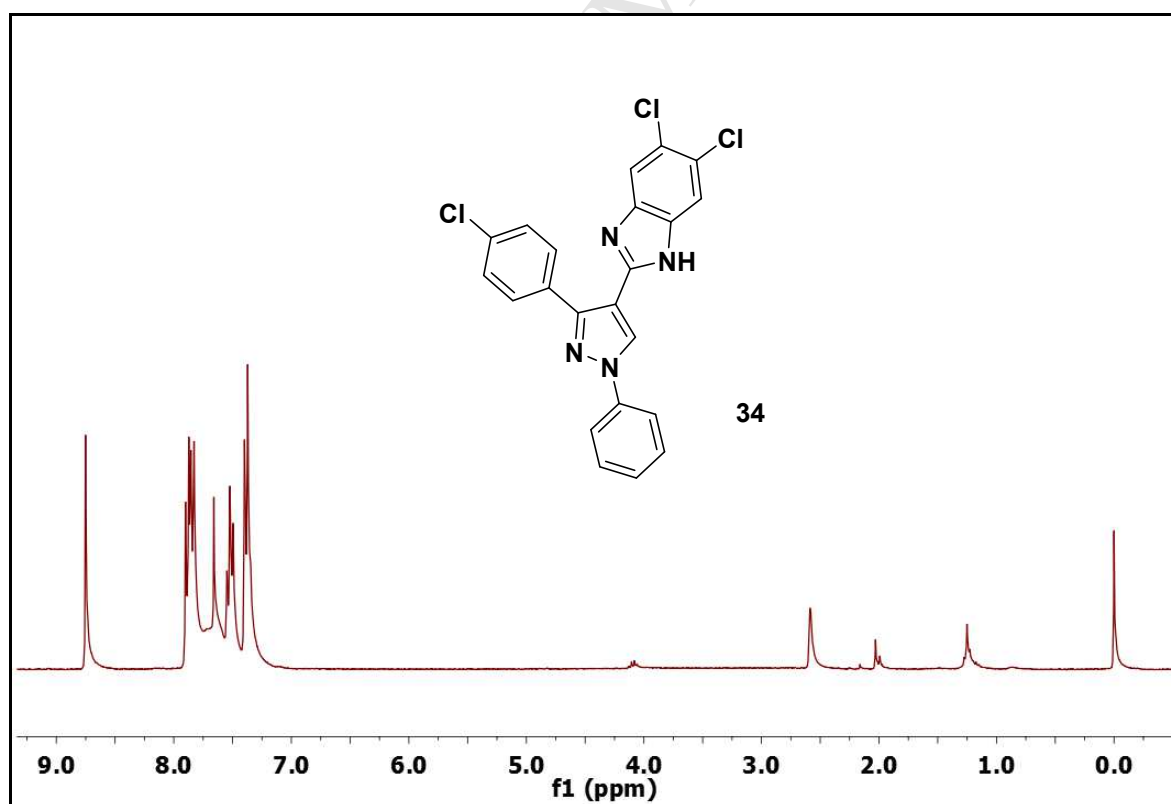
 ^{13}C NMR spectra of compound 28 ^1H NMR spectra of compound 29

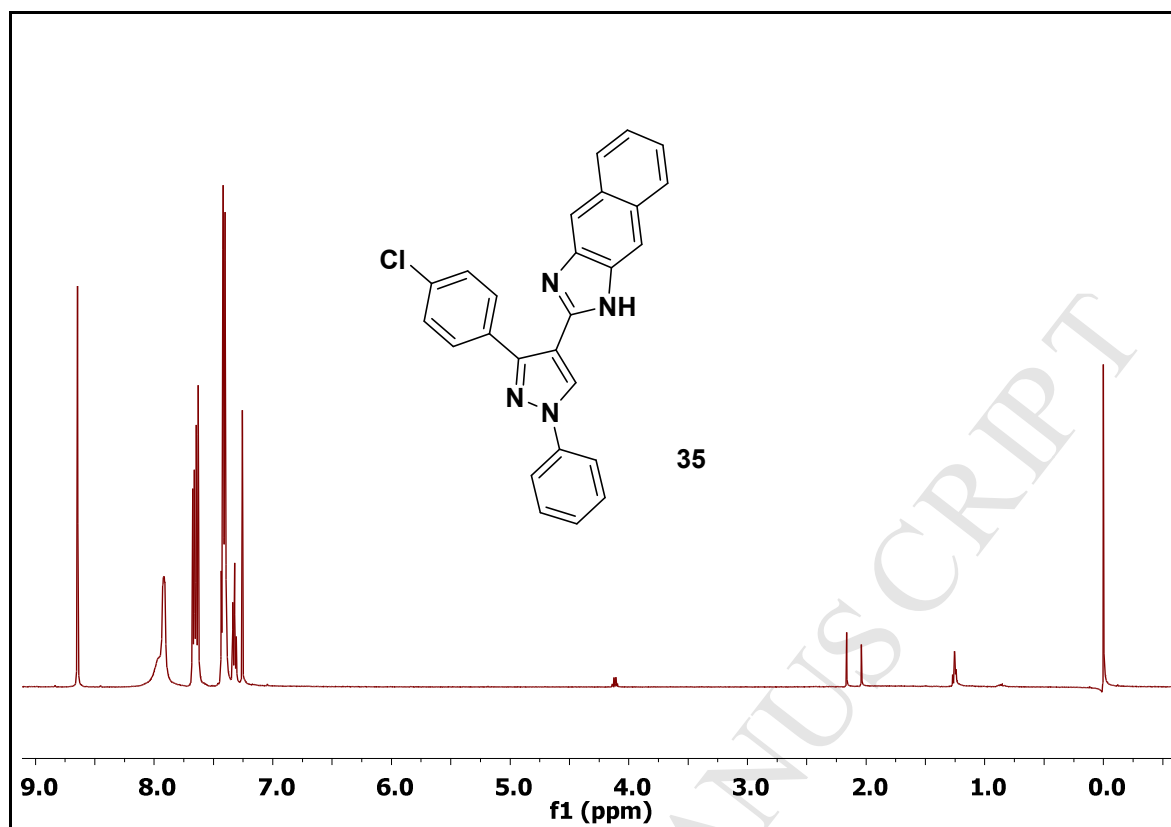
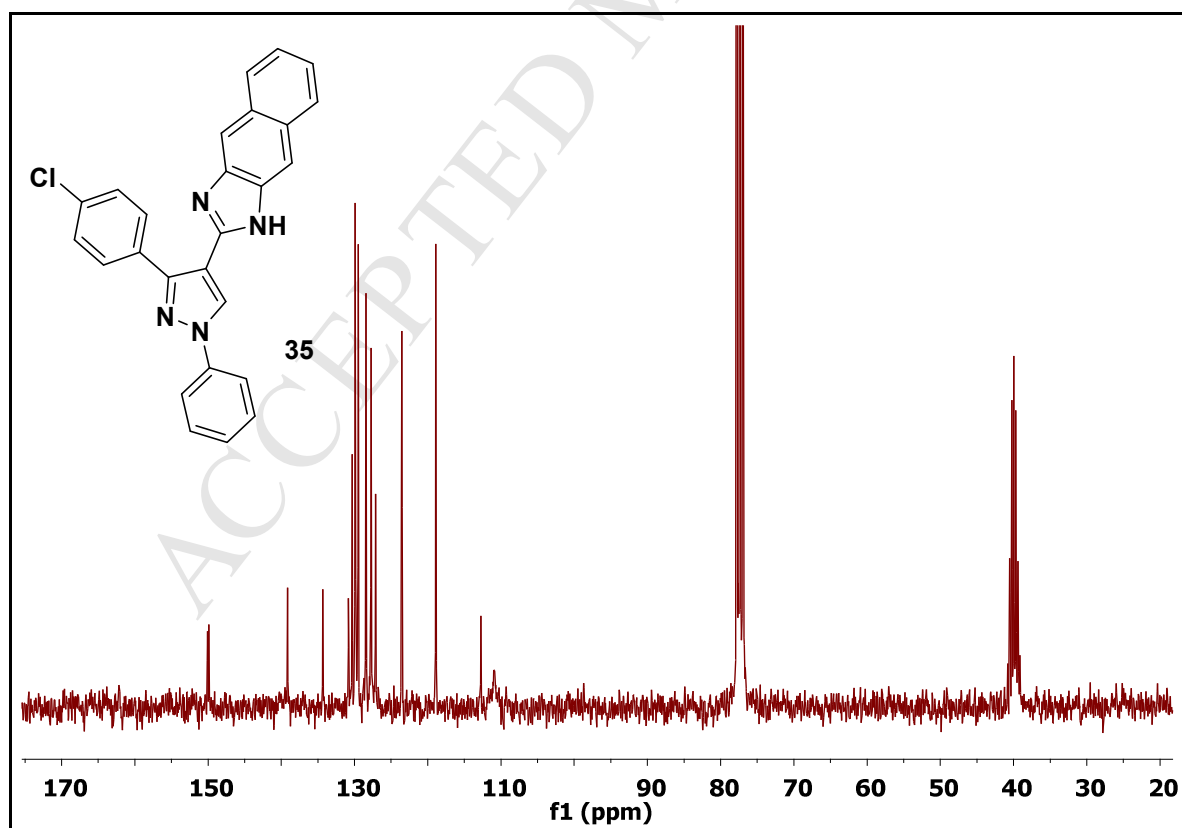
 ^{13}C NMR spectra of compound 29 ^1H NMR spectra of compound 30

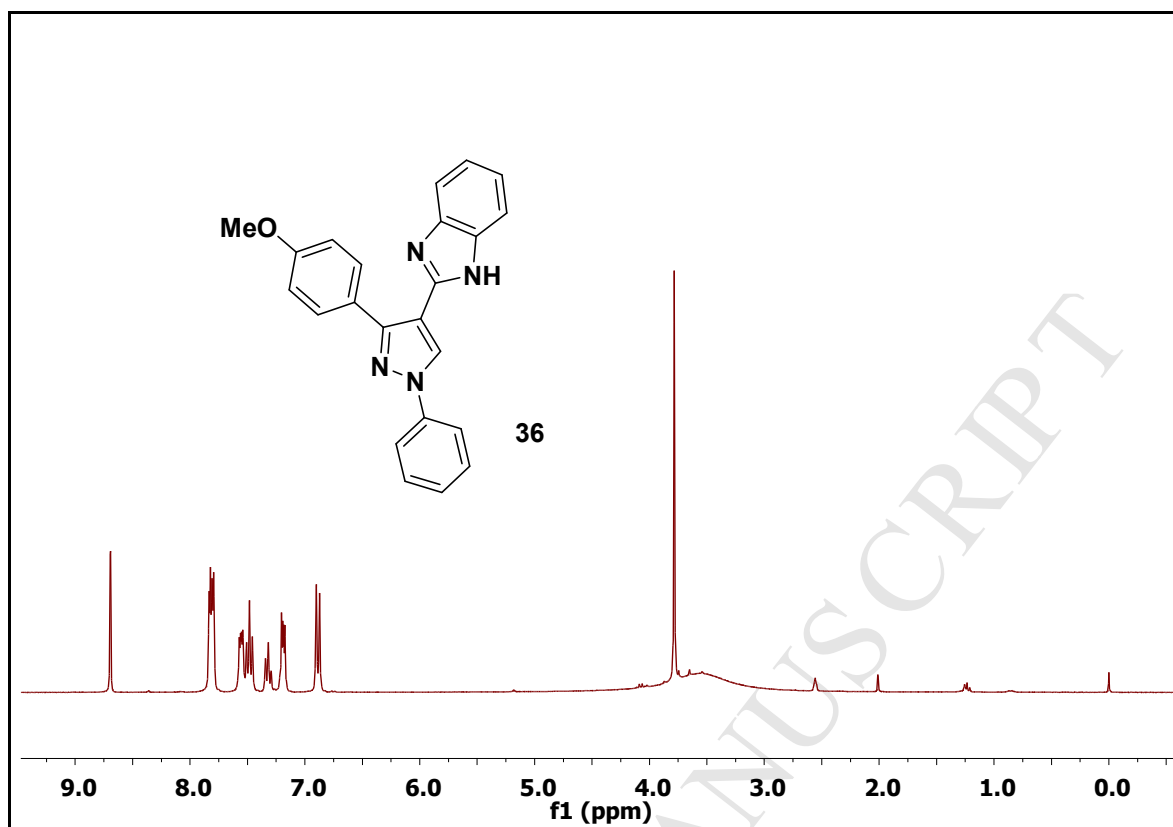
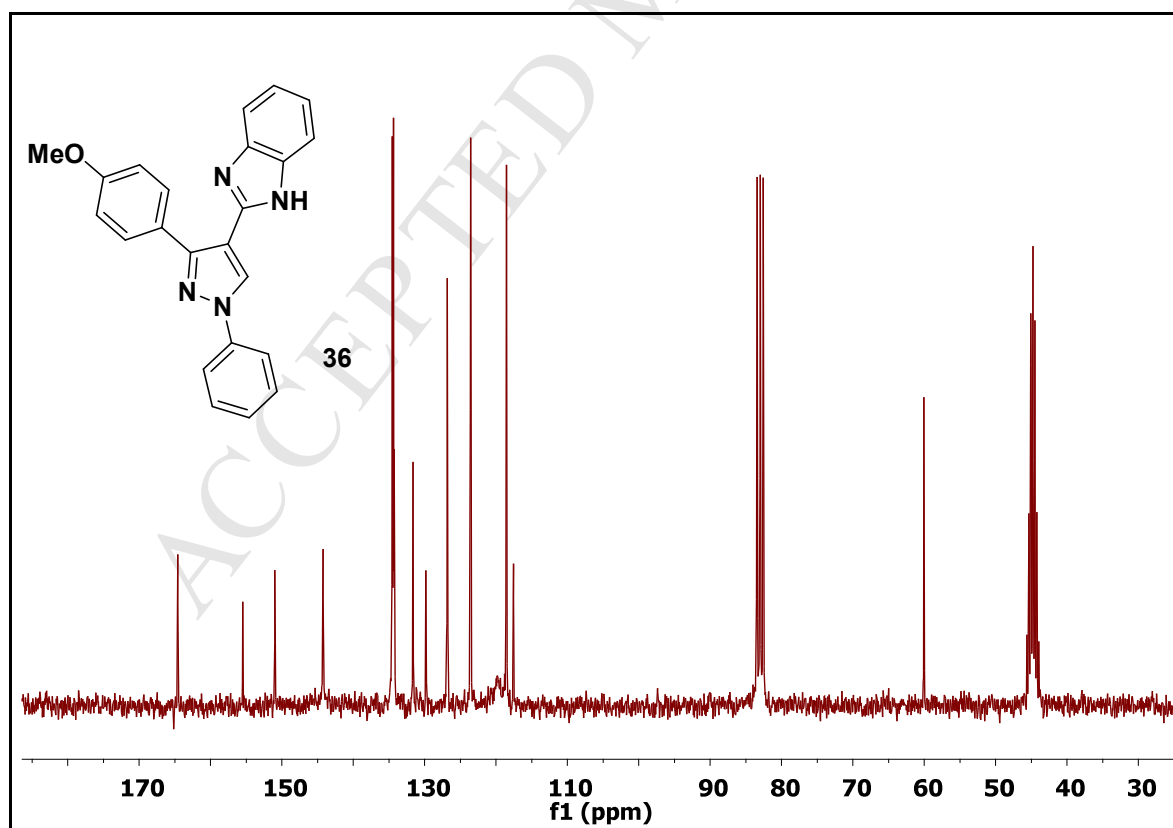
 ^{13}C NMR spectra of compound 30 ^1H NMR spectra of compound 31

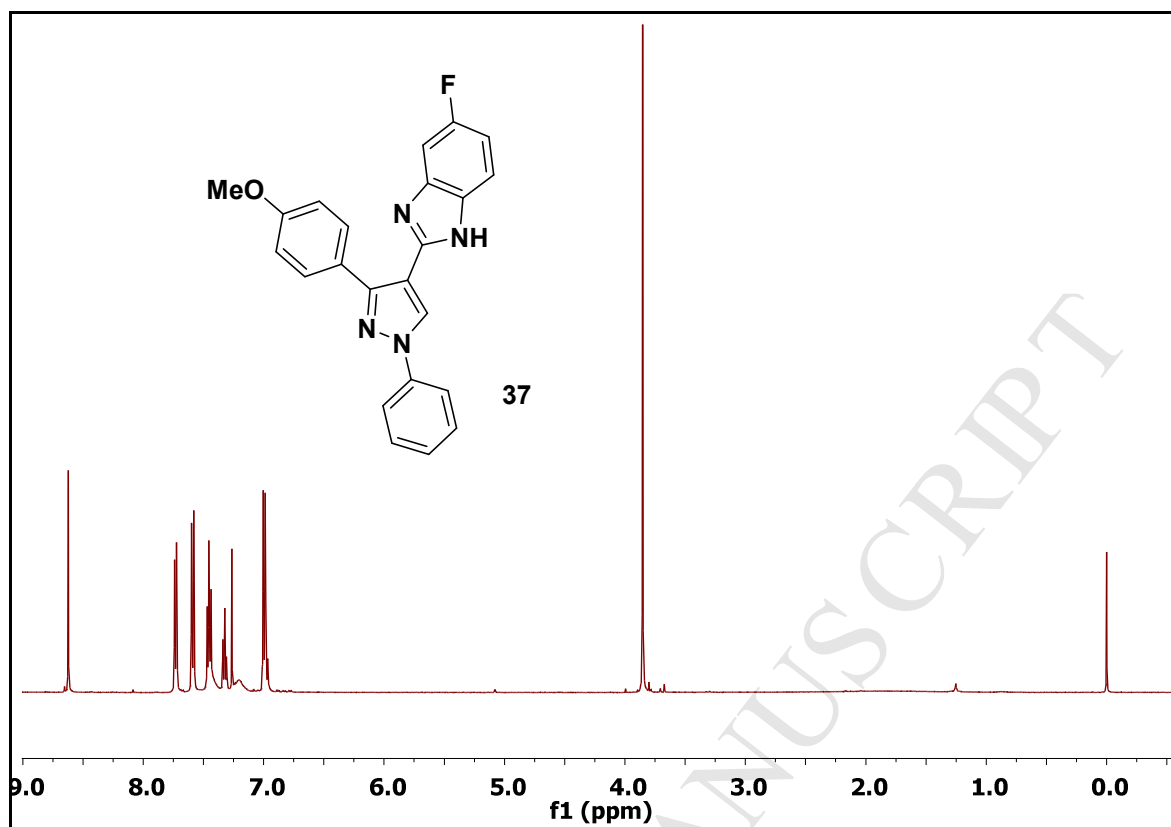
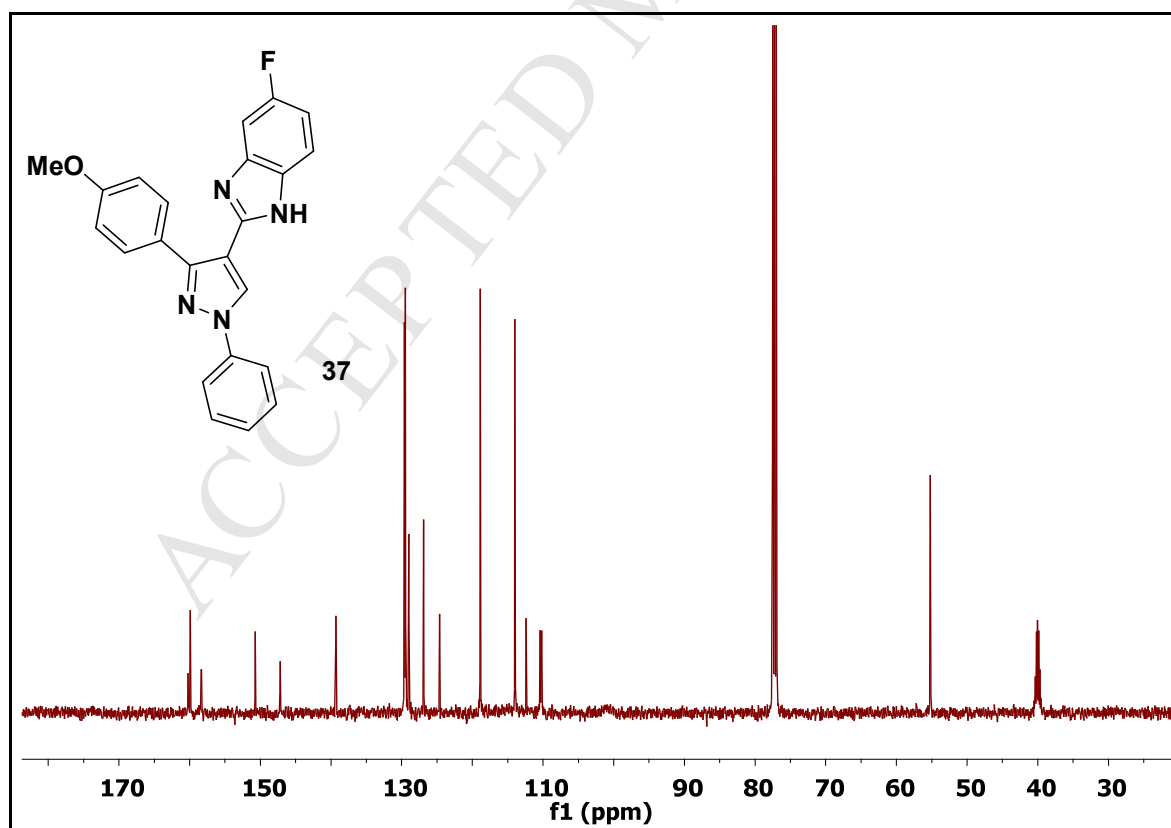
 ^{13}C NMR spectra of compound **31**HRMS spectra of compound **31**

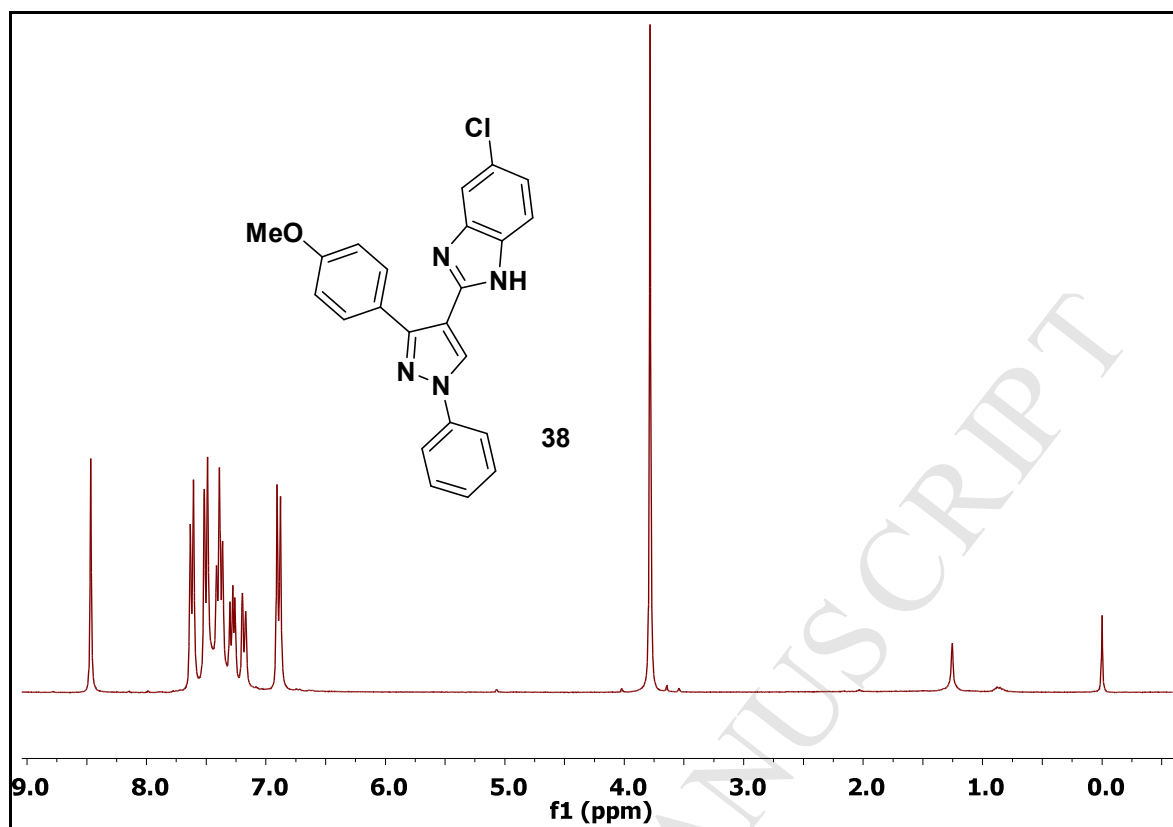
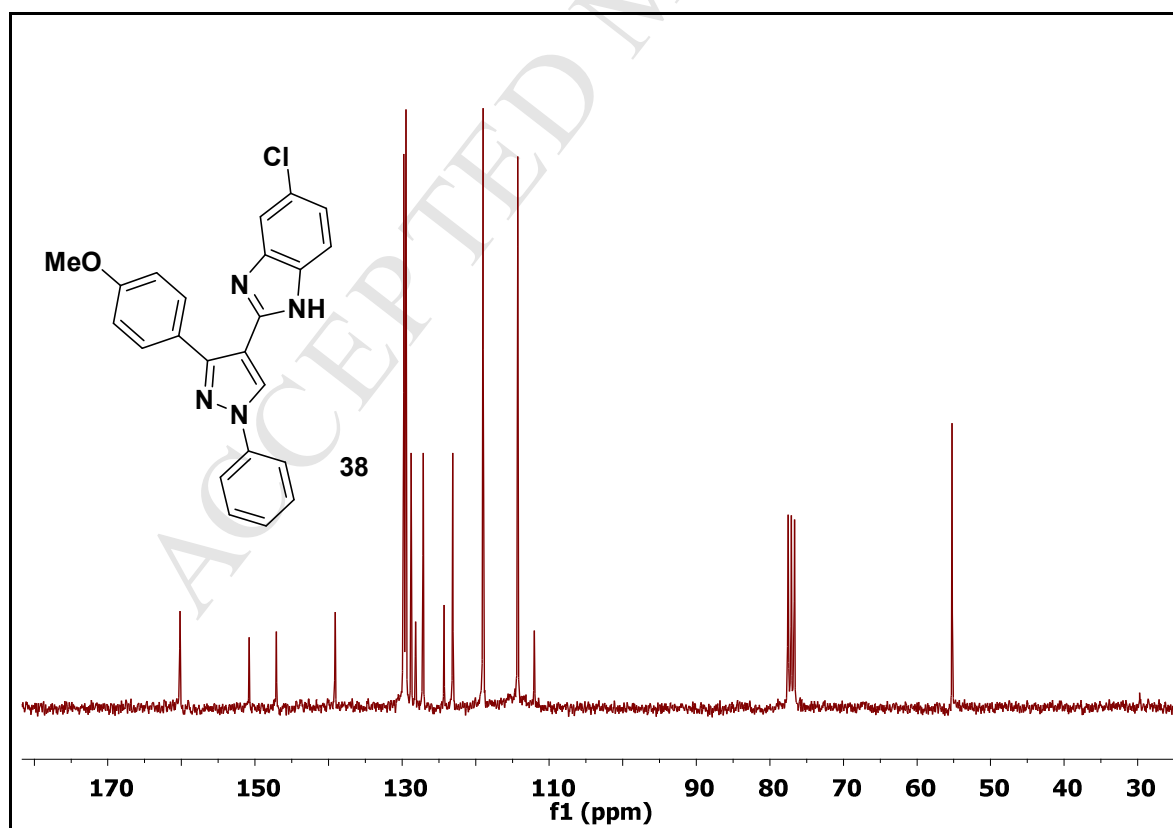
 ^1H NMR spectra of compound 32 ^{13}C NMR spectra of compound 32

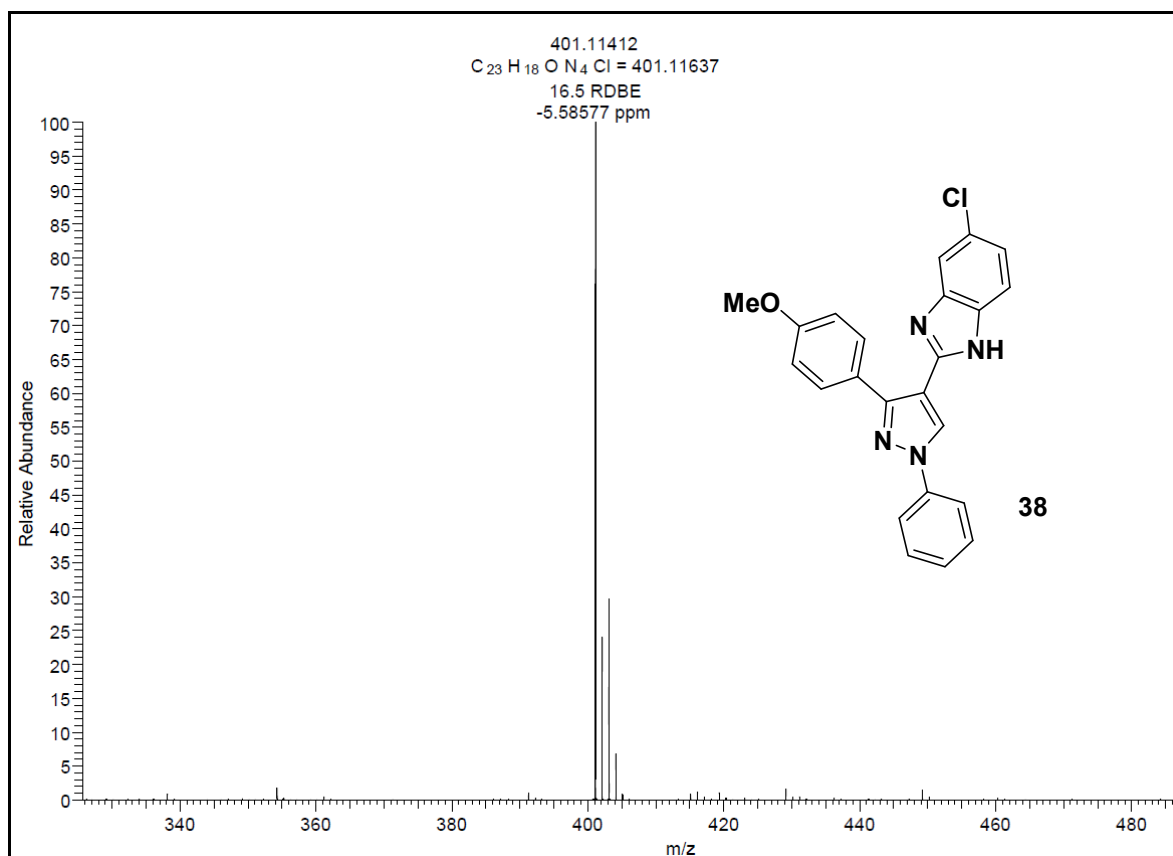
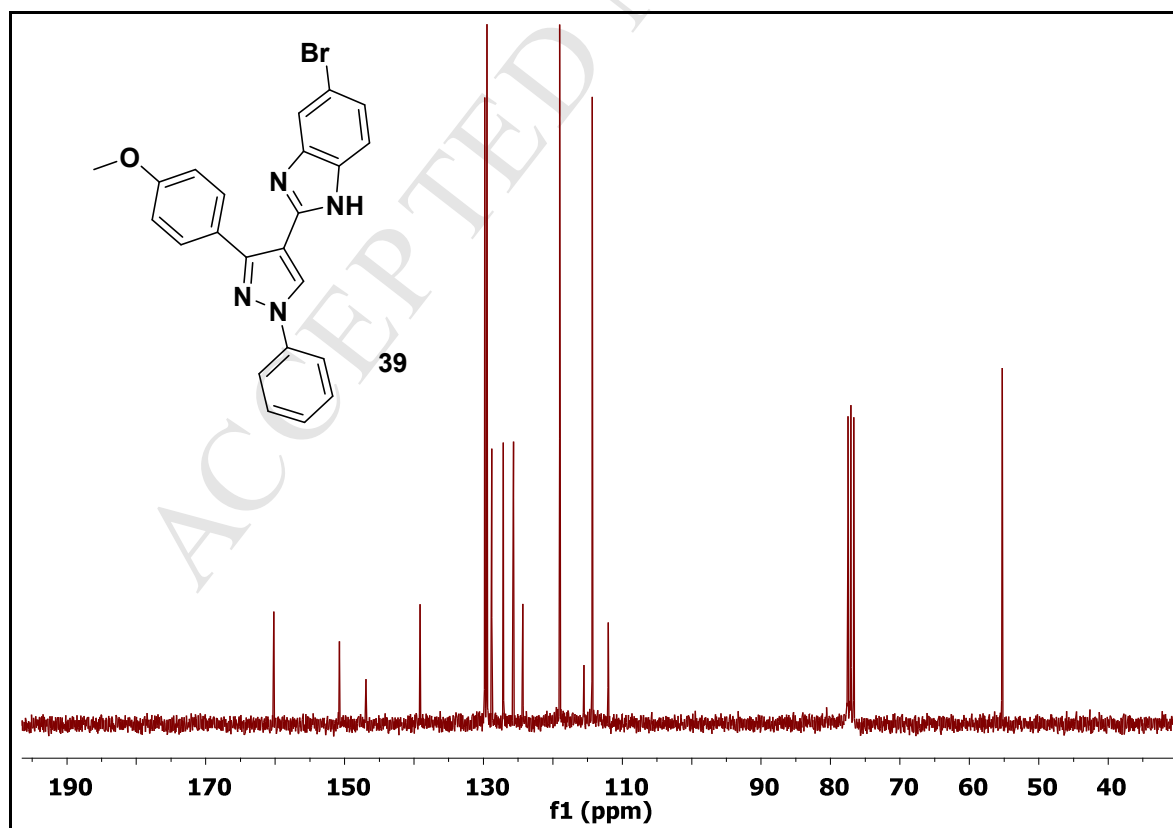
¹H NMR spectra of compound 33¹H NMR spectra of compound 34

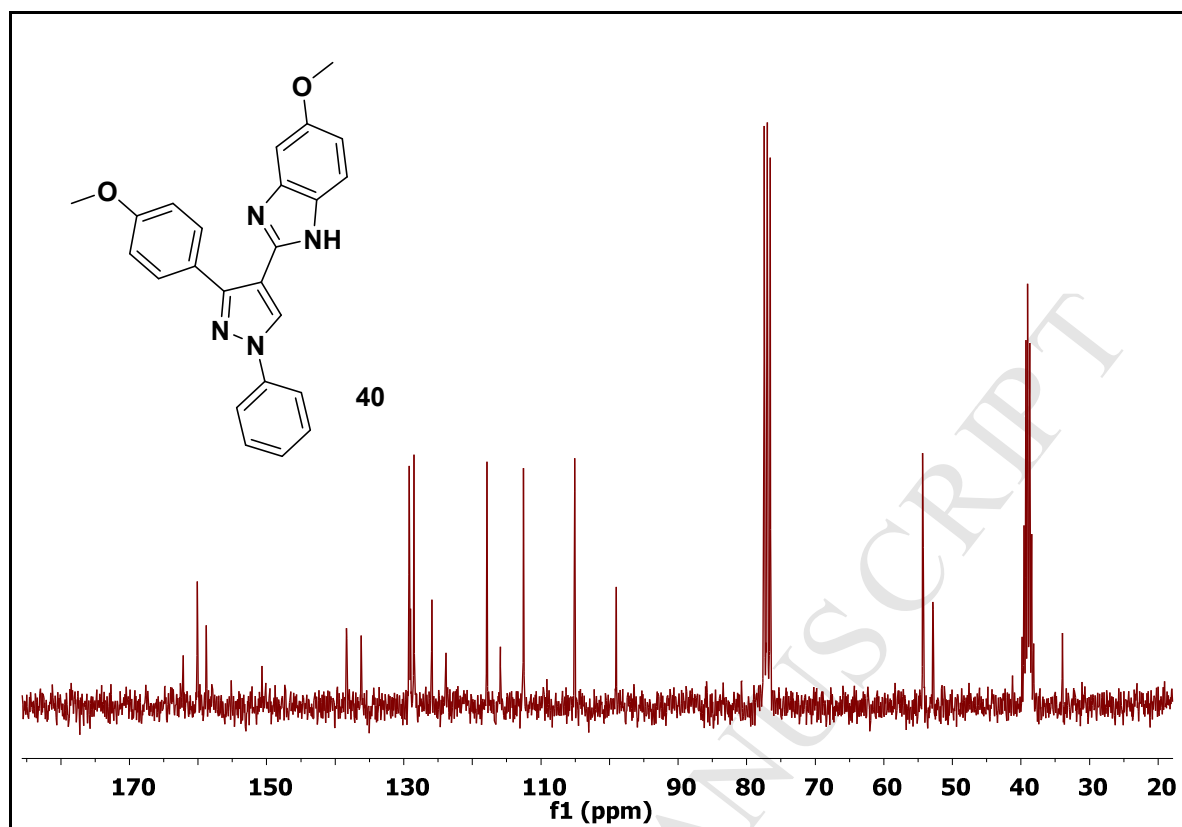
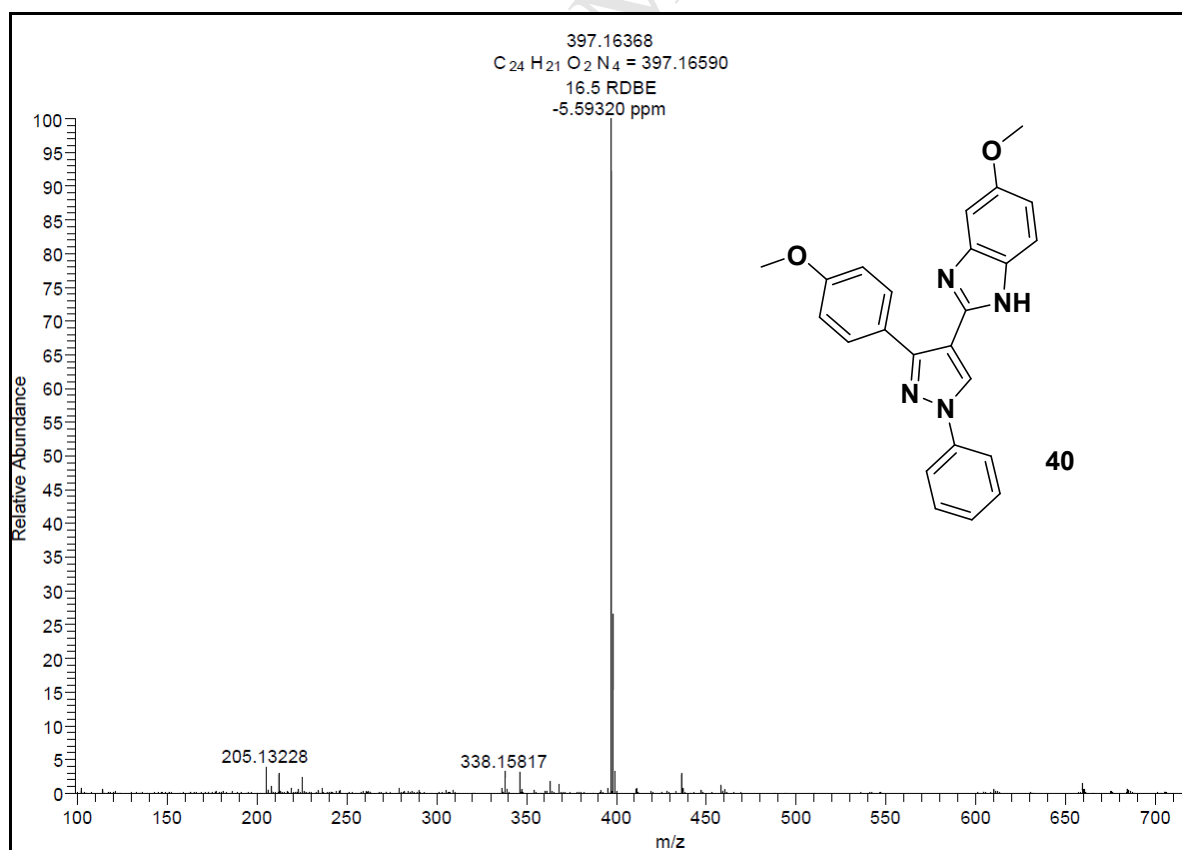
 ^1H NMR spectra of compound 35 ^{13}C NMR spectra of compound 35

¹H NMR spectra of compound 36¹³C NMR spectra of compound 36

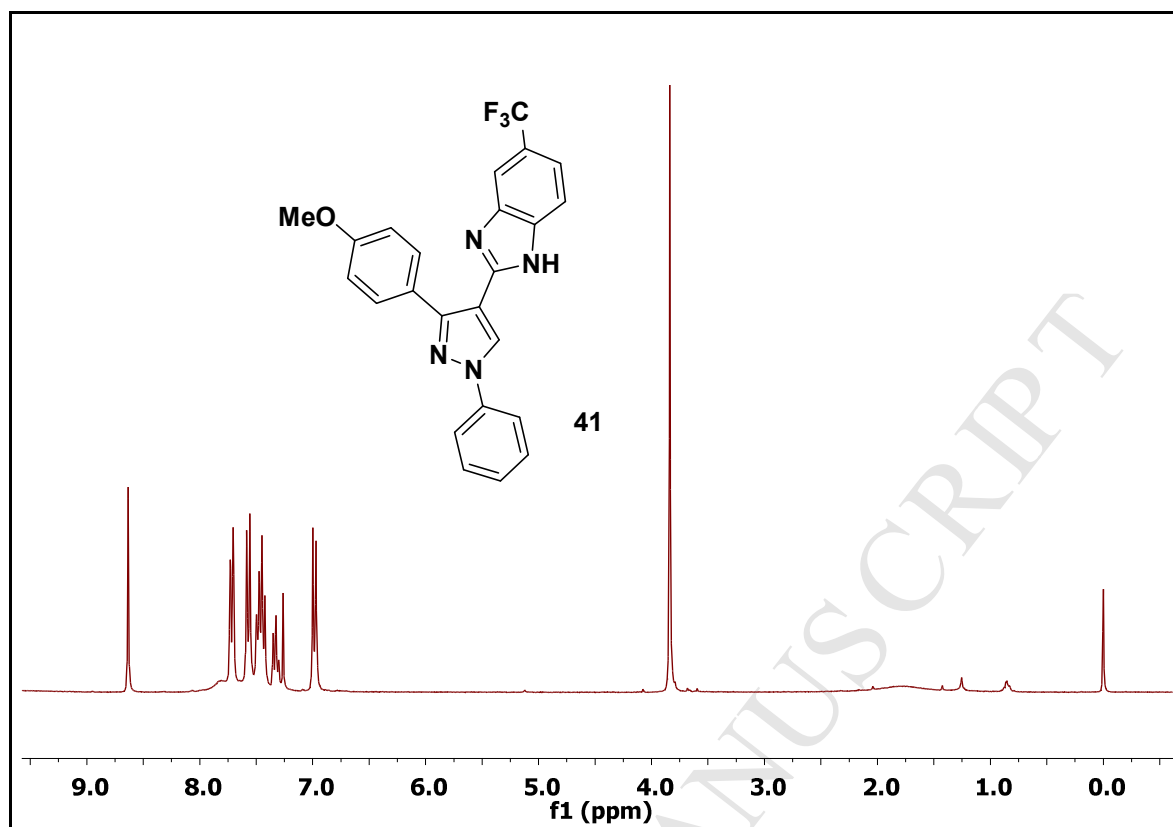
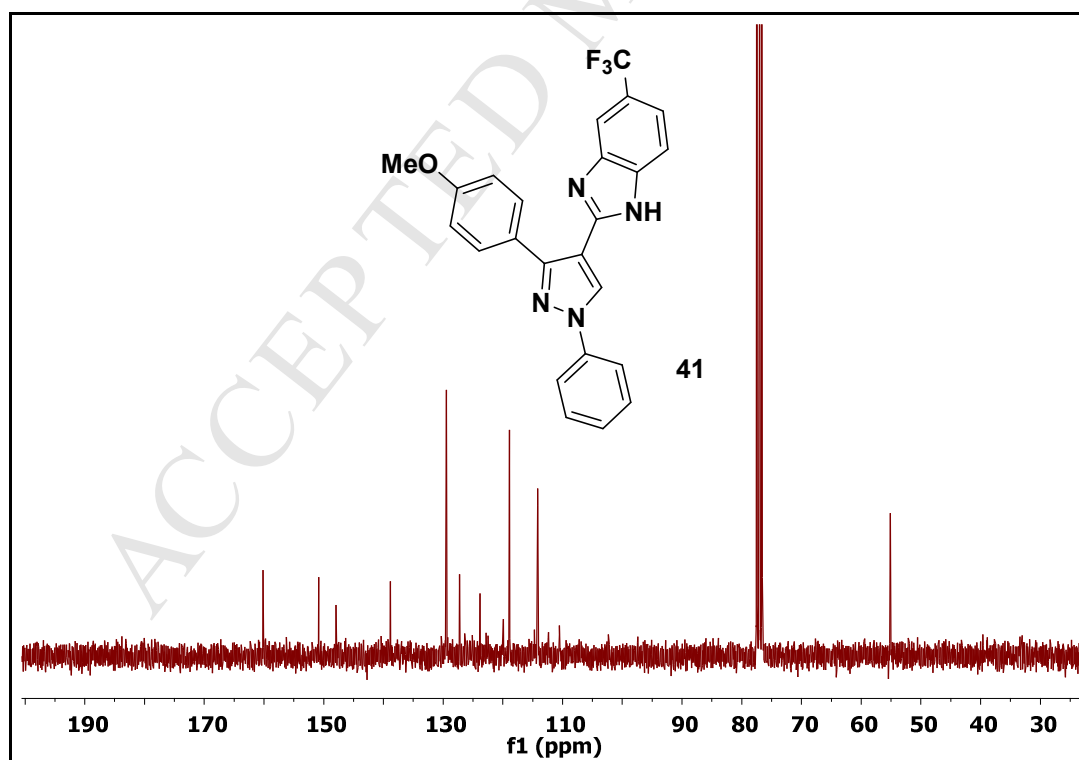
¹H NMR spectra of compound 37¹³C NMR spectra of compound 37

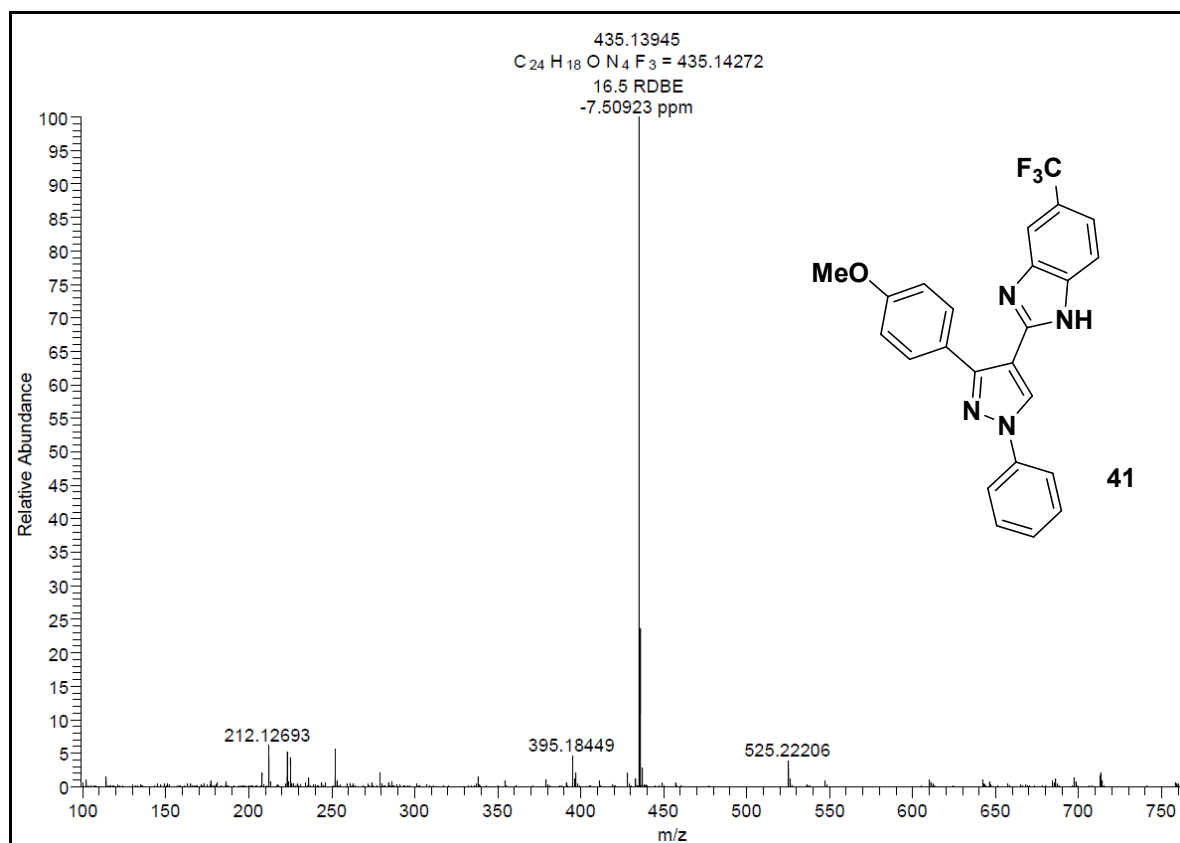
 ^1H NMR spectra of compound 38 ^{13}C NMR spectra of compound 38

HRMS spectra of compound **38**¹³C NMR spectra of compound **39**

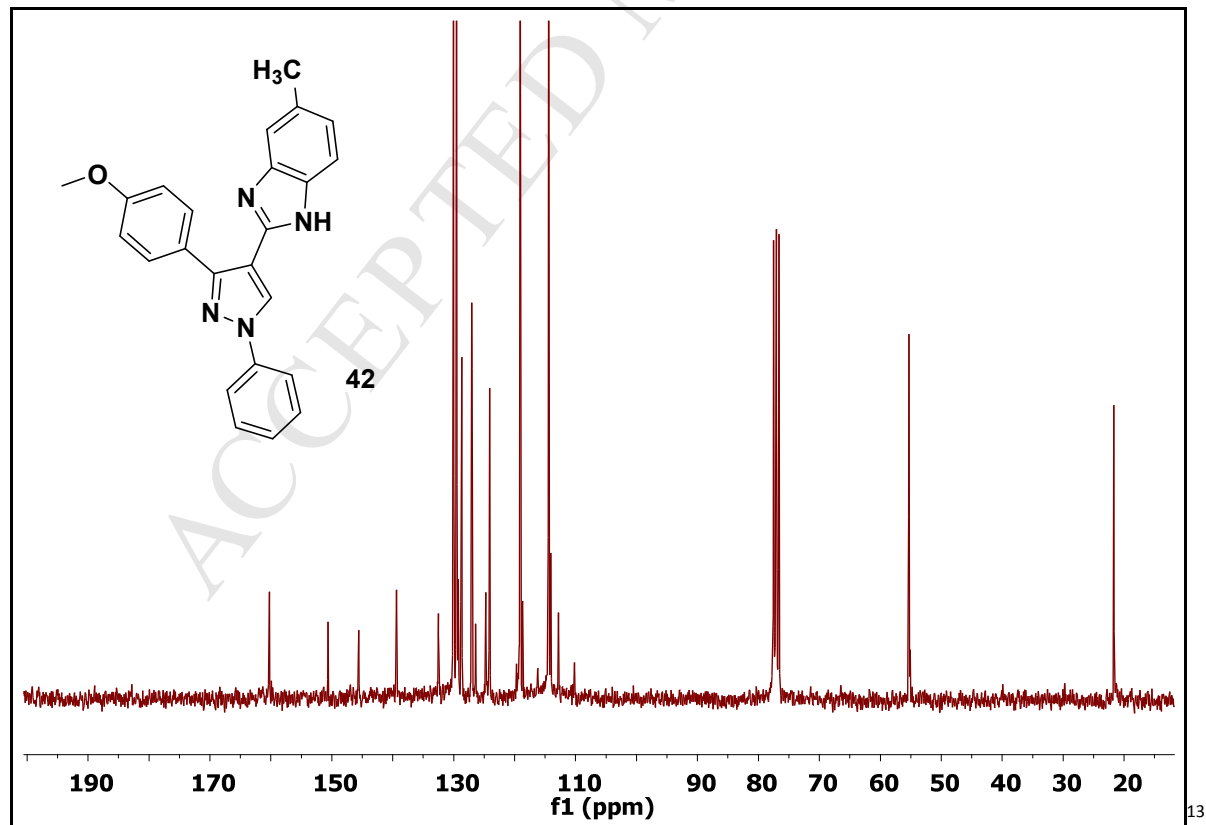
 ^{13}C NMR spectra of compound 40

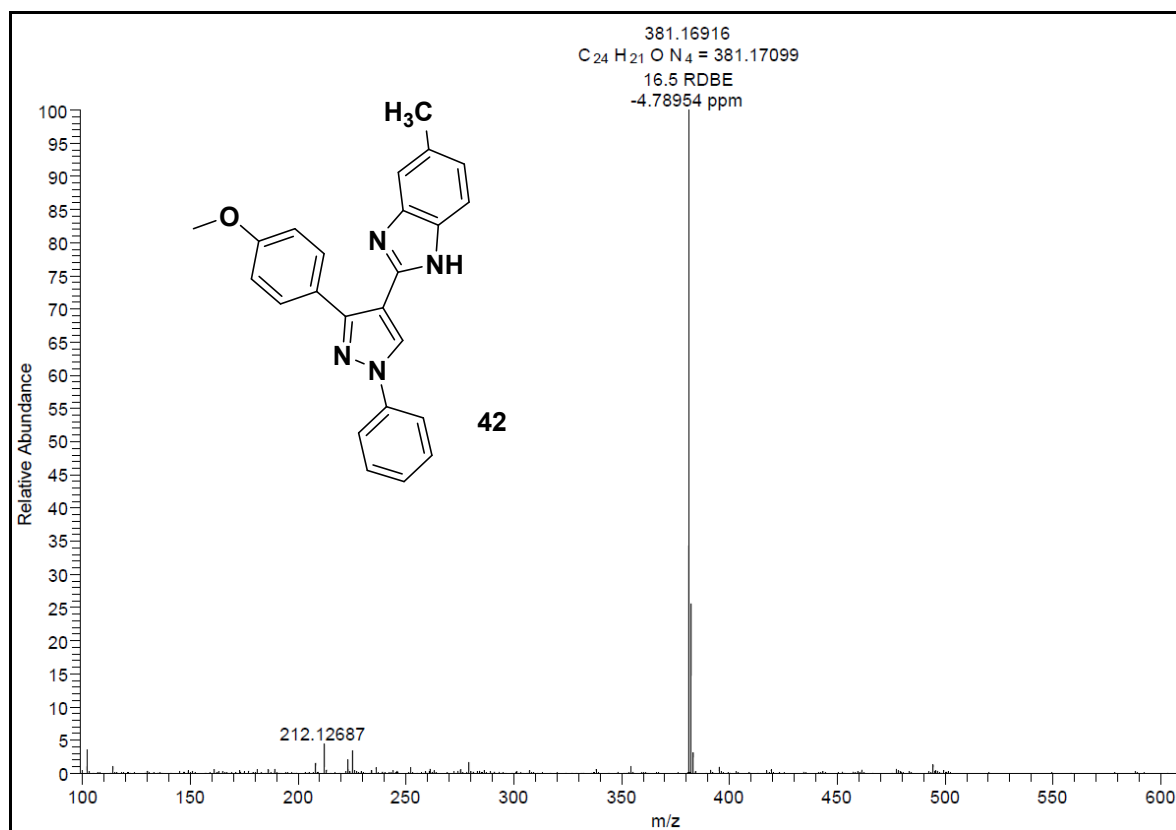
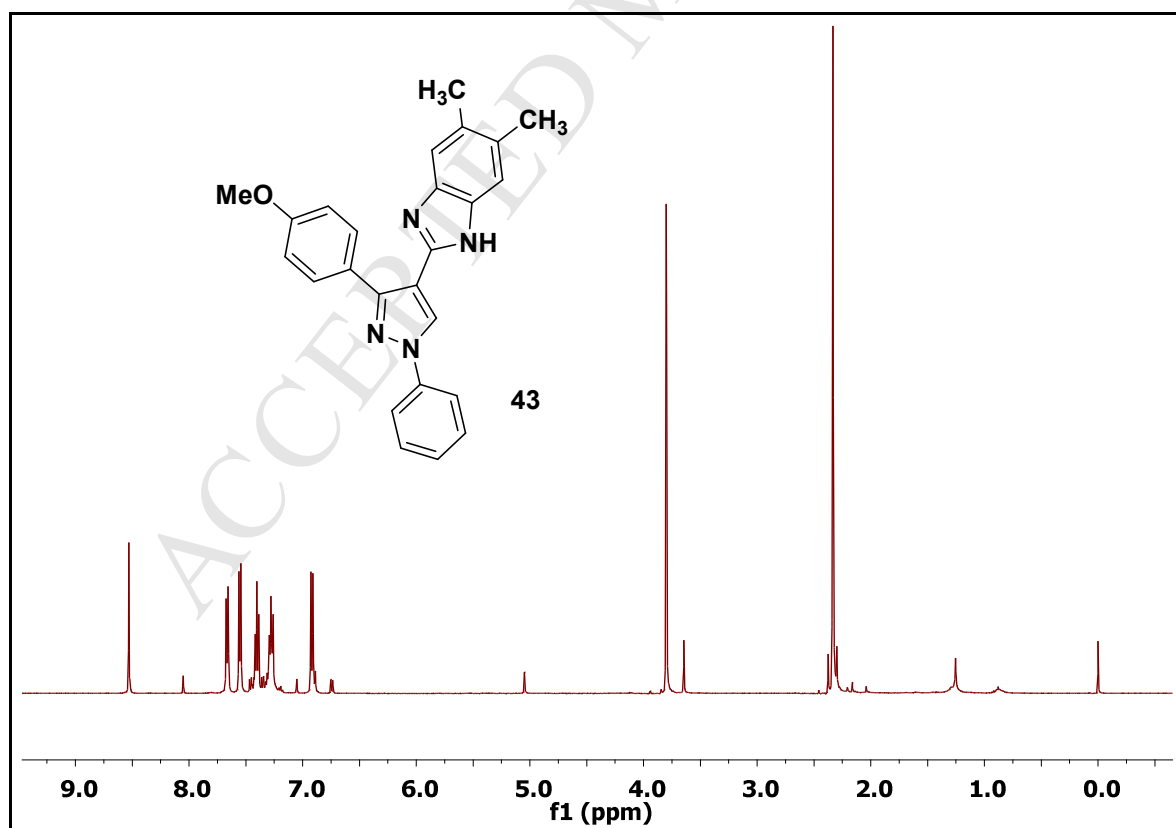
HRMS spectra of compound 40

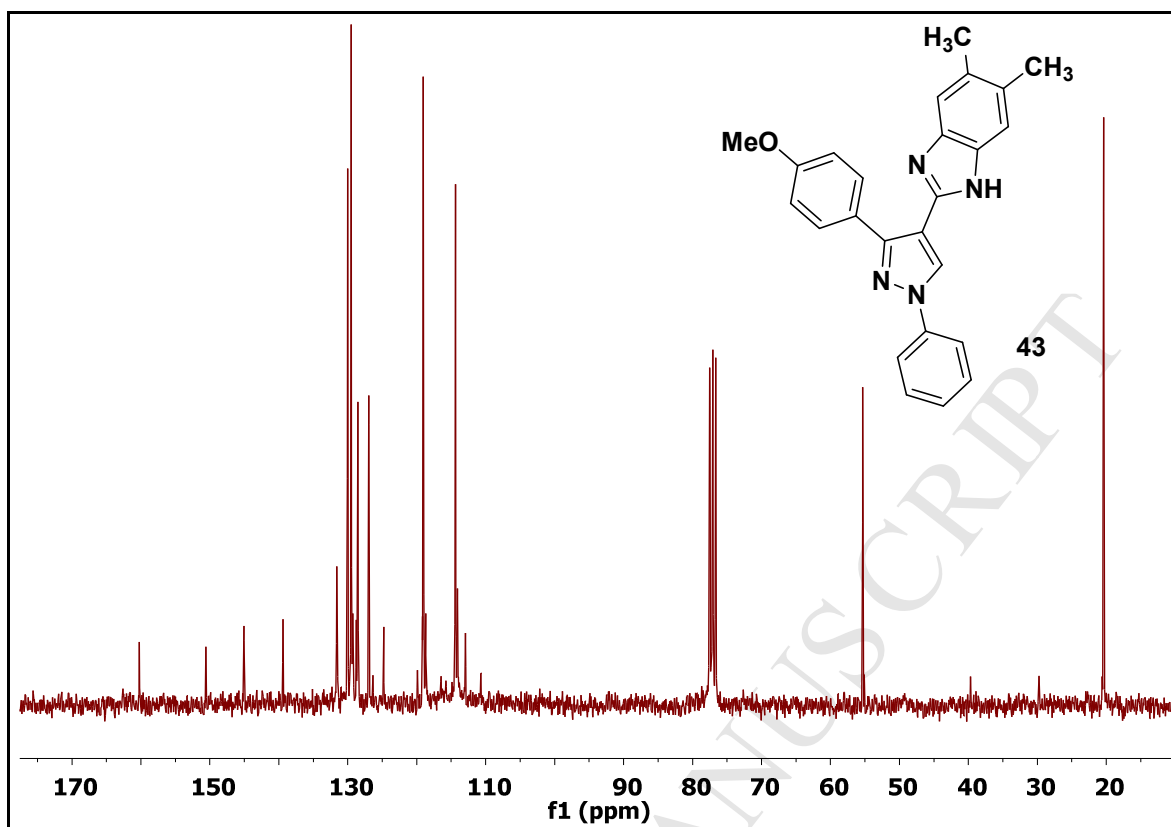
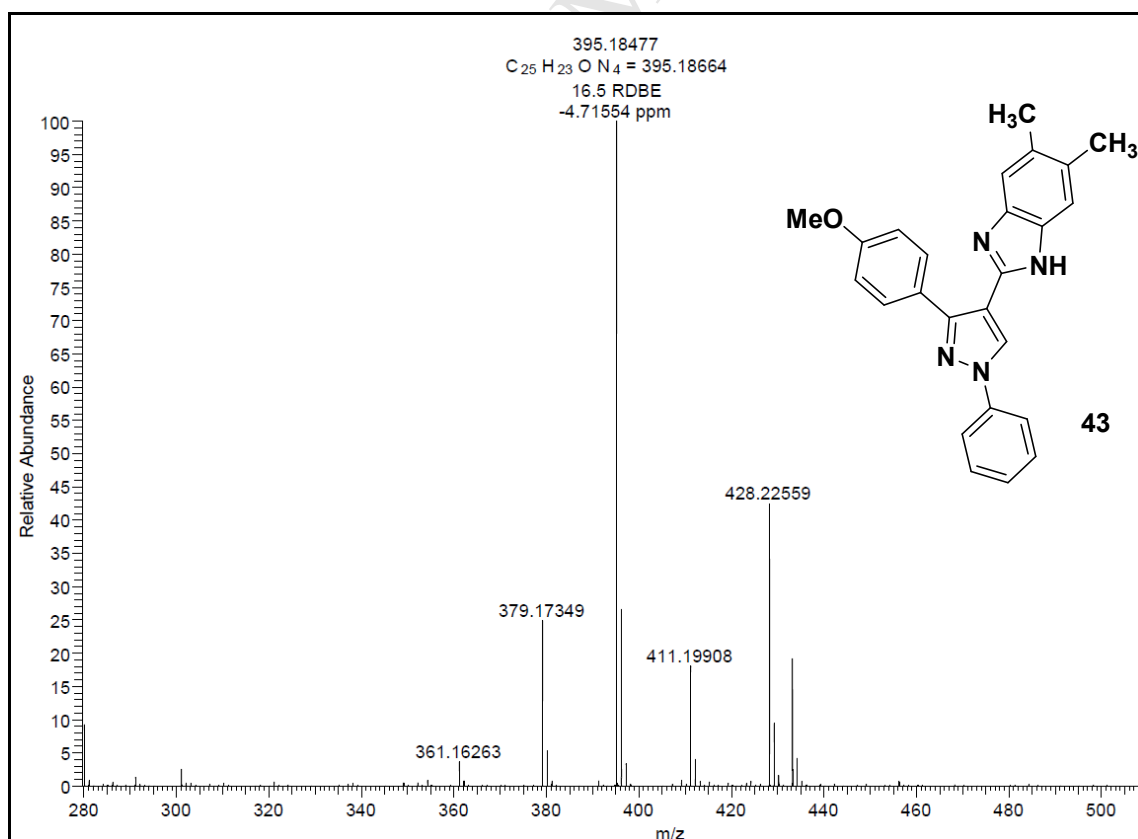
 ^1H NMR spectra of compound 41 ^{13}C NMR spectra of compound 41



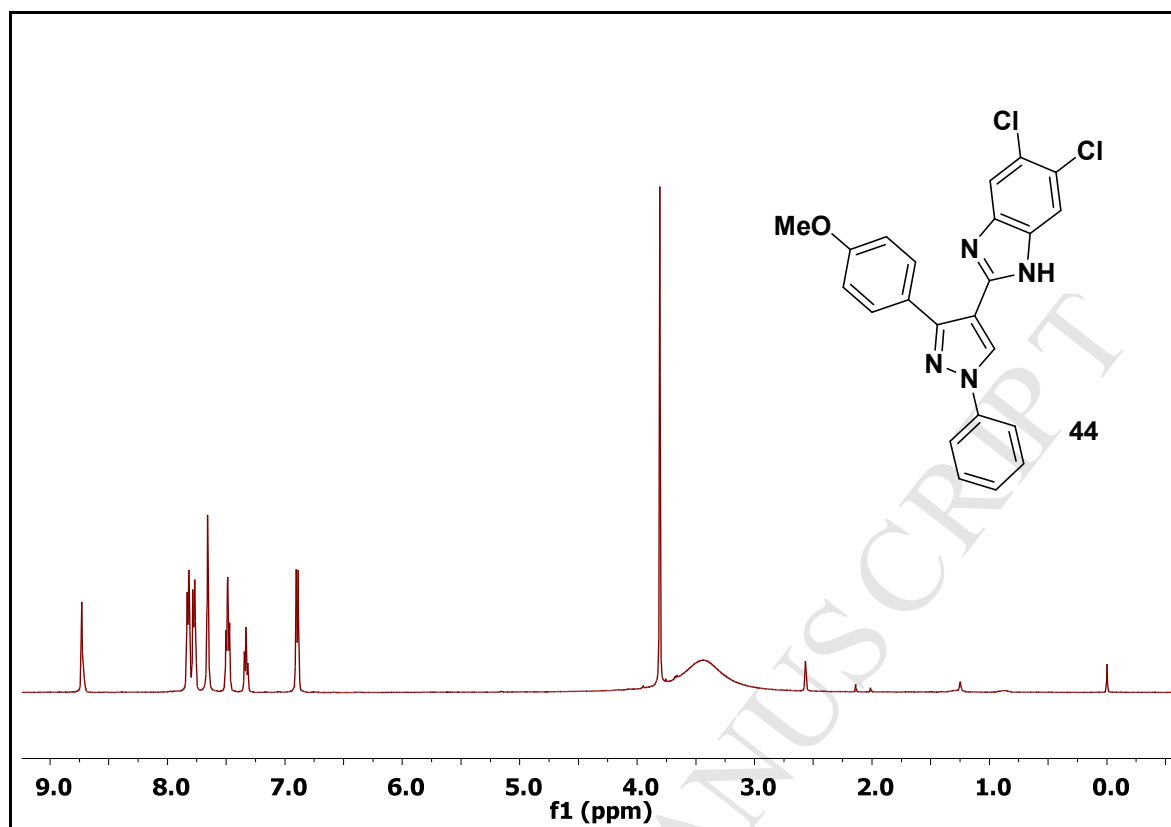
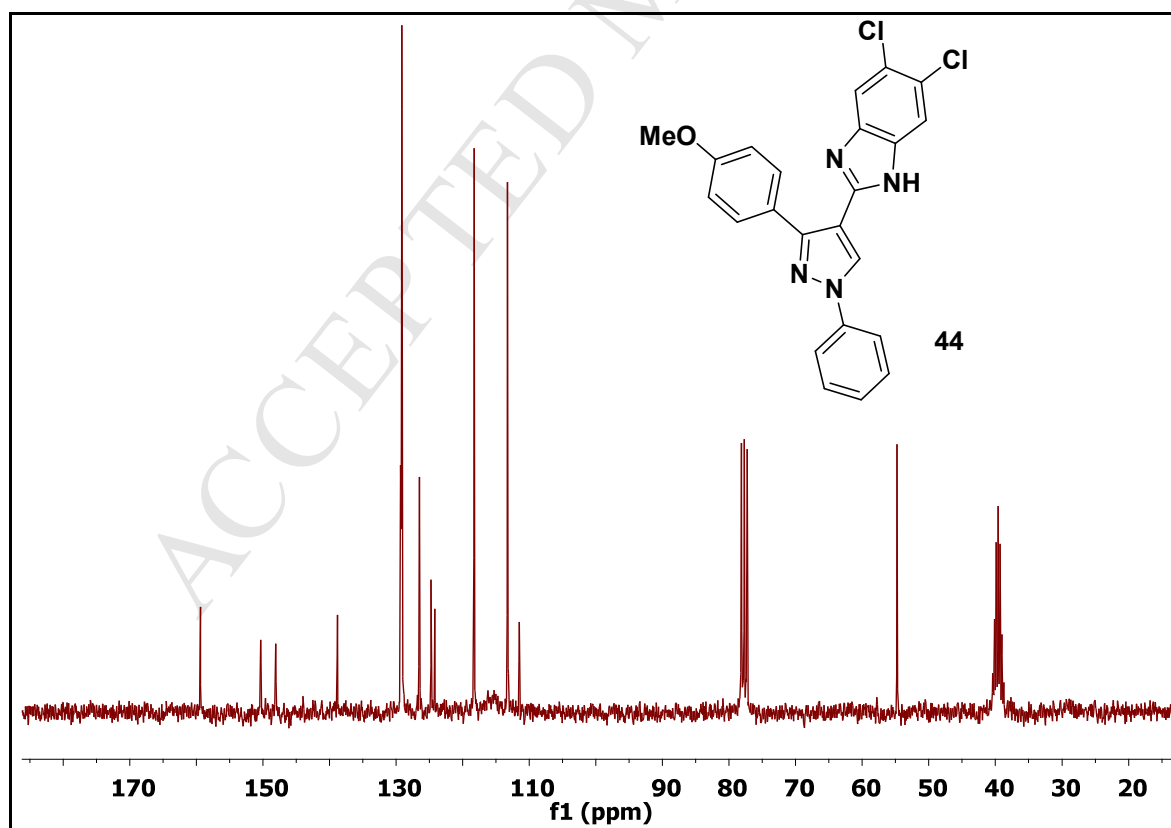
HRMS spectra of compound 41

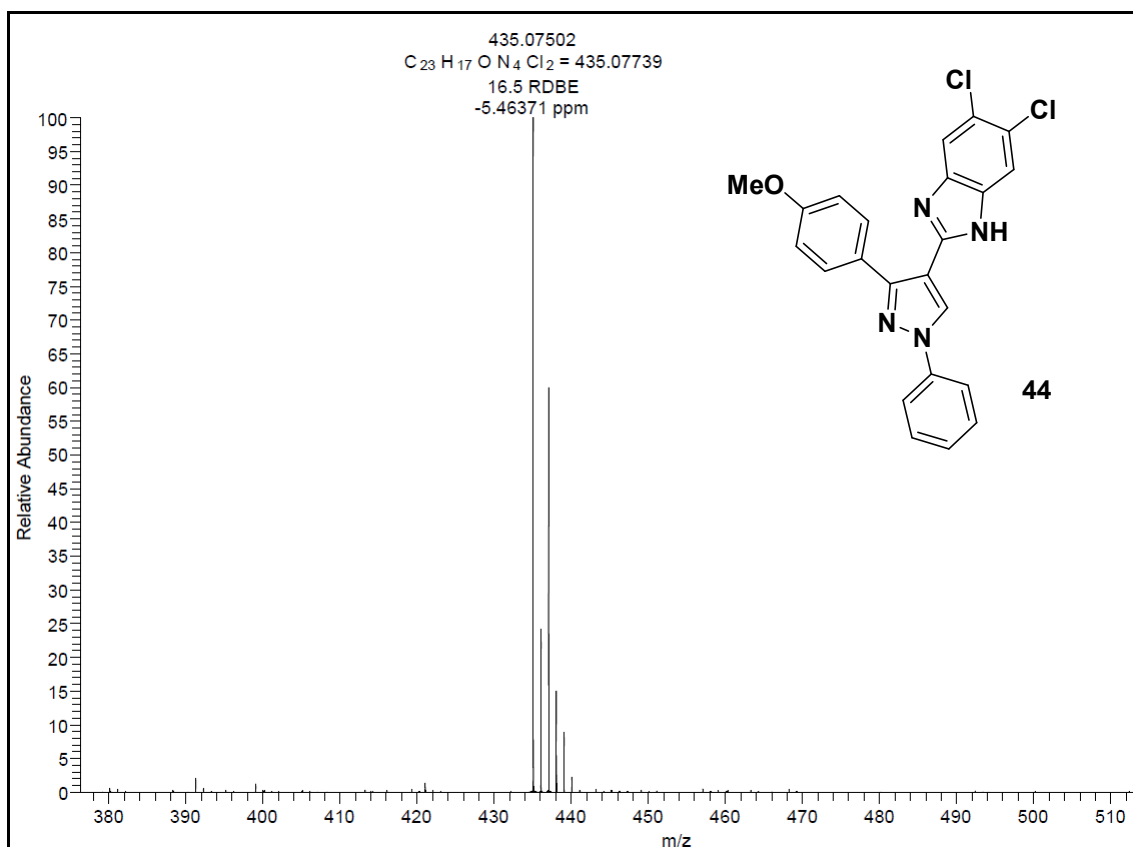
¹³C NMR spectra of compound 42

HRMS spectra of compound **42** 1H NMR spectra of compound **43**

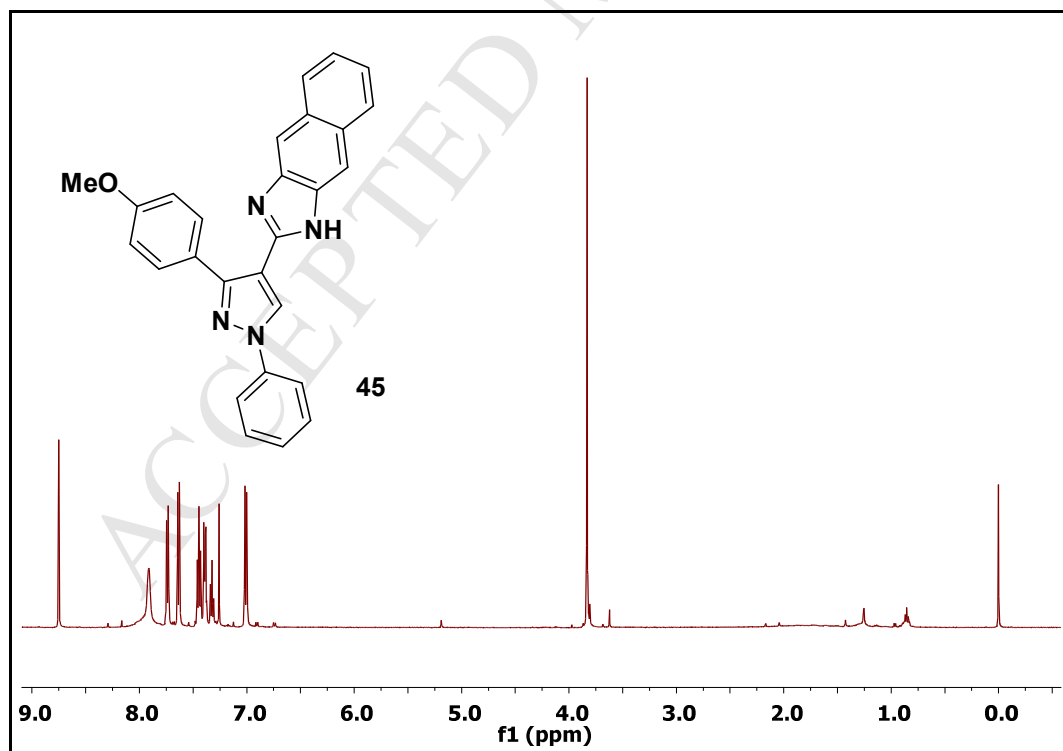
 ^{13}C NMR spectra of compound 43

HRMS spectra of compound 43

 ^1H NMR spectra of compound 44 ^{13}C NMR spectra of compound 44



HRMS spectra of compound 44

¹H NMR spectra of compound 45